MASTER IN BIOCHEMISTRY AND MOLECULAR AND CELL BIOLOGY RESEARCH FOCUS

Study of the putative roles of sirtuins 1 and 3 in the aristolochic acid I-induced cytotoxicity in human kidney-2 cells

Harvent, Marianne

Award date:
2019

Awarding institution:
University of Namur

Faculté des Sciences

Study of the putative roles of sirtuins 1 and 3 in the aristolochic acid I-induced cytotoxicity in human kidney-2 cells

Mémoire présenté pour l'obtention

du grade académique de master 120 en biochimie et biologie moléculaire et cellulaire

Marianne HARVENT

Août 2019

Université de Namur

FACULTE DES SCIENCES

Secrétariat du Département de Biologie

Rue de Bruxelles 61 - 5000 NAMUR

Téléphone: + 32(0)81.72.44.18 - Téléfax: + 32(0)81.72.44.20

E-mail: joelle.jonet@unamur.be - http://www.unamur.be

Study of the putative roles of sirtuins 1 and 3 in the aristolochic acid I-induced cytotoxicity in human kidney-2 cells

HARVENT Marianne

Abstract

Aristolochic acid nephropathy is characterized by a progressive interstitial fibrosis located in the superficial cortex, along with a tubular atrophy and a loss of proximal tubules due to the ingestion of aristolochic acids. In different study models of nephropathy, the effects of sirtuins 1 and 3 have already been investigated as they have been shown to have protective roles against oxidative stress or mitochondrial impairment. However, the roles of these enzymes have never been investigated in a model of aristolochic acid nephropathy. In the first part of this study, an aristolochic acid I (AAI)-induced cytotoxicity *in vitro* model is used on human kidney-2 cells to determine these putative roles. To allow sirtuins 1 and 3 gene expression analysis in cells exposed to an AAI, independently of cell death, we have characterized the effects of low concentrations (0, 0.1, 0.25, 0.5, 0.75 or 1 µM) of AAI on cell proliferation and cell toxicity by MTT and LDH assays for 12, 24, 48 or 72 h. After setting up the cell model, the second part concerns the analysis of the ATP content of cells incubated with low concentrations of AAI by a bioluminescent method. Indeed, mitochondrial fragmentation observed in cells exposed to a toxic AAI concentration might be accompanied by ATP production alterations. These low concentrations don't affect the ATP contents. The third part of this work covers the investigation of the putative effects of low concentrations of AAI on the abundance of sirtuins 1 and 3 at the transcriptomic and protein levels. No significant difference is observed on the expression of sirtuin 1 and sirtuin 3. The last part relates to the impact of the activation or the inhibition of sirtuins 1 and 3, by the use of four molecules. In order to evaluate a putative sensitisation by sirtuins inhibitors (3-TYP and EX527) or a potential protection by sirtuins activators (Coumarin and SRT2104) against the AAI-induced cytotoxicity, western blot analysis, MTT and LDH assays are performed. A slight activation of sirtuin 3 was noted with the use of 10 µM of Coumarin. No change is observed in the cytotoxicity by the use of 10 µM of 3-TYP, whereas a decrease of the cell proliferation is observed. As regards sirtuin 1, a reduction of the cell proliferation and an increase in the cytotoxicity are observed with the use of 25 µM of SRT2104. Moreover, a decrease of the cell proliferation is observed 72 hours after the incubation with 10 µM of EX527. This study opens the scope for additional experiments such as the analysis of the morphology of the mitochondrial population in human kidney-2 cells exposed to low concentrations of aristolochic acid I or an increase of the concentrations of activators or inhibitors of sirtuins used in this work, in order to obtain a more marked effect of these four molecules.

Mémoire de master 120 en biochimie et biologie moléculaire et cellulaire

Août 2019

Promoteur: N. CARON

Co-promoteur: T. ARNOULD

Université de Namur
FACULTE DES SCIENCES
Secrétariat du Département de Biologie
Rue de Bruxelles 61 - 5000 NAMUR
Téléphone: + 32(0)81.72.44.18 - Téléfax: + 32(0)81.72.44.20
E-mail: joelle.jonet@unamur.be - http://www.unamur.be

Étude des rôles potentiels des sirtuines 1 et 3 dans la cytotoxicité induite par l'acide aristolochique I dans les cellules rénales humaines

HARVENT Marianne

Résumé

La néphropathie aux acides aristolochiques est caractérisée par une fibrose interstitielle progressive au niveau du cortex superficiel ainsi que d'une atrophie tubulaire et d'une perte des tubules proximaux suite à l'ingestion d'acides aristolochiques. Les effets des sirtuines 1 et 3 ont déjà été investigués dans différents modèles d'étude de néphropathie, montrant des rôles protecteurs contre le stress oxydatif ou les altérations mitochondriales. Cependant, les rôles potentiels de ces deux enzymes n'ont jamais été étudiés dans la néphropathie aux acides aristolochiques. Dans la première partie de ce travail, un modèle *in vitro* de cytotoxicité induite par l'acide aristolochique I (AAI) est utilisé sur des cellules rénales humaines pour déterminer ces rôles potentiels. Afin d'analyser l'expression génique des sirtuines 1 et 3 dans des cellules exposées à l'AAI, indépendamment de la mort cellulaire, les effets de faibles concentrations (0, 0,1, 0,25, 0,5, 0,75 ou 1 µM) d'AAI sur la prolifération et la toxicité cellulaires ont été déterminés par des tests MTT et LDH durant 12, 24, 48 ou 72 heures. Après cette mise au point, la seconde partie concerne l'analyse des niveaux d'ATP des cellules incubées avec les faibles concentrations d'AAI choisies, niveaux évalués par une méthode de bioluminescence. En effet, la fragmentation mitochondriale observée dans des cellules exposées à une concentration toxique d'AAI pourrait être accompagnée d'altérations de la production d'ATP. Ces faibles concentrations n'affectent pas le contenu en ATP. La troisième section de ce travail couvre l'examen des effets potentiels de faibles concentrations d'AAI sur l'abondance des sirtuines 1 et 3 au niveau transcriptomique et protéique. Aucune différence significative n'a été observée au niveau de l'expression de *sirtuine 1* et de *sirtuine 3*. La dernière partie de ce travail est relative à l'activation ou l'inhibition des sirtuines 1 et 3 par l'usage de quatre molécules. Afin d'évaluer la sensibilisation potentielle par les inhibiteurs (3-TYP ou EX527) ou une potentielle protection par les activateurs (Coumarin ou SRT2104) de sirtuines contre la cytotoxicité induite par l'AAI, les méthodes de western blot, MTT et LDH furent appliquées. Une faible activation de la sirtuine 3 a été constatée lors de l'utilisation de 10 µM de Coumarin. Aucun changement n'a été observé dans la cytotoxicité en utilisant 10 µM de 3-TYP, tandis qu'une diminution de la prolifération cellulaire a été relevée. En ce qui concerne la sirtuine 1, une diminution de la prolifération cellulaire et une augmentation de la cytotoxicité ont été constatées en utilisant 25 µM de SRT2104. De plus, une réduction de la prolifération cellulaire a été observée 72 heures après incubation avec 10 µM d'EX527. Cette étude ouvre le champ à des expériences additionnelles telles que l'analyse de la morphologie de la population mitochondriale dans des cellules rénales humaines soumises à de faibles concentrations d'AAI ou une augmentation de la concentration des activateurs ou inhibiteurs de sirtuines utilisés dans ce travail afin d'obtenir un effet plus marqué des quatre molécules.

Mémoire de master 120 en biochimie et biologie moléculaire et cellulaire

Août 2019

Promoteur: N. CARON

Co-promoteur: T. ARNOULD

Acknowledgements

This work is the result of a « team of teams »[1]. To help craft the study into a clear narration, I relied on the advice and wisdom of professionals, classmates and friends.

My supervisors from UNamur have been essential in shaping my dissertation, offered me the opportunity to do and learn cell culture - with the entire rigor that this requires -, and contributed to the development and improvement of one year of business. Professors Nathalie CARON and Thierry ARNOULD, Doctors of Science, were especially helpful in assisting me by mentoring my project, giving effective advice on the work's structure and content, reading the different drafts, and providing support, patience and encouragement in a long process. Thanks to Inès JADOT, my tutor, and Pauline MOSSERAY, PhD Student, who provided advice throughout the development process.

I have also to mention the contribution and the support of my supervisors and Patsy RENARD and their teams of the laboratories of URPhym and URBC.

And special thanks to Marino, Julie, Damien, Morgane, PhD students, as well as to Christoph and Sébastien, who helped and provided assistance during the experiments and the meetings.

Dr. Olivier DEVUYST, MD, PhD, PI, provided valuable feedback and information that shaped elements of the study.

Marie ROMMELAERE and Dominique BECKER, MD, nephrologists, read final drafts and provided invaluable feedback in the late stages of intensive editing.

Although we could not begin to thank every single person involved in this project and the learning moments, Mrs Huguette DEBAIX, Senior Technician, gave helpful comments on methods.

Thank you to the members of the jury for their evaluation of this thesis.

We could not have produced this work without relying on the research and great works of many scientists and authors in a wide variety of fields.

[1] Initial expression of General Stanley Mac CHRYSTAL, US Army, retired

Table of content

Table of figures

Table of abbreviations

A	Ampere
Å	Angström
AA	Aristolochic acid
AAN	Aristolochic acid nephropathy
AceCSs	Acetyl-CoA-synthase
ADP	Adenosine diphosphate
AKI	Acute kidney injury
AL	Aristolactam
ATCC	American Type Cell Collection
ATP	Adenosine triphosphate
ATPS-β	Adenosine triphosphate synthase subunit β
BEN	Balkan-endemic nephropathy
BPE	Bovine pituitary extract
BSA	Bovine Serum Albumin
CD	Collecting duct
cDNA	complementary Desoxyribo Nucleic Acid
cm^2	Square centimetre
COX1	Cytochrome c oxidase subunit 1
CtBP	Carboxy-terminal-binding protein
CWE	Column wash solution
CYP	Cytochrome P
Da	Dalton
DBC1	Deleted in breast cancer 1
DCT	Distal convoluted tubule
DMSO	Dimethylsulfoxide
DNA	Desoxyribo Nucleic Acid
Drp	Dynamin-related protein
Drp1-dependent	Dynamin-related protein-dependent
DTNB	Dithiobis 2-nitrobenzoic acid
DTT	Dithiothreitol
E2F1	E2 promoter binding factor 1
EDTA	Ethylene diamine acid tetra acetic

EGF	Epidermal growth factor
ERRα	Estrogen-related receptor α
ETC	Electron transport chain
FCCP	Carbonyl cyanide-4 (tri-fluoromethoxy) phenylhydrazone
Fis	Fission
FOXOs	Forkhead box, group O (FOXO) subfamily of forkhead transcription factor
g	Gram
GDH	Glutamate dehydrogenase
GLUT	Glucose transporter
GSH	Glutathione
GSSG	Glutathione regeneration from oxidized glutathione
h	Hour
H1C1	Hypermethylated in cancer 1
HD	Huntington disease
HIF-2α	Hypoxia-inducible factor-2 alpha
HK	Human kidney
HL	Henle's loop
HL-60	Human promyelocytic leukemia
HLA	Human histocompatibility antigen
HPV-16	Human papillomavirus-16
IDCR	Ionic Detergent Compatibility Reagent
IDH2	Isocitrate dehydrogenase 2
IdMOC	Integrated discrete multiple organ co-culture
IKK	IκB kinase
IKKβ	Subunit of activated IκB kinase
IL-1β	Interleukin 1 beta
IL-6	Interleukin 6
ISOM	Inner stripe of the outer medulla
kDa	kilo Dalton
kg	Kilogram
K-SFM	Keratinocyte serum-free medium
L	Litre
LBA	Lysis buffer

LDH	Lactate dehydrogenase
LDLR	Low-density lipoprotein receptor
LRP2	Low-density lipoprotein-related protein-2
Lys	Lysine
M	Molar
Mff	Mitochondrial fission factor
Mfn	Mitofusin
mg	Milligram
MgCls	Magnesium chloride
min	Minute
mL	Millilitre
mM	Millimolar
MPS	Micro-physiological system
mRNA	messenger RNA
MRP	Multidrug resistance-associated proteins
mtDNA	Mitochondrial DNA
MTT	3-[4,5-dimethylthiazol-2-yl]-2,5 diphenyl tetrazolium bromide
NAD	Nicotinamide adenine dinucleotide
NAD(P)H or NADPH	Nicotinamide Adenine Dinucleotide Phosphate
NAM	Nicotinamide
NAMPT	Nicotinamide mononucleotide adenyltransferase
nDNA	Nuclear DNA
NDUFB8	Nicotinamide adenine dinucleotide: ubiquinone oxidoreductase subunit B8
NEP	Neutral endopeptidase
NF-κB	Nuclear factor-kappa B
ng	Nanogram
nm	Nanometer
NMN	Nicotinamide mononucleotide
NMNAT	Nicotinamide phosphoribosyltransferase
NQO	NAD(P)H:quinone oxidoreductase
NRF	nuclear respiratory factor
OAT	Organic anion transporter
OK	Opossum kidney

OPA-1	Optic atrophy-1
OSOM	Outer stripe of the outer medulla
OxPHOS	Oxidative phosphorylation
PBS	Phosphate buffer saline
PCNA	Proliferating cell nuclear antigen
PCT	Proximal convoluted tubule
PGC-1α	Peroxisome proliferator-activated receptor γ coactivator-1 alpha
pH	Hydrogen potential
PIB	Phosphatase inhibitor buffer
PIC	Protease inhibitor cocktail
PINK1	PTEN-induced putative kinase 1
PLA_2	Phospholipase A2
POR	NADPH:CYP oxidoreductase
$PPAR_{\gamma}$	Peroxisome proliferator-activated receptor-γ
PPM1A	Protein phosphatase magnesium-dependent 1A
PTC	Proximal tubular cells
PTEC	Proximal tubular epithelial cells
PTEN	Phosphatase and Tensin homolog
PVDF	PolyVinyliDene Fluoride
qPCR	Polymerase chain reaction
RBP	Retinol binding protein
RNA	Ribo Nucleic Acid
ROS	Reactive Oxygen Species
rRNA	Ribosomal Ribo Nucleic Acid
RT-qPCR	Reverse transcription polymerase chain reaction
RWA	RNA wash solution
s	Second
SDH	Succinate dehydrogenase
SDS	Sodium dodecyl sulfate
SEM	Standard error of the mean
ser	Serine
SGLT	Sodium-dependent glucose transporter
SIRT	Sirtuin
SOD2	Superoxide dismutase 2

SULT	Sulfotransferase
TFAM	transcription factor A mitochondrial
TGF-β1	Transforming growth factor beta 1
TNB	2-nitro-5-thiobenzoic acid
TNF-α	Tumour-necrosis factor alpha
V	Volt
vs	*versus*
Zn	Zinc
µg	Microgram
µL	Microliter
µM	Micromolar
µm	Micrometre
µmol	Micromole
°C	Degrees Celsius
%	Percentages

Introduction

I. The kidneys

a) Anatomy

The kidneys are located in the abdominal cavity, under the diaphragm, in the retroperitoneum. They are vascularized by the renal arteries, which give birth to segmental arteries and then to interlobate, arcuate and interlobular arteries that supply afferent arterioles and the glomerulus where the filtration occurs. Blood then goes to the efferent artery, which gives birth to *vasa recta* that give birth to venous system (Figure 1) (Gueutin et al., 2012).

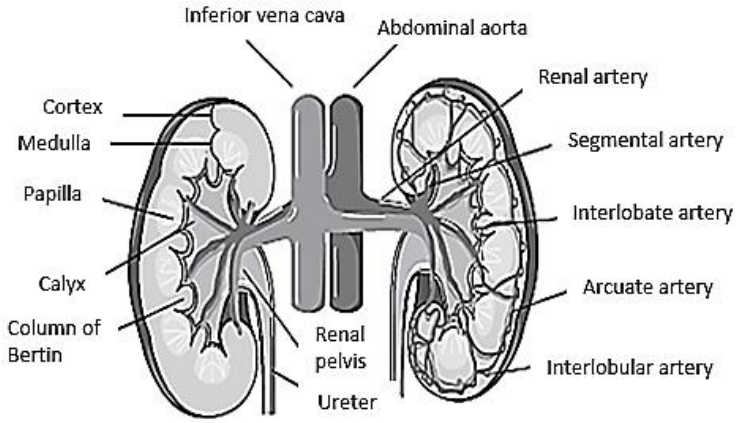

Figure 1: Renal anatomy and vascularization*. Modified from (Gueutin et al., 2012).*

From the outside to the inside, the composition of the kidney is the following: 1) cortex, 2) outer stripe of the outer medulla (OSOM), 3) inner stripe of the outer medulla (ISOM) and 4) inner medulla (Figure 2). The primitive urine flows through the proximal convoluted tubule (PCT), the Henle's loop (HL), then the distal convoluted tubule (DCT), and finally, through the collecting duct (CD) where the reabsorption and secretion mechanisms allow to modulate the urinary concentration (Gueutin et al., 2012).

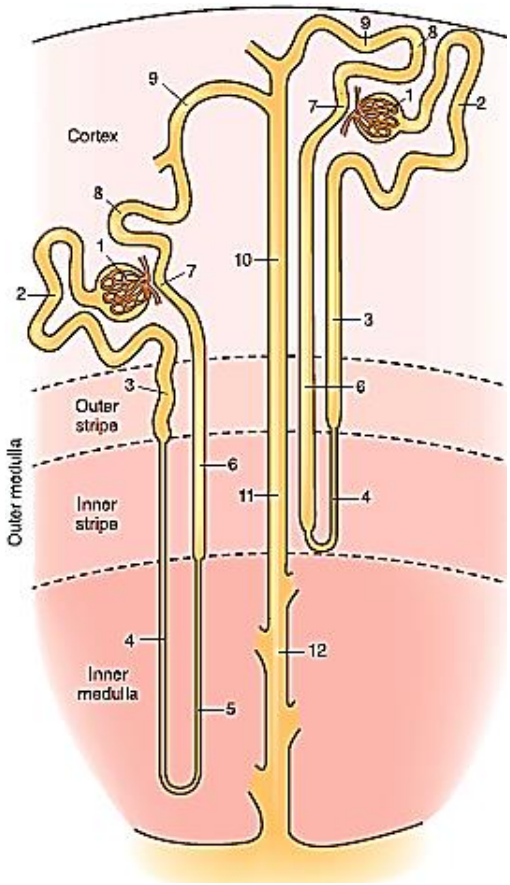

Figure 2 : Illustration of a nephron, the functional unit of kidneys, forming by glomerulus and renal tubules. *1, glomerulus; 2, proximal convoluted tubule; 3, proximal straight tubule; 4, descending thin limb; 5, ascending thin limb; 6, thick ascending limb; 7, macula densa; 8, distal convoluted tubule; 9, connecting tubule; 10, cortical collecting duct; 11, outer medullary collecting duct; 12, inner medullary collecting duct (Mount, 2014).*

b) Functions

The kidneys ensure several functions: elimination of degradation products of the cellular metabolism such as urea, maintenance of the composition of the inner medium (water and electrolyte homeostasis) and synthesis of renin[2], erythropoietin[3] and calcitriol[4] (Lacour, 2013). They are also in charge of the regulation of intra-/extracellular volume, acid-base status, pH regulation, erythropoiesis and calcium and phosphate concentration homeostasis (Gueutin et al., 2012).

These organs filter every day about 150 to 180 L of blood to produce 1 to 2 L of urine, which is composed of metabolic waste products such as nitrogenous waste and extra fluids. Kidneys constitute a frequent target of toxicity induced by drugs, xenobiotics (Bajaj et al., 2018) and cytotoxins (Hagos and Wolff, 2010). Indeed, the renal proximal tubules, part of the nephron in charge for secretion and reabsorption, have number of secretory transporters. So, kidneys possess a lot of passages and are most affected by the intoxication of toxic molecules. In addition, if transporters have an activity default, which can decrease their secretion activity, the toxic can potentially accumulate in the concerned cells (Hagos and Wolff, 2010).

[2] Molecule synthetized by juxtaglomerular cells after a decrease of the blood pressure. That allows the transformation of angiotensinogen to angiotensin I (Lacour, 2013)
[3] Molecule produced by the kidney and essential for the production of erythrocytes (Lacour, 2013)
[4] Or active vitamin D, increases the calcium and phosphate absorption by the organism and regulates also the parathormone in order to regulate the osteoblast activity (Lacour, 2013)

The nephron constitutes the functional unit of the kidney since it is able to achieve all the kidney functions, and it is composed of a glomerulus and of renal tubules (Callard, 2016). The PCT allows the most important reabsorption of water, sodium, bicarbonate, amino acids and small filtered proteins (Gueutin et al., 2012). The tubular reabsorption is the passage of a solute from urine to blood (Lacour, 2013) and so the proximal tubule allows a quantitative and qualitative modifications of urine (Callard, 2016). Indeed, the PCT possesses cubic epithelial cells with a lot of mitochondria, which offer the energy supply necessary for their function (Lacour, 2013). A major feature of proximal tubular cells (PTC) is the brush border in the lumen which contains microvilli (Callard, 2016). The different functions of PCT (Figure 3), mentioned above, are: 1) a total absorption for glucose, amino acids and low molecular weight proteins[5]; 2) an almost total reabsorption of bicarbonates and phosphates; 3) the reabsorption of other ions such as Na^+, K^+, Cl^-, Ca^{2+} and water that represent 75 % of filtered quantities, except for the Mg^{2+}, and 4) the secretion of H^+ ions and NH_3 (Lacour, 2013).

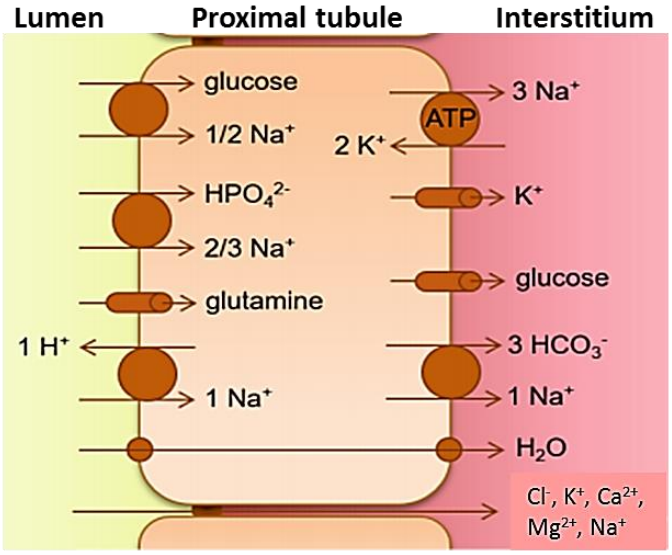

***Figure 3: Schematic illustration of PCT's functions**, based on (Zhuo and Li, 2013).*

II. Aristolochic acid nephropathy

a) History and clinical features

Aristolochic acid nephropathy (AAN) was initially described in the early 1990s in Belgium, when several young women were hospitalized with an interstitial nephritis from unknown origin. Rapidly, their nephritis appeared to be due to the use of slimming pills containing Chinese herbs (Vanherweghem et al., 1993). These patients received pills in which the harmless herb *Stephania tetrandra* was accidentally substituted by *Aristolochia fangchi*, which contains aristolochic acids (AA). Renal biopsies of these patients revealed that their kidneys were shrunk and asymmetric (Figure 4 A). In addition, the cortex was thinner than the cortex of a healthy kidney (Nortier et al., 2015). Histologically, the glomeruli seemed unaffected while an extensive and progressive interstitial fibrosis, mainly located in the cortex, was observed along with atrophy of proximal tubules (Figure 4 B). Additionally, interstitial infiltration by inflammatory cells was reported (Debelle et al., 2008; Jadot et al.,

[5] Such as parathormone, growth factors or β2-microglobulin (Yu et al., 1983)

2017b). Indeed, it was described that proximal tubular epithelial cells (PTEC) constitute the preferential target of AA in kidneys (Debelle et al., 2008).

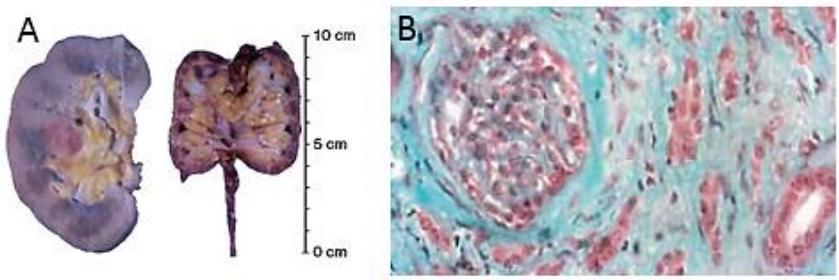

Figure 4: Comparison between a healthy kidney and a kidney intoxicated by AA *(A) (Nortier et al., 2015).* ***Histological representation of kidney from patients with AAN*** *which shows interstitial fibrosis and tubular atrophy (B) (Debelle et al., 2008).*

In addition, other features that support alterations of the kidney function are observed in patients intoxicated with AA. These alterations can be an increase in serum creatinine, a decrease in urinary excretion of neutral endopeptidase (NEP) which is found in brush border of proximal tubule and a proteinuria of low molecular weight proteins. These proteins are β2- and α1-microglobulin, cystatin C, Clara cell protein and retinol binding protein (RBP) (Jadot et al., 2017b; Nortier et al., 2015). Finally, these patients also frequently developed urothelial malignancies (Debelle et al., 2008; Vanherweghem et al., 1993). The abundance of several low molecular weight protein markers (filtered by glomerulus and then completely reabsorbed by proximal tubule where there are degraded) can be followed to assess kidney function alterations (Yu et al., 1983).

The accumulation of α1-microglobulin in urine is an indirect reflect of tubular impairment. This protein (30 kDa), mainly synthetized in liver and kidney, is a lipocalin and can bind small hydrophobic ligand, such as steroids and retinoids. Compared to other protein markers of tubulopathies, the α1-microglobulin possesses the advantages to be stable in urine, even acid, and thus represents a sensitive marker of tubulopathies (Penders and Delanghe, 2004; Yu et al., 1983). This protein exerts several functions such as the inhibition of lymphocyte activation in response to protein antigens, the stimulation of lymphocyte division or the inhibition of neutrophil granulocyte migration *in vitro* (Penders and Delanghe, 2004). A second protein used as a kidney function alteration, the β2-microglobulin (11.8 kDa), is the light chain common to the HLA-A, -B, and -C major histocompatibility complex antigens, and thus, is expressed on the surface of all normal nucleated cells (Bethea and Forman, 1990) and found in most biological fluids, including serum, urine and synovial fluid (Li et al., 2016). A serum elevation of this protein appears in kidney's diseases but also in lymphoid malignancies, some chronic inflammatory or possibly autoimmune conditions (Bethea and Forman, 1990). In kidneys, the dysfunction of glomeruli would cause an increase in blood and a decrease in urine while, in contrast, the dysfunction of tubules would cause an increase in urine and a decrease in blood (Li et al., 2016). A third protein used as a marker is the retinol-binding protein 4 (RBP4) (21 kDa), a lipocalin synthetized by the liver and adipocytes, which can bind molecules such as steroids, bilins, retinoids and some lipids. It transports the vitamin A in the circulation in retinol form, from liver to target tissues (skin, mucosa and retina). It can also serve as a marker to malnutrition, type II diabetes or tubular nephropathy (Biomnis, 2012). The fourth protein used as a marker, the cystatin C (13.2 kDa), is synthetized in a stable rate, not influenced by renal factors (Murty et al., 2013), produced by all investigated nucleated cells (Coll et al., 2000) and widely distributed in human body fluids. It inhibits the activity of lysosomal cysteine proteinases and plays a key role in various diseases. The cystatin C exerts several functions, among which: 1) direct inhibition of

endogenous or exogenous cysteine peptidases; 2) a modulation of the immune system and 3) antibacterial and antiviral activities (Mussap and Plebani, 2004). The last protein, Clara cell protein (15.8 kDa), is produced and secreted by only a few cell types (epithelial cells …). It has the anti-inflammatory property by the inhibition of the phospholipase A_2 (PLA_2) (Jorens et al., 1995; Kabanda et al., 1995).

The presence of these five low molecular weight proteins attests that tubules are injured after AA intoxication. Moreover, 1) low molecular weight proteins/albumin ratio - higher in patients with tubular diseases than in patients with glomerular diseases -, 2) decrease in the urinary level of NEP[6], 3) decrease in the megalin[7] expression, which is in conjunction with the inhibition of receptors-mediated endocytosis of low molecular weight proteins, and 4) transport of AA by organic anion transporter (OAT) - expressed in membranes of PTEC -, indicate PTEC as the main target of AA (Debelle et al., 2008). Indeed, PTEC reabsorb proteins mainly by receptor-mediated endocytosis. That implies 1) the binding to a receptor in the luminal membrane of epithelial cells, 2) the endocytosis of the protein-receptor complex, 3) the catabolism of the protein in lysosomes and 4) the receptor recycling to the luminal membrane (Lebeau et al., 2001). This process of reabsorption involves megalin and cubilin[8] receptors, located both in the brush border of PTEC (Li et al., 2018; Sansoe et al., 2006; Verroust et al., 2000). An exposure of 20 µmol/L of AA on opossum kidney (OK) cells for 24 h decreases the megalin expression (Lebeau et al., 2001). In addition to the proteins mentioned above, several proteins present in brush border have a modified level after an exposure to AA. These proteins are leucine aminopeptidase, N-acetyl-β-D-glucosaminidase and α-glutathione S-transferase. Moreover, PTEC show morphological changes, including the loss of brush border (Lebeau et al., 2005).

b) Balkan-endemic nephropathy or BEN

As already mentioned, AAN has been described in Belgium only in the early 1990s (Vanherweghem et al., 1993). In fact, the true incidence of AAN was and remains largely unknown and probably underestimated due to the use of AA in traditional medicine in Asia and the availability of AA-containing products on Internet. In addition, AA have also been found to be the toxicological agent responsible for the Balkan-endemic nephropathy (BEN). Many people are intoxicating mainly in rural areas of the Balkan countries (Bosnia, Bulgaria, Croatia, Romania and Serbia) by eating contaminated food. In fact, these individuals have a chronic dietary intoxication from bread which is made from wheat flour contaminated with *Aristolochia*. This plant grows in wheat fields of endemic areas and is mixed with wheat grain (Figure 5). BEN, recognized since late 1950s, is characterized by a tubulointerstitial fibrosis, slow progression to end-stage renal disease (for 20 years or more) and urothelial malignancy. In these countries, 25000 people are suffering from BEN and more than 100000 people are at risk. So the impact of AA exposure has a worldwide impact (Debelle et al., 2008; Nortier et al., 2015). However, BEN and AAN, although sharing similar features, present differences mainly in the clinical course. Indeed, AA are ingested in small doses in BEN whereas in AAN induced by slimming pills, AA are ingested in higher doses (0.65 ± 0.56 mg/g of powder in

[6] Membrane-bound Zn-metallo-endopeptidase of the brush border membrane of PTEC, which degrades several peptides (atrial natriuretic peptide or endothelin-1) and produces the vasoconstrictor polypeptide endothelin-1 from circulating precursors (Sansoe et al., 2006)

[7] Megalin, or low-density lipoprotein-related protein-2 (LRP2), is a 600-kDa protein that belongs to the low-density lipoprotein receptor (LDLR) family. It is membrane-anchored ligand highly expressed on the apical surface of PTEC, where it plays an important role in the reabsorption of filtered vitamins and proteins from the glomeruli; it binds and internalizes proteins with a molecular weight lower than albumin, and is implicated in vitamin D uptake (Li et al., 2018)

[8] Cubilin, or receptor for the intrinsic factor-vitamin B12 complex, is a 460-kDa protein that helps the megalin in the reabsorption of proteins and vitamins into PTEC (Verroust et al., 2000)

pills) (Jadot et al., 2017b; Vanherweghem and al., 2003). Still, BEN can be considered as an environmental form of AAN (Jadot et al., 2017b).

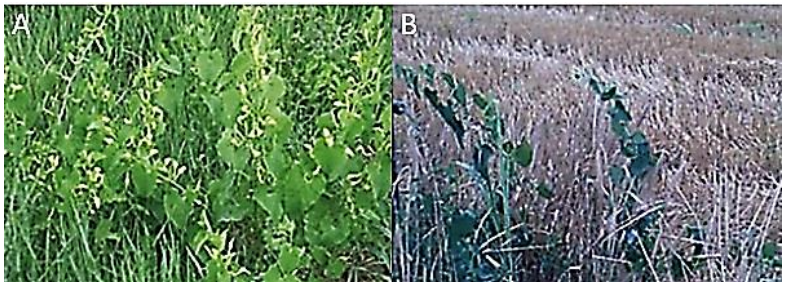

Figure 5: Plants of Aristolochia growing in fields *in Serbia (A) and Croatia (B) (Nortier et al., 2015).*

III. Aristolochic acid

a) Aristolochic acid structure and activity

AA, that plays a major role in kidney toxicity, is composed of a mixture containing AAI (8-methoxy-6-nitro-phenanthro-(3,4-d)-1,3-dioxolo-5-carboxylic acid) and AAII (6-nitro-phenanthro-(3,4-d)-1,3-dioxolo-5-carboxylic acid) which are nitrophenanthrene carboxylic acids (Figure 6) found in the roots and leaves of *Aristolochia* species. Both compounds have similar genotoxic and carcinogenic potential and are both cytotoxic, but only AAI is nephrotoxic (Romanov et al., 2015; Shibutani et al., 2007). Indeed, according to Shibutani and his colleagues, AAI-treatment in C3H/He mice is associated with strong nephrotoxic effects characterized by acute tubular necrosis, extensive cortical interstitial fibrosis, mild interstitial inflammation and occasional tubular apoptosis, compared to control mice. In addition, treatment with AAII only induced a slight acute necrosis without renal interstitial fibrosis (Shibutani et al., 2007). Moreover, levels of AAI-DNA adducts (metabolite that will be explained in the following section) observed in kidneys are more abundant than in other organs such as stomach, spleen or lung. Furthermore, levels of AAII-DNA adducts in non-target tissues (liver, intestine, stomach and lung) are less abundant than those in mice treated with AAI. These results suggested that kidneys are the primary target of AA and that AAI is the chemical species responsible for the nephrotoxic effects of AA. It is due to the presence of an O-methoxy group at position C-8 in the nitrophenanthrene ring, only in AAI. Indeed, its derived-metabolite such as AAIa, generated by demethylation of the O-methoxy group, is not toxic for renal epithelial cells in culture (Shibutani et al., 2007).

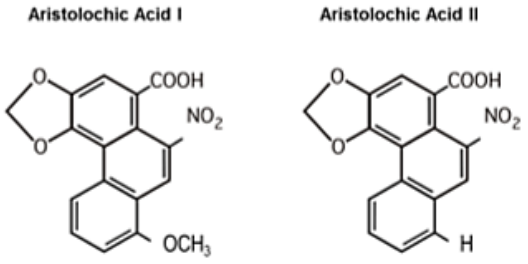

Figure 6: Molecular structure of aristolochic acids I and II. *Formula of the major compounds of the Aristolochia species, aristolochic acid I (AAI) and aristolochic acid II (AAII) (Jadot et al., 2017b).*

b) Aristolochic acid transport and metabolization

After oral ingestion, AA are absorbed from the gastrointestinal tract and distributed throughout the body in a systemic manner. In addition, once in blood circulation, AAI is able to bind to plasma proteins such as albumin (Jadot et al., 2017b). As a consequence of this

binding, AAI cannot be filtered in the glomerulus and goes through the peritubular capillaries. AAI is then transported by organic anion transporters (OAT) 1, OAT2 and OAT3 at the basolateral membrane of PTEC (Jadot et al., 2017b). In fact, the hydrophobic moiety of substrate of OAT1 must be of 4-10 Å and that of AAI is about 7-8 Å (Xue et al., 2011). In addition, AAI competitively inhibits anion transport mediated by OAT1, OAT3 and OAT4, in a dose-dependent manner, and with a stronger effect on OAT1 and OAT3 (Babu et al., 2010; Bakhiya et al., 2009). AAI metabolites are then secreted in the proximal tubular lumen by OAT4 or, hypothetically, by multidrug resistance-associated proteins (MRP) 2 and 4 at the apical membrane. The major metabolites, called the aristolactams, are sequestered inside the cell due to the formation of DNA adducts (Figure 7) (Jadot et al., 2017b). So, OATs contribute to the accumulation of AAI and AAI metabolites in the cells (Bakhiya et al., 2009). However, the role of OATs in an AA nephropathy requests more investigations (Jadot et al., 2017b). It is possible to block the entry of AA in PTEC by triggering the inhibition of OATs by using of probenecid, an OAT inhibitor (Bakhiya et al., 2009; Baudoux et al., 2012). This compound is considered as a renal protective effect as it reduces the histopathologic injuries in mice exposed to AA (Xue et al., 2011). The OATs inhibition leads to a reduction of AA-DNA adduct and a preservation of cell viability, in addition to a reduction in the abundance of proliferating cell nuclear antigen (PCNA), a marker of DNA-damage-repair. However, in response to the inhibition of OAT, it appears that AAI can enter by other endogenous transmembrane transporters or by passive diffusion (Baudoux et al., 2012).

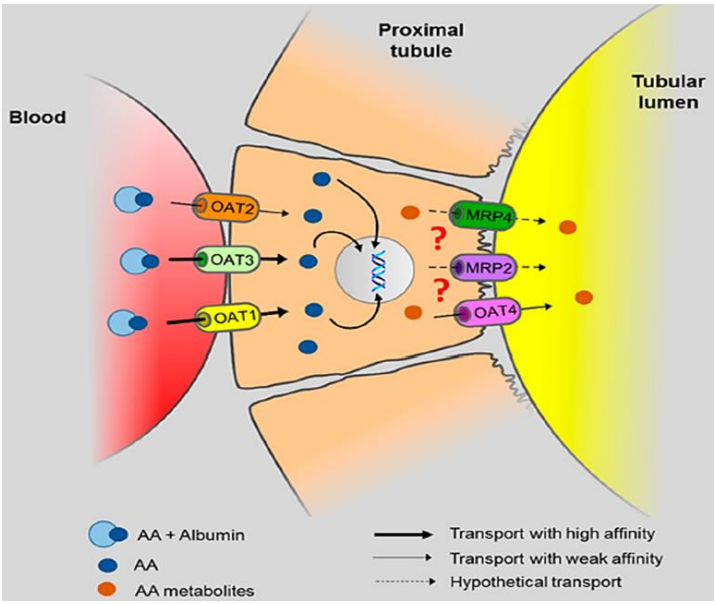

Figure 7: AAI transport in PTEC. *After binding to albumin, AAI is transported through the basolateral membrane via OAT1, OAT2 and OAT3 and then metabolized in aristolactams. The formation of DNA adducts is induced by the binding of AA metabolites to DNA. The metabolites are secreted through the apical membrane via OAT4 and hypothetically via MRP2 and 4 (Jadot et al., 2017b).*

After reduction, AAI is metabolized in N-hydroxyaristolactam I and it is further reduced to cyclic N-acylnitrenium ions, to 7-hydroxyaristolactam I or to aristolactam I, the major metabolite of AAI. The nitrenium ion displays a delocalized positive charge able to bind to the exocyclic amino groups of purine bases and, ultimately, to form AA-DNA adducts (Stiborova et al., 2017). DNA adducts induce DNA damage with severe nuclear alterations, cell cycle arrest and apoptosis and may lead to urothelial malignancies, carcinoma and upper urinary tract cancers (Li et al., 2006; Shibutani et al., 2007). They are detected by high-performance liquid chromatography coupled with mass spectrometry (Yuan

et al., 2009), by ^{32}P-postlabelling technique or with rabbit monoclonal anti-AL adduct antibodies (Chang et al., 2017; Shibutani et al., 2007). They can thus be used as biomarkers after exposure to AA (Jadot et al., 2017b; Nortier et al., 2015; Schmeiser et al., 1996; Stiborova et al., 2017).

Several enzymes are critical in AA metabolism (Figure 8). The major enzymes for the oxidation of AAI are the human cytochrome P450 (CYP) enzymes CYP1A1 and 1A2. Other enzymes (CYP2C, CYP3A…) can act but with less efficiency due to their lower affinity for AAI. Some enzymes are implicated in the reduction of AAI. The major reductase is the cytosolic NAD(P)H:quinone oxidoreductase (NQO1). In addition, it has been shown in human kidney (HK)-2 cells that sulfotransferase SULT1A1 potentiates the activation of AAI and N-hydroxyaristolactam I even if, in others studies, SULT has no action on the bioactivation of AAI or AAII. A third enzyme, the NADPH:CYP oxidoreductase (POR) interacts in the reduction of AAI on a minor manner. CYPs have two actions: they reduce AAI and AAII and, in addition, they oxidize AAI. The fact that CYP1A1 and CYP1A2 act as oxidant and reductive enzymes is important, because a balance between detoxification and activation reactions of AAI is a critical determinant in the development of AAN or BEN. Additionally, several endogenous factors might also contribute to disease development such as the expression levels and activities of biotransformation enzymes dependent on their basal expression, regulation, induction and/or inhibition. Other factors are the genetic and phenotypic polymorphisms of these enzymes (Stiborova et al., 2017).

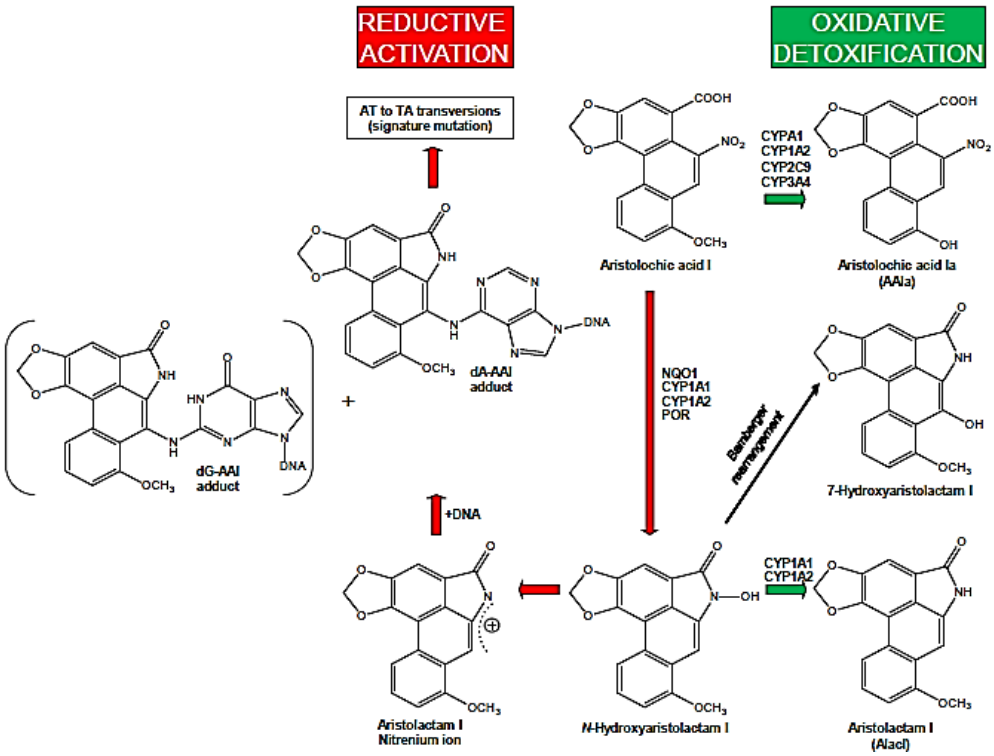

Figure 8: Metabolism of AAI. *There are two pathways for AAI metabolism: the activation or the detoxification. Formation of N-hydroxyaristolactam I is mediated by reduction of AAI and this metabolite is either further reduced to aristolactam I (the major metabolite of AAI) or rearranged to 7-hydroxyaristolactam I. In addition, AAIa is formed through O-demethylation of AAI. CYP: hepatic microsomal cytochrome P450, NQO1: hepatic and renal cytosolic NAD(P)H:quinone oxidoreductase, POR: kidney microsomal NADPH:CYP oxidoreductase (Stiborova et al., 2017).*

c) Aristolochic acid effects

AA can induce inflammation by the decrease in the protein phosphatase magnesium-dependent 1A (PPM1A) expression, which leads to the enhanced phosphorylation of IKKβ

and activation of inflammatory genes driven by nuclear factor-kappa B (NF-κB) transcription factor (Sun et al., 2009). PPM1A, an IKKβ phosphatase (subunit of activated IκB kinase), can dephosphorylate IKKβ at Ser177 and Ser181 (essential for activation of IKKβ by tumour-necrosis factor alpha - TNF-α) and terminate IKKβ-mediated NF-κB activation. After phosphorylation and activation of IKKβ by TNF-α, IKKβ binds to PPM1A, but when the expression of PPM1A is reduced, this binding does not happen (Sun et al., 2009). However, AA are also known as anti-inflammatory compounds in traditional medicine in Asia (Chen et al., 2010). On the one hand, AAI inhibits PLA_2 activity in human neutrophils. But on the other hand, a daily treatment of male Wistar rats with AA leads to massive interstitial inflammation. The use of AAI induces a decrease in the DNA-binding activity of NF-κB by an inhibition of the phosphorylation of IκBα, an inhibitor of NF-κB. Overall suggests that AAI prevents NF-κB activation by blocking IκBα phosphorylation (Liu et al., 2011).

It was also reported that AAI causes mitochondrial alterations. Mitochondria are involved in several essential cellular functions such as cell cycle, growth, differentiation and death. The organelle, providing ~90 % of cellular ATP by oxidative phosphorylation (OxPHOS), is a significant source of reactive oxygen species (ROS), which, produced in excess, can lead to mitochondrial dysfunction, disruption and cell death. Mitochondria are composed of: 1) the outer membrane, permeable barrier to metabolites and small peptides (< 5000 Da) and with a similar composition to the plasma membrane, 2) the inner membrane, electrical insulator (Benigni et al., 2016), 3) an intermembrane space, which separate the both membranes and whom the composition is similar to the cytosol and 4) the matrix, the site of the tricarboxylic acid/Krebs cycle (Cooper, 2000). The structure and function of mitochondria are perpetually remodelled in response to metabolic changes and are controlled by fusion, fission, motility and morphological process. These changes refer to mitochondrial dynamics and help to maintain mitochondrial functional integrity. Fusion is mediated by mitofusin (Mfn) 1 and 2 for the outer membrane and optic atrophy protein 1 (OPA-1) for the inner membrane. While fission is mediated by cytosolic dynamin-related protein (Drp) 1 and its outer membrane receptors (mitochondrial fission factor (Mff), fission 1 (Fis1) and the 49 and 51 kDa mitochondrial dynamics proteins (MiD49-51)) (Figure 9) (Benigni et al., 2016).

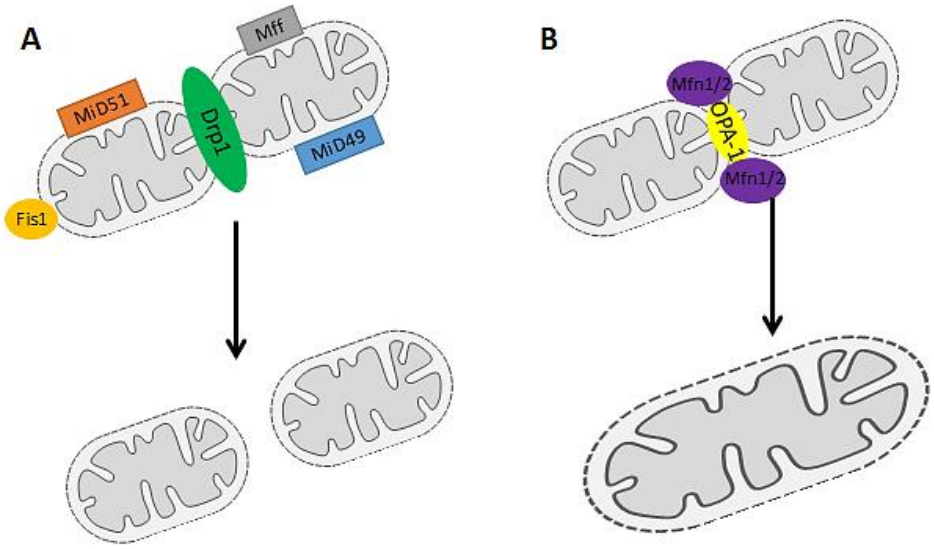

Figure 9: Mitochondrial dynamics. *Mitochondrial fission (A) and mitochondrial fusion (B). Drp1, dynamin-related protein 1; Fis1, fission 1; Mff, mitochondrial fission factor; MiD49 and MiD51, mitochondrial dynamics proteins of 49 and 51 kDa; Mfn1/2, mitofusin 1 and 2; OPA1, optic atrophy protein 1.*

As PTEC possess number of mitochondria, these cells are much vulnerable to mitochondrial dysfunction. The impairments that AAI can induce: 1) mitochondrial swelling,

2) leakage of Ca^{2+}, 3) membrane depolarisation and 4) release of cytochrome c from kidney mitochondria. In addition, rats intoxicated with 5 mg/kg/day have proximal tubular enlarged, dysmorphic mitochondria, mitochondrial swelling and small vacuoles. The degradation and the decrease in the number of mitochondria are proportional to the AAI concentration used (Jiang et al., 2013). The ATP content also decreases in response to AA exposure in a concentration-dependent manner and a depletion of mitochondrial DNA (mtDNA) can also be observed (Jiang et al., 2013). Nuclear DNA (nDNA) is less susceptible to damage induced by AAI than mtDNA, due to the absence of efficient DNA repair mechanisms in mitochondria and the lack of protective histones in mtDNA (Jiang et al., 2013; Tabara et al., 2014). Moreover, with an exposure of 5 µM of AAI for 24 h, a decrease in the cellular content of ATP is observed in HK-2 cells (Qi et al., 2007). Finally, to accompanied these mitochondrial modifications, the production of ROS is increased (Shui et al., 2017).

AA also play a role in fibrosis. Indeed, in the HK-2 cells exposed to AA, the expression of phosphatase and tensin homolog (PTEN), which interacts with PPM1A[9] by stabilizing its expression, is reduced. This reduction of PTEN expression induces three reactions: 1) a reduction of total PPM1A expression, 2) a decrease in nuclear PPM1A levels and 3) an increase in PPM1A in the cytosolic fraction. Finally, the TGF-β1/Smad3 signalling is activated after an increase in Smad2/3 phosphorylation (Figure 10). There is then the association of Smad2/3 with Smad4 and an increase in Smad2 accumulation in the nucleus as well as the enhancement of the production of fibrotic factors (Figure 10) (Lin et al., 2006; Samarakoon et al., 2016).

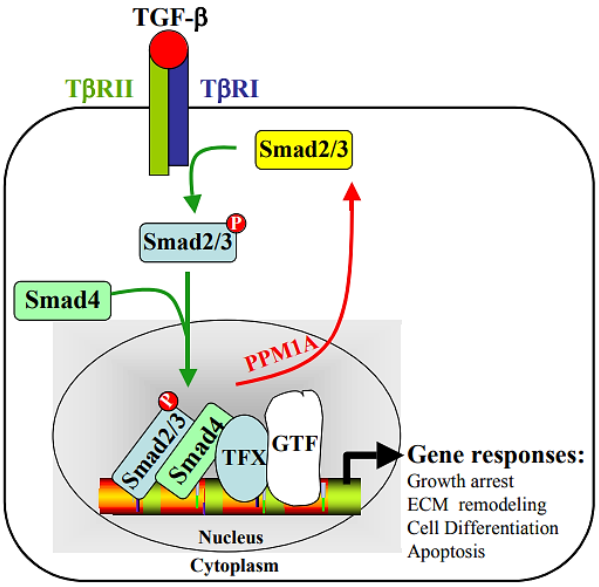

Figure 10: Schematic representation of role of PPM1A on the TGF-β1 signalling. *Phosphorylation of Smad2/3 is essential for the association with Smad4 and the nuclear import. PPM1A binds to phosphorylated Smad2/3, promoting the dissociation of the Smad2/3-Smad4 complex and so facilities nuclear export of Smad2/3. TβRI, type I TGF-β receptor; TβRII, type II TGF-β receptor; TFX, hypothetical DNA-binding cofactor for Smads; GTF, general transcription machinery (Lin et al., 2006).*

As regards oxidative stress, it has been shown that AAI-intoxication induces glutathione (GSH) depletion in rats. A hypothesis is that rat organic anion transporter (OAT) serves as a bidirectional transporter for the organic anion/GSH exchange (Yu et al., 2011).

[9] Monomer located in cytosol, cytoplasmic vesicle, nucleus and membrane, which binds 2 magnesium or manganese ions per subunit. This protein is member of the PP2C family of serine/threonine protein phosphatases, which is known to be negative regulators of cell stress response pathways (websites of antibodies-online and uniprot)

At the present time, sirtuins expression and activity in response to AA exposure as well as the mechanism triggered by these proteins to reduce cytotoxicity and nephrotoxicity remain poorly investigated.

IV. Sirtuins

a) Structure, function and catalysed activities

Sirtuins are a well-conserved evolutionary family of nicotinamide adenine dinucleotide (NAD+)-dependent enzymes with deacetylase, mono-ADP-ribosyltransferase, demalonylase or desuccinylase activity (Houtkooper et al., 2012; Nogueiras et al., 2012; Polak-Jonkisz et al., 2013). Sirtuins target histones and non-histone proteins, among which transcription factors (nuclear factor-kappa B - NF-κB, or peroxisome proliferator-activated receptor-γ - PPARϒ), metabolic enzymes (glutamate dehydrogenase - GDH, or acetyl-CoA-synthase - AceCSs) and antioxidant enzymes (isocitrate dehydrogenase 2 - IDH2, or superoxide dismutase 2 - SOD2) (Nogueiras et al., 2012; Yu and Auwerx, 2009). As sirtuins activities are dependent of NAD^+ concentrations, they are called "cellular energy sensors" which directly link them to metabolism (Nogueiras et al., 2012). As represented in Figure 11, sirtuins deacetylate proteins or enzymes in the presence of NAD^+ used as a co-substrate. First, sirtuins catalyse the cleavage of NAD^+, producing nicotinamide (NAM) and 2'-O-acetyl-ADP-ribose. NAM is then regenerated into NAD^+ thanks to several enzymes (Kupis et al., 2016).

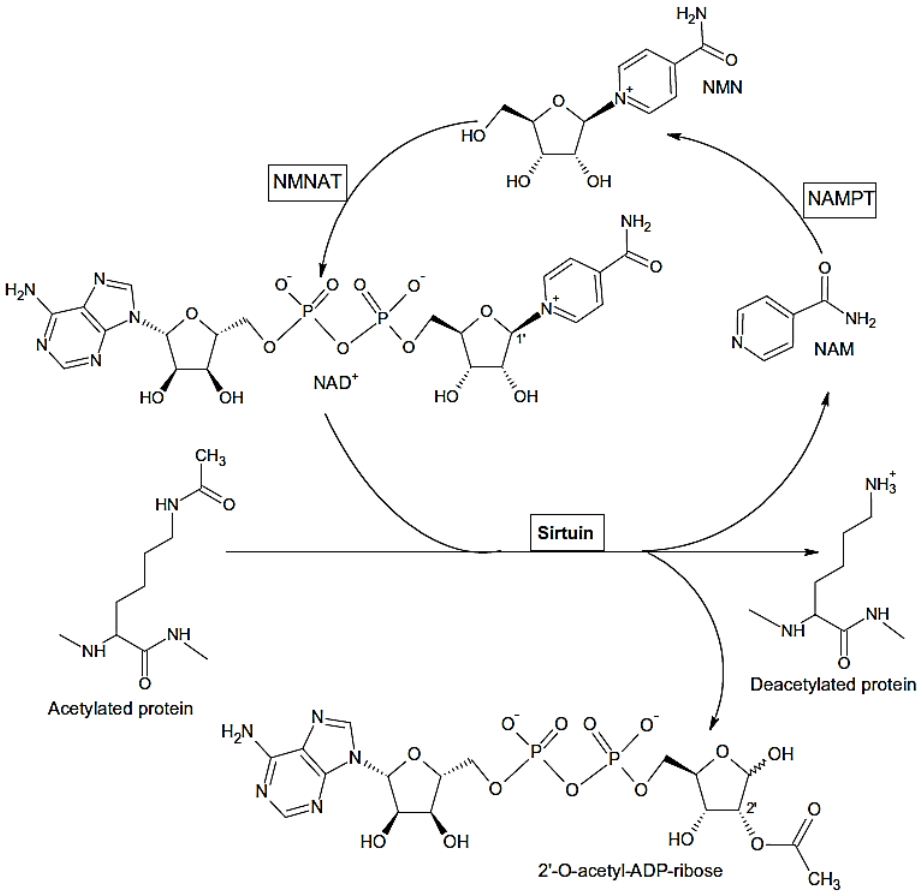

Figure 11: Deacetylation mechanism of sirtuins *(Kupis et al., 2016).*

Mammals possess seven sirtuins (SIRT1-7) sharing a conserved catalytic domain, flanked by the N- and C-terminal sequences of variable length (Carafa et al., 2012). These sequences

are the targets for post-translational modifications affecting the functions and/or the activity of sirtuins (Figure 12) (Carafa et al., 2012; Yamamoto et al., 2007).

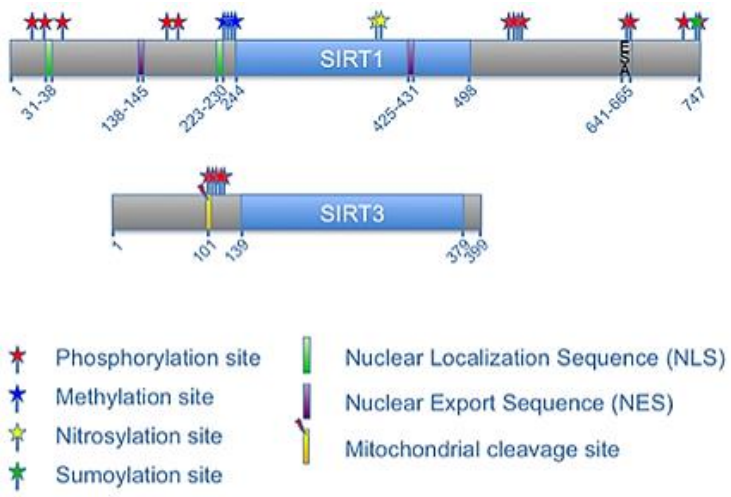

Figure 12: Post-translational modifications of SIRT1 and SIRT3. *Blue boxes, catalytic core domain; grey boxes, N- and C-terminal sequences; ESA, essential for SIRT1 activity. Modified from (Flick and Luscher, 2012).*

However, these proteins are localized in different subcellular compartments and have different functions (Carafa et al., 2012; Yamamoto et al., 2007). The eukaryotic sirtuins were divided into four phylogenetic categories: SIRT1, SIRT2 and SIRT3 composing the class I (deacetylase), SIRT4 constituting the class II (ADP-ribosyltransferase), SIRT5 for the class III (deacetylase, demalonylase or desuccinylase) and, finally, SIRT6 and SIRT7 as the class IV (deacetylase/ADP-ribosyltransferase and deacetylase, respectively). SIRT 1, 6 and 7 are nuclear, SIRT2 is cytosolic and SIRT 3, 4 and 5 are mainly localized into mitochondria (Carafa et al., 2012; Houtkooper et al., 2012).

Protein	Class	Localization	Function(s)
SIRT1	I	Nucleus	Deacetylase
SIRT2	I	Cytosol	Deacetylase
SIRT3	I	Mitochondria	Deacetylase
SIRT4	II	Mitochondria	ADP-ribosyltransferase
SIRT5	III	Mitochondria	Deacetylase/ demalonylase/ desuccinylase
SIRT6	IV	Nucleus	Deacetylase/ ADP-ribosyltransferase
SIRT7	IV	Nucleus	Deacetylase

Figure 13: Summary of classes of sirtuins *(Carafa et al., 2012; Houtkooper et al., 2012).*

b) Sirtuins 1 and 3 regulation

The regulation of SIRT1 expression and activity is complex. Firstly, the gene promoter is positively and negatively regulated by the binding of various transcription factors. Hypermethylated in cancer 1 (H1C1) is a transcriptional repressor and the repression is mediated by carboxy-terminal-binding protein (CtBP) which is also a transcriptional repressor. E2 promoter binding factor 1 (E2F1) is a positive regulator of SIRT1 and p53 is a negative regulator. Finally, FOXO3a inhibits the suppressive action of p53 (Figure 14)

(Zschoernig and Mahlknecht, 2008). The acetylation and activity of these factors are in turn controlled by SIRT1. Secondly, the SIRT1 mRNA is regulated by the RNA binding protein HuR and miR-34A, a p53-regulated microRNA. Thirdly, SIRT1 protein activity is regulated positively and negatively by interacting proteins (active regulator of SIRT1 - AROS, and deleted in breast cancer 1 - DBC1) and by NAD^+/NADH ratio (Figure 14) (Finkel et al., 2009; Houtkooper et al., 2012).

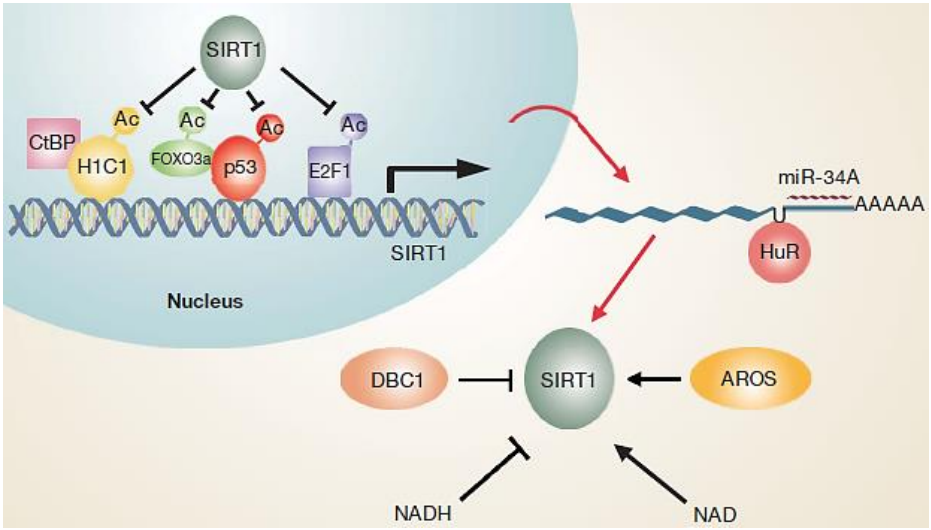

Figure 14: Regulation of SIRT1 activity *(Finkel et al., 2009).*

The expression of SIRT3 is activated by estrogen-related receptor-α (ERRα). In addition to ERRα that binds to SIRT3 promoter, peroxisome proliferator-activated receptor γ coactivator-1 alpha (PGC-1α) binds the transcription factor (co-activator) and controls the expression of genes involved in the biogenesis of mitochondria, brown adipose tissue development and function (Houtkooper et al., 2012). A major function of PGC-1α is the detoxification of ROS which are generated during the mitochondrial respiration. PGC-1α controls the removal of ROS by the regulation of the expression of several enzymes of detoxification such as SOD2. In addition, PGC-1α increases the expression of the transcription factors nuclear respiratory factors (NRF), which regulate the expression of several mitochondrial genes. For example, PGC-1α actives NRF1 in order to regulate the expression of transcription factor A mitochondrial (TFAM), which is responsible for the transcription and replication of mitochondrial genes from the mitochondrial genome (Austin and St-Pierre, 2012).

c) Sirtuins 1 and 3 functions

SIRT1 deacetylates target proteins involved in several cellular processes such as cell cycle, mitochondrial biogenesis, metabolism, inflammation, fibrosis and adaptation to cellular stress (Kitada et al., 2013; Nogueiras et al., 2012).

The activation of SIRT1 prevents renal fibrosis, that may be caused by AA, in response to the deacetylation of Smad3 (that inhibits the activity of the transforming growth factor beta 1 (TGF-β1)) inhibiting the cell signalling triggered by this transcription factor. The TGF-β1 is a cytokine known to positively control the expression of genes encoding collagen IV and fibronectin contributing, after deposition, to fibrosis (Kitada et al., 2013), a major characteristic of chronic kidney injury (Jadot et al., 2017b).

Furthermore, SIRT1 was shown to be protective against oxidative stress, a process mediated, for example, by the deacetylation and activation of hypoxia-inducible factor-2 alpha (HIF-2α), by the deacetylation of peroxisome proliferator-activated receptor γ

coactivator-1 alpha (PGC-1α) or by the activation of FOXOs factors. For example, they induce the antioxidative response triggered by catalase or superoxide dismutase 2 (SOD2) (Nogueiras et al., 2012).

SIRT1 was also described as protective against inflammation. For example, SIRT1 deacetylates the p65 subunit of the transcription factor NF-κB leading to its inhibition and a reduced expression of several pro-inflammatory genes encoding cytokines such as interleukin 1 beta (IL-1β), interleukin 6 (IL-6) and tumour-necrosis factor alpha (TNF-α) (Kitada et al., 2013).

The human SIRT3 protein is found in both long and short isoforms and present in mitochondria (short isoform) or nuclei (long isoform). In addition, three isoforms of SIRT3 were reported in mice; the first and the second one possess a nuclear localization while the third one is located into mitochondria (Cooper et al., 2009). These enzymes mainly regulate mitochondrial energy metabolism and redox status, more specifically in response to stress and are thus an adaptive regulator of several cells and mitochondrial responses (Nogueiras et al., 2012).

It is known that SIRT3 controls mitochondrial dynamics and degradation. Indeed, it inhibits the Drp1-dependent fission and by upregulation of OPA-1, by preventing the loss of membrane potential and PTEN-induced putative kinase 1–related (PINK1-related) mitophagy (Morigi et al., 2015; Perico et al., 2016). It allows a protection against mitochondrial fragmentation and cell death. SIRT3 also maintains basal ATP levels by a dual mechanism: 1) prevention of excessive electron leakage and so oppose to the increase in ROS generation by the regulation of the function of the electron transport chain (ETC) complexes I and III; 2) ROS detoxification by the activation of mitochondrial antioxidant enzymes (SOD2 or IDH2) (Benigni et al., 2016). Indeed, an elevated expression and activation of SIRT3 result in a reduction of oxidative stress following SOD2 activation by deacetylation. In addition, IDH2 enzyme is activated by deacetylation. Its activation leads to the catalysis of isocitrate in α-ketoglutarate, producing NADPH, an important redox equivalent required for GSH regeneration from oxidized glutathione (GSSG) (Kincaid and Bossy-Wetzel, 2013). The SIRT3 activation induces an increase of GSH/GSSG ratio and so, a decrease of oxidative stress (Ouyang et al., 2019).

These different roles of sirtuins 1 and 3 (SIRT 1 and 3), under oxidative stress or mitochondrial injury, are relevant. Indeed, accumulation of ROS and mitochondrial impairment were reported during AA-intoxication of rats, in particular in proximal tubular epithelial cells, the preferential cells targeted by AA (Figure 15) (Debelle et al., 2008; Galvan et al., 2017; Jadot et al., 2017b; Nortier et al., 2015).

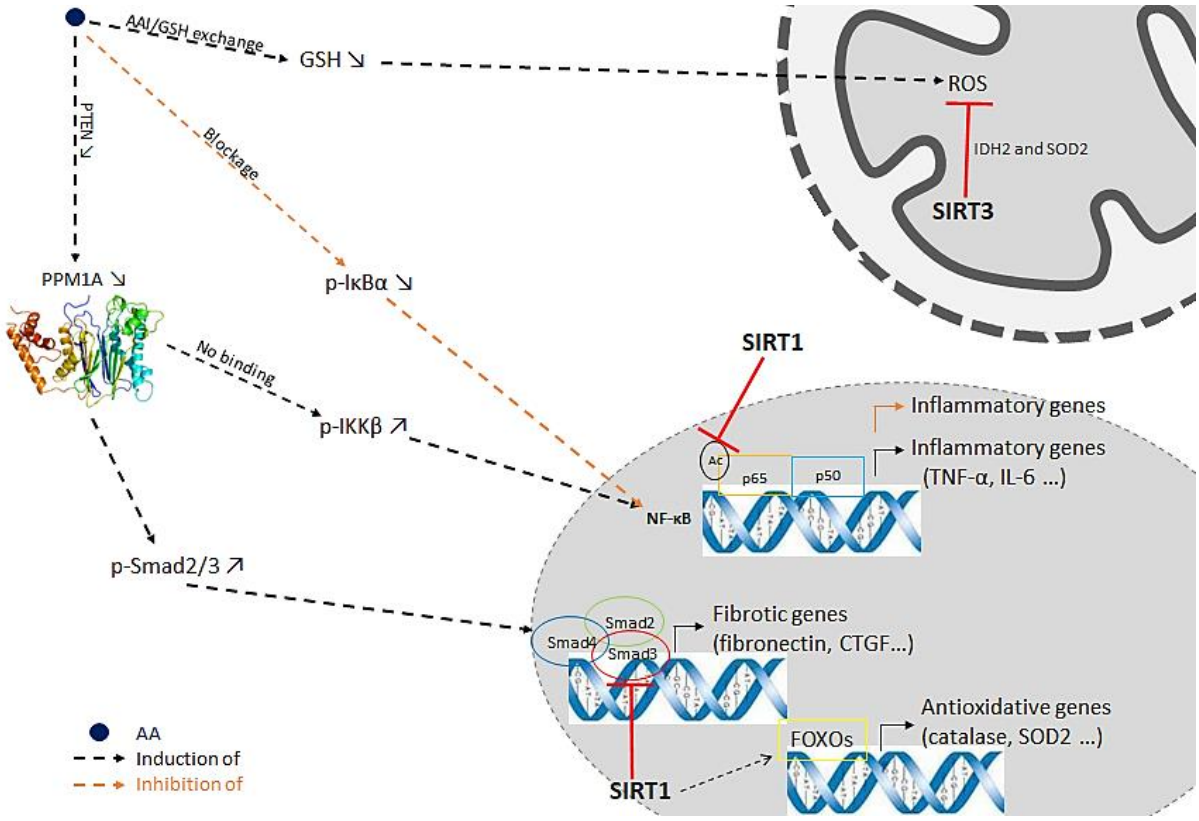

Figure 15: Schematic illustration of putative roles of SIRT 1 and 3 in a context of oxidative stress, inflammation or fibrosis induced by AA*. AAI, aristolochic acid I; CTGF, Connective tissue growth factor; ERK1/2, extracellular signal-regulated kinase 1/2; FOXOs, forkhead transcription factor; GSH, glutathione; IDH2, isocitrate dehydrogenase 2; IKKβ, subunit of IκB kinase; IL-6, interleukin-6; NF- κB, Nuclear factor-kappa B; p, phosphorylated; PPM1A, phosphatase magnesium-dependent 1A; PTEN, Phosphatase and Tensin homolog; ROS, reactive oxygen species; SOD2, superoxide dismutase 2; TNF-α, Tumour-necrosis factor alpha.*

V. Cell line used in this master thesis

We used HK-2 cells for experiments, which are proximal tubular cells from normal adult human kidney, immortalized by HPV-16 E6/E7 genes in order to retain relatively normal phenotypic expression. Due to the characteristics of primary proximal tubular cells (PTC) - inability to survive serial passages, variability amongst sequential PTC preparations and laborious isolation -, we chose HK-2 cells. Indeed, these cells display the same characteristics than PTC namely: 1) typical brush border membrane-associated enzymes, 2) recognition by antibodies directed against cytokeratin, vimentin, fibronectin and α3β1 integrin, 3) same functional characteristics of *in vivo* proximal tubules and primary PTC cultures, 4) maintenance in glucose-free medium, and 5) ability to ensure gluconeogenesis (Ryan et al., 1994). These five features indicate a proximal tubular origin and phenotype, intact transport mechanisms and an ability to produce and store glycogen. HK-2 cells have also an EGF-dependent anchorage showing an immortalized cell line, besides the fact that these cells are a major advantage relative to animal or human embryonic-derived cell lines (Ryan et al., 1994).

VI. Previous work

Previous work in our laboratory (Mosseray, 2018) used toxic concentrations (10, 25, 50, 75 and 100 µM) of AAI *in vitro* on HK-2 cells and *in vivo* on C57Bl/6 mice (3.5 mg/kg).

Previous data has shown that AAI impairs renal function as demonstrated by an increase in proteinuria, a disorganization of the proximal tubular epithelial cells' (PTEC) brush border or a necrosis of the proximal tubules in mice. *In vivo*, the expression of SIRT1 was reported as oscillating with a decrease after 12, 48, 96 h or 10 days whereas the expression of SIRT3 was decreased after 12 hours of exposure to AAI.

In vitro, a concentration-dependent decrease in the cell viability was observed and the highly toxic concentration of 50 µM was chosen to study the toxic effect of AAI. In this previous work, mitochondrial fragmentation in HK-2 cells was observed (Figure 16). At that high concentration, preliminary data revealed that the relative mRNA expression of *SIRT1* was increased after 12 h of cell incubation with AAI while the relative mRNA abundance of *SIRT3* was increased after 24 h of treatment.

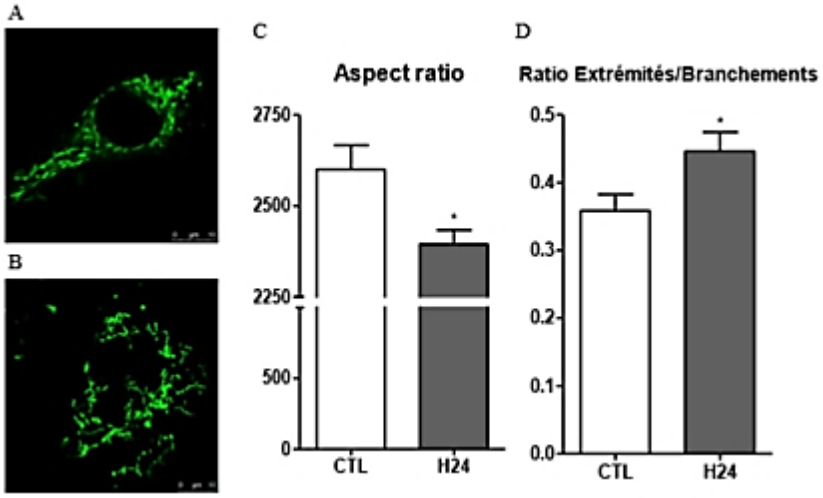

Figure 16: Mitochondrial morphology *visualized by confocal microscopy on control cells (A) and cells incubated for 24 h with 50 µM of AAI (B). Aspect ratio (C) and ratio between end points and branched points (D). Data are expressed as means ± SEM, 30 cells analysed per group. Statistical analyses were performed using a t-Student test. *p≤0.05 vs control group. Pauline Mosseray data (Mosseray, 2018).*

However, the analysis of gene expression modifications in a context of cell toxicity and cell death is difficult and generated results which might be contaminated by confounding factors other than the effects of the molecule of interest.

VII. Goal of the current work

The main goal of this work is to study the putative role of sirtuins (SIRT) 1 and 3 (SIRT1 and 3) in cytotoxicity induced by AAI.

SIRT3 has already been studied in a model of sepsis-induced acute kidney injury (AKI) triggered by the ligation of the caecum at the colon juncture followed by puncturing or a lacing to the abdomen (Zhao et al., 2016). The authors highlighted that SIRT3 exerted protective effects against mitochondrial damage in the kidney as evidenced by a decrease in mitochondrial abundance and an increase in the mitochondrial permeability transition pore when the enzyme is less active (Zhao et al., 2016). In addition, the overexpression of SIRT3 protected mice in a cisplatin-induced AKI model, a protective effect mediated by the enhancement of mitochondrial dynamics (Morigi et al., 2015). SIRT1 was also reported as

protective against oxidative stress triggered by ischemia-reperfusion in C57Bl/6 mice (Hasegawa et al., 2010). These different studies suggest protective effects of these sirtuins during AKI. However, sirtuins expression and activity in response to AA exposure as well as the mechanism triggered by these proteins to reduce cytotoxicity and nephrotoxicity remain poorly investigated.

In this regard, the major objectives of the present study are: 1) to determine the optimal concentration and incubation time of HK-2 cells with AAI that are minimizing the toxicity, 2) to measure the ATP content after AAI treatment and 3) to test an interferential approach using inhibitors and activators of SIRT1 and SIRT3 on the AAI-induced toxicity in HK-2 cells. These experiments have been performed in order to test the modulation of enzyme activity on AAI-induced cell toxicity.

Material and methods

I. Cell culture

Human kidney-2 (HK-2) cells are proximal tubular epithelial cells obtained from normal adult human kidney, and immortalized by human papillomavirus-16 (HPV-16). HK-2 cells were obtained from American Type Cell Collection (ATCC CRL-2190TM, Belgium) and cultured in "Keratinocyte serum-free medium" (K-SFM/ThermoFisher Scientific, USA) supplied with bovine pituitary extract (BPE – 0.05 mg/mL) and human recombinant epidermal growth factor (EGF – 5 ng/mL) as recommended by manufacturer (Ryan et al., 1994). For cell culture maintenance, cells were incubated in T75 culture flasks (75 cm^2) (Corning-Costar®, USA) in a humidified atmosphere maintained at 37 °C and 5 % of CO_2. When routinely cultured, cells were diluted 1:2 to obtain 80 % of cell culture confluence every three days. For the different experiments, cells were incubated in T25 culture flasks (25 cm^2) (Corning-Costar®, USA) at the density of 1.25 $x10^6$ cells/flask or in 24-well culture dishes (Corning-Costar®, USA) at the density of 100000 cells/well.

II. Cell incubation with aristolochic acid I

A stock solution of AAI was made by diluting AAI powder (Sigma-Aldrich, USA) in dimethylsulfoxide (DMSO, Sigma-Aldrich, USA) to obtain a concentration of 15 mM. To allow the solubilisation of AAI in DMSO, the solution was heated at 60 °C in a water bath for 30 min, vortexed every 10 min and sterilized with a 0.2 µm Filtropur filter (Sarstedt, The Netherlands). The stock solution was stored at room temperature for one month and protected from light. Cells were incubated with freshly prepared sterile K-SFM media containing different concentrations of AAI (0.1, 0.25, 0.5, 0.75, 1, 2.5, 5, 7.5, 10, 20, 30, 40 or 50 µM).

III. Cell viability assays

a) Cell seeding

HK-2 cells were seeded into 24-well culture dishes (Corning-Costar®, USA) at the density of 100000 cells/well. The next day and depending the experiment performed (as indicated in the legend of the figures), cells were incubated with fresh culture media containing AAI at 0, 0.1, 0.25, 0.5, 0.75 or 1 µM for 12, 24, 48 or 72 h (with or without medium change every 24 h), or at 0, 1, 2.5, 5, 7.5, 10 or 50 µM during 12, 24, 48 or 72 h. In several experiments, the concentration of 10 µM was used as a positive control able to induce toxicity. Then, MTT (3-[4,5-dimethylthiazol-2-yl]-2,5 diphenyl tetrazolium bromide) and LDH (lactate dehydrogenase) assays were performed to assess cell viability/cytotoxicity.

b) MTT assay

The MTT assay was performed to assess cell viability (van Meerloo et al., 2011). This assay is based on the activity of the succinate dehydrogenase (SDH), a mitochondrial enzyme that catalyses the oxidation of succinate to fumarate in the Krebs/citric acid cycle in the mitochondrial matrix and transfers electrons to ubiquinone without pumping protons across the mitochondrial inner membrane (Huang and Millar, 2013). First, cells were seeded into 24-well culture dishes (Corning-Costar®, USA) at the density of 100000 cells/well. Then cells were incubated with fresh culture media containing AAI at 0, 0.1, 0.25, 0.5, 0.75 or 1 µM for 12, 24, 48 or 72 h (with or without medium change every 24 h). At the end of the incubation time, culture media were replaced by a PBS buffer containing MTT (Sigma-

Aldrich, USA) diluted at 2.5 mg/mL mixed with K-SFM medium 1:1 (v:v) for a 2 h-incubation period at 37 °C in a humidified atmosphere. This step allows SDH of active metabolic cells to reduce MTT in formazan, forming purple crystals in aqueous medium. The MTT solution was then removed and 500 µL of lysis buffer (30 % sodium dodecyl sulfate (SDS), Fisher, USA, diluted in distilled water; N,N-dimethyl-formamide 2:1 (v:v), Rooth, France; pH 4.7) were added. Samples were placed on a rotary plate for 1 h at 37 °C. Finally, absorbance was measured at 570 nm in a spectrophotometer (xMark™ Microplate, BioRad, Belgium) to determine the quantity of reduced MTT and thus, estimate cell viability.

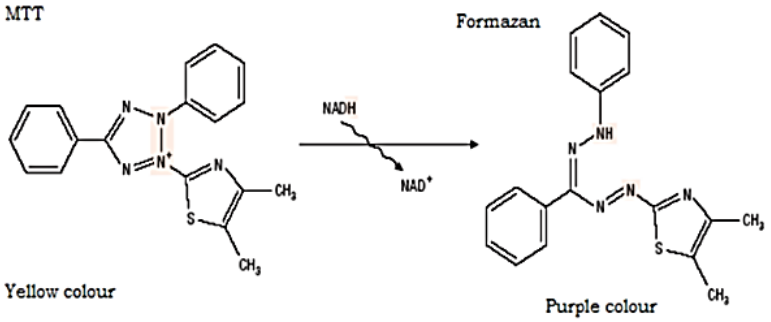

Figure 17: Principle of MTT assay and reaction catalysed by the SDH *(Prakash, 2011).*

Results were calculated with the following formula:

$$\text{Cell viability (\%)} = \frac{(sample\ test\ absorbance - blank)}{(control\ cell\ absorbance - blank)} \times 100$$

In this work, the MTT assay was also used to assess cell proliferation and results were calculated with the following formula:

$$\text{Absorbance} = \frac{(sample\ test\ absorbance - blank)}{(control\ cell\ absorbance - blank)}$$

The blank represents the measure of the lysis buffer absorbance and the control cell absorbance represent the measure of cells which are not treated with AAI.

c) LDH assay

A LDH assay was used to assess cytotoxicity of AAI by measuring the release of the intracellular enzyme LDH. An increase in LDH release is a marker of cell damage (defect of the integrity/permeability of the plasma membrane) (Abe and Matsuki, 2000; Allen et al., 1994). In this assay, released LDH by damaged cells reduces NAD^+ in NADH + H^+. Then NADH reduces tetrazolium salt to formazan in the presence of electron coupling agents (Abe and Matsuki, 2000).

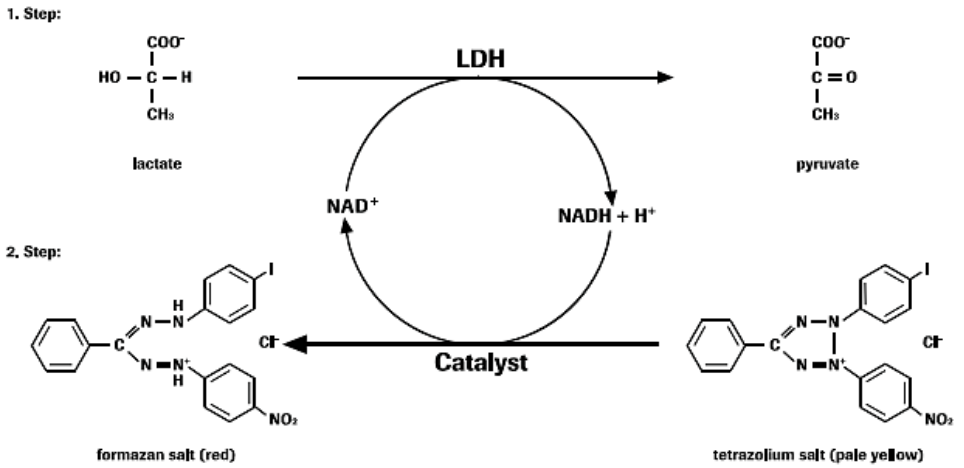

Figure 18: Principle of LDH assay *(Cytotoxicity Detection Kit, Roche, USA).*

First, cells were seeded into 24-well culture dishes (Corning-Costar®, USA) at the density of 100000 cells/well. Then cells were incubated with fresh culture media containing AAI at 0, 0.1, 0.25, 0.5, 0.75 or 1 µM for 12, 24, 48 or 72 h (with or without medium change every 24 h). Positive control cells were obtained with cells incubated with PBS containing 2 % Triton X-100 for 1 h in order to release the maximum of LDH. At the end of the incubation time, supernatants, or also named centrifuged conditioned-culture media, were collected and centrifuged for 5 min at 0.4 g. Next, a volume of 250 µL of PBS containing 2 % Triton X-100 was added for 10 min on the adherent cell monolayers (on agitation) (then called lysates) to permeabilize the cells. Conditioned-culture media and cell lysates were collected separately. Cell pellets, obtained after centrifugation (0.4 g) of cell conditioned-culture media, were also lysed in 250 µL of PBS containing 2 % Triton X-100 for 10 min. Samples were placed into 96-well microplate (Greiner Bio-One, Germany) in the following way:

- 100 µL of centrifuged conditioned-culture media, or
- 100 µL of cell lysates recovered cell pellets, or
- 5 µL of cell lysates and 95 µL of PBS containing 2 % Triton X-100, or
- 100 µL of K-SFM medium (blank for conditioned-culture media from control cells),
- 100 µL of K-SFM added each AA concentration (blank for conditioned culture media for AA-incubated cells),
- 100 µL of PBS containing 2 % Triton X-100 (blank for cell pellets and cell lysates).

Next, 100 µL of the reaction mixture (Cytotoxicity Detection Kit (LDH), Roche, USA) were added. Finally, the absorbance was measured in a spectrophotometer (xMark™ Microplate, BioRad, Belgium) (490 nm – sample – and 655 nm – reference –) every 5 min until values reach an absorbance between 2 and 3.

Results were calculated using the following formula:

$$\text{Cytotoxicity (\%)} = \frac{((lysate\ from\ cell\ pellet - blank) + ((centrifuged\ conditioned - culture\ media - blank)x2))}{(lysate\ from\ cell\ pellet - blank) + ((centrifuged\ conditioned - culture\ media - blank)x2) + ((cell\ lysate\ from\ cell\ monolayers - blank)x20)} x100$$

Factors 2 and 20 adjust the base formula as a result of the use of 250 µL de PBS containing 2 % Triton X-100.

IV. Protein assay by Folin-phenol reagent

Briefly, in alkaline condition, the Folin reagent (phosphomolybdic phosphotungstic complex) is reduced by the phenolic ring of tyrosine residues of proteins. This reaction gives a blue coloration which allows a colorimetric assay. Cooper sulphate is added to make the reaction more sensitive and promote electron transfer (Lowry et al., 1951). HK-2 cells were seeded at a density of 10000, 25000, 50000, 75000 and 100000 cells/well in 24-well culture dishes (Corning-Costar®, USA) and were incubated for 6, 24, 48 or 72 h in a humidified atmosphere, 5 % CO_2 and 37 °C. Cells were rinsed twice with 1 mL of PBS at room temperature. A volume of 200 µL of 0.5 N NaOH was added for 30 min. At the end of the alkaline hydrolysis, cell hydrolysates were collected for the protein assay. A calibration curve was done with known concentrations of Bovine Serum Albumin (BSA, ThermoFisher Scientific, USA) (0, 0.025, 0.05, 0.1 and 0.15 µg/µL). For the protein assay, 150 µL of hydrolysate were mixed with 750 µL of the solution A (2 % Na_2CO_3; 2 % sodium and potassium tartrate; 1 % $CuSO_4$) for 10 min. Finally, 75 µL of Folin reagent (Merck, Germany), diluted twice in distilled water, were added every 30 s and samples were vortexed. At the end of a 30 min-incubation at room temperature, the absorbance was measured in a spectrophotometer (Ultrospec, Biochrom, England) at 740 nm. Protein assay was also used to monitor cell proliferation exposed at 0, 0.1, 0.25, 0.5, 0.75, 1 or 10 µM during 12, 24, 48 or 72 h. For this experiment, HK-2 cells were seeded in 24-well culture plates (Corning-Costar®, USA) at 100000 cells/well.

Results were calculated using the following formula:

$$y = ax + b$$

V. ATP assay

HK-2 cells were incubated with AAI solution freshly prepared and containing 0, 0.1, 0.5, 1 or 50 µM for 24, 48 or 72 h, or containing 0, 1, 2.5, 5, 7.5, 10 or 50 µM for 3, 6, 12, 24 or 48 h. Cells were also incubated with fresh culture medium containing 0, 1, 5, 10, 20, 30, 40 or 50 µM during 24, 48 or 72 h, with or without medium change every 24 h to assess (even indirectly) the stability of the AAI, before ATP content was determined.

First, cells were seeded into 24-well culture dishes (Corning-Costar®, USA) at a density of 100000 cells/well. The next day, culture media were replaced either by fresh K-SFM medium (control cells) or by K-SFM medium containing the different concentrations of AAI. At the end of the incubation period, cells were rinsed twice with sterile PBS. Then, 200 µL of "somatic cell ATP releasing reagent" (Sigma-Aldrich, USA) were added. After 10 s of incubation, solution was collected and placed in microtubes (4 °C). Cells were then rinsed with sterile PBS and 250 µL of 0.5 N NaOH were added for 30 min at room temperature. A protein assay was then done (Folin method as described in section IV) on cell proteins harvested to normalize the results of ATP content. For the ATP assay, samples were diluted 100 times in distilled water and 100 µL of samples were mixed with 100 µL of ATP mixture. This mixture is composed of (a) reaction mixture, (b) luciferin buffer (2 mg/mL) and (c) luciferase buffer. The reaction mixture (a) was composed of 75 mM glycine, 75 mM Hepes; pH 7.7, 75 µM DTT (dithiothreitol), 125 µM EDTA and 6.25 mM $MgCl_2$. The luciferin buffer (b) was composed of 25 mM Tris; pH 7.75, 125 µM EDTA, 75 µM DTT, 6.25 mM $MgCl_2$ and luciferin. The luciferase buffer (c) was composed of 0.5 M glycine; pH 7.7, and luciferase. The reaction (Figure 19) catalysed by the luciferase produces photons that are measured with a luminometer (Lucetta™ Luminometer, Lonza, USA).

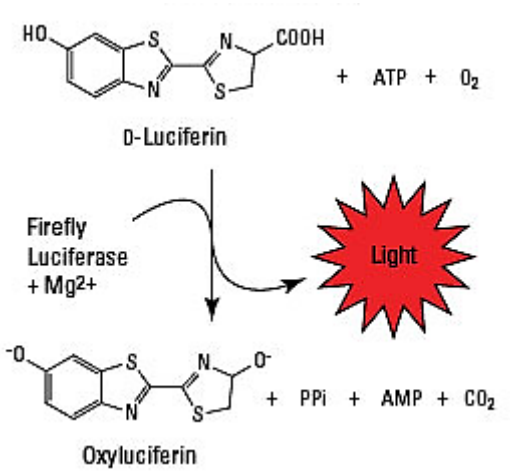

Figure 19: Reaction produced by the assay. *Bioluminescence is emitted from the reaction of luciferase enzyme and its substrate, firefly luciferase and luciferin, respectively. Co-substrates are ATP and O_2. ATP is hydrolysed and light is emitted when firefly luciferase catalyses the oxidation.*

VI. Activation or inhibition of SIRT1 and SIRT3

Before inducing either the activation or the inhibition of SIRT1 and SIRT3, the toxicity of each activator or inhibitor (see Figure 20) has been tested by MTT and LDH assays (as described in section III). Cells were seeded at a density of 100000 cells/well. When 80 % of confluence were reached, cells have been incubated for 24, 48 or 72 h with EX527 (Santa Cruz Biotechnology, USA), SRT2104 (Selleckchem, USA), 3-TYP (Selleckchem, USA) or 7-hydroxy-3-(4'-methoxyphenyl) Coumarin (Synquest Laboratories, USA) at different concentrations.

	Inhibitor	**Activator**
SIRT1	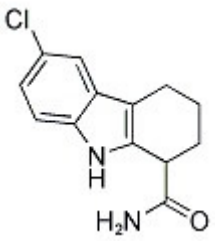 EX527	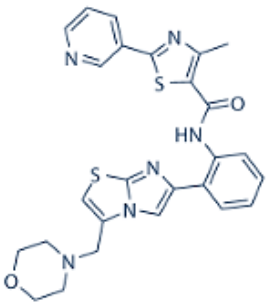 SRT2104
SIRT3	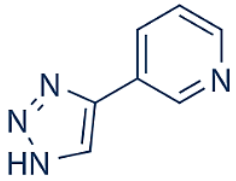 3-TYP	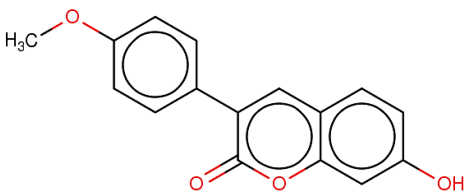 7-hydroxy-3-(4'-methoxyphenyl) Coumarin

Figure 20: List of inhibitors and activators *of SIRT1 and SIRT3 used in this investigation.*

The optimal concentration of each activator or inhibitor was then chosen for concentrations that were not toxic based on the assays performed. HK-2 cells were seeded in T25 culture dishes (Corning-Costar®, USA) and, 24 h later, cell culture media were replaced by fresh K-SFM medium (control cells) or by fresh K-SFM medium containing activators or inhibitors. The following concentrations were used: 10 µM of EX527, 3-TYP and 7-hydroxy-3-(4'-methoxyphenyl) Coumarin and 25 µM of SRT2104. After a pre-incubation of the cells for 3 h with the inhibitor of sirtuins (EX527 or 3-TYP) for SIRT1 or SIRT3, respectively, cells were incubated with media containing 1 µM of AAI in the presence of the sirtuin 1 or 3 inhibitor. After a pre-incubation of the cells for 3 h with the activator of sirtuins (SRT2104 or 7-hydroxy-3-(4'-methoxyphenyl) Coumarin) for SIRT1 or SIRT3, respectively, cells were incubated with media containing 10 or 50 µM of AAI in the presence of the sirtuin 1 or 3 activator. Cells were then incubated for 24, 48 or 72 h and media were changed every 24 h. At the end of the incubation period, cell lysates were prepared as described in section VIII and samples were prepared for western blot analysis. In addition, MTT and LDH assays were performed, as described in section III.

VII. RT-qPCR

RT-qPCR allows to quantify the relative expression of a gene. The expression of *SIRT1* and *SIRT3* genes was quantified in HK-2 cells incubated with different concentrations of AAI. The *18S* gene, coding for rRNA, was used as a housekeeping gene due to its constant expression level in these experimental conditions. HK-2 cells were seeded in T25 culture dishes (Corning-Costar®, USA) and 24 h later, cell culture media were replaced by fresh K-SFM medium (control cells) or by fresh K-SFM medium containing 0, 0.1, 0.5, 1, 10, 30 or 50 µM of AAI. Cells were then incubated for 24, 48 or 72 h in a humidified atmosphere containing 5 % of CO_2 and at 37 °C.

a) RNA extraction

This step was performed in "RNA^{se}-free" conditions. At the end of the incubation period, the conditioned culture media were replaced by 500 µL of Lysis buffer (LBA)-thioglycerol (Promega, USA) and cell lysates were then collected in microtubes. A volume of 170 µL of isopropanol was added to provide ideal binding conditions and the mixture was homogenized. Then, 400 µL of lysate/isopropanol were collected and poured on a column placed on a collection tube (Promega, USA) and centrifuged for 30 s at 12000 g. The remaining sample was then poured on the same column and also centrifuged for 30 s at 12000 g. Next, 500 µL of RNA wash solution (RWA) were added in order to rinse membrane-bound RNA and sample was centrifuged for 30 s at 12000 g. A mixture containing 3 µL of DNAse I enzyme (Promega, USA), 24 µL of yellow core buffer (Promega, USA) and 3 µL of 0.09 M $MnCl_2$ (Promega, USA) was prepared to remove residual amounts of DNA. A volume of 30 µL of this mixture was poured on the column for 15 min at room temperature. Afterwards, 200 µL of column wash solution (CWE) were added and centrifuged for 15 s at 12000 g. The column was then rinsed with 500 µL of RWA, diluted in ethanol, and centrifuged for 15 s at 12000 g. A volume of 300 µL of RWA was added and centrifuged for 2 min at 12000 g. Finally, the column was placed in a microtube of 1.5 mL and 50 µL of RNA^{se}-free water were added, to elute RNA. This final product was centrifuged for 1 min at 12000 g. Measurement of RNA concentration was performed with a Nanodrop 1000 spectrophotometer (Isogen Life Science, The Netherlands). RNA was finally stored at –80 °C in microtubes until use.

b) Reverse transcription

Following the manufacturer's instructions (GoScript™ Reverse Transcriptase, Promega, USA) and to obtain cDNA, 2 µg of RNA were diluted in RNA^{se}-free water up to a volume of 12 µL and the samples were incubated for 5 min at 70 °C to denature RNA (Promega, USA). Then, a volume of 8 µL of the reaction mixture (Buffer Mix Random Primer; Enzyme mix; RNA^{se}-free water) (Promega, USA) was added and samples were then successively incubated for 5 min at 25 °C (primers hybridization), for 60 min at 42 °C (cDNA extension) and for 15 min at 70 °C (enzyme inactivation). Finally, cDNA was stored at –20 °C in microtubes until use.

c) qPCR

For the qPCR in real time, a mixture, composed of 10 µL of SyberGreen (GoTaq® qPCR Master Mix, Promega, USA) and 5 µL of forward and reverse primers (Figure 21), was loaded in a 96-well plate (ThermoFisher Scientific, USA) and combined with 5 µL of cDNA. Finally, the plate was centrifuged for 1 min at 12000 g and inserted in the Step One Plus™ Real-Time PCR System (ThermoFisher Scientific, USA). The amplification was followed during 40 cycles: 15 s at 95 °C, 10 s at 60 °C, and 20 s at 72 °C.

Results were analysed by $2^{-\Delta\Delta Ct}$ method (Bustin et al., 2009), using the following formula:

$$1)\ \Delta C_t = C_{t\ gene\ of\ interest} - C_{t\ housekeeping\ gene}$$

$$2)\ \Delta\Delta C_t = \Delta C_{t\ condition\ of\ gene\ of\ interest} - \Delta C_{t\ control\ of\ gene\ of\ interest}$$

$$3)\ 2^{-\Delta\Delta Ct}$$

Gene	Direction	Primer sequence (5' → 3')
SIRT1	Forward	TAGCCTTGTCAGATAAGGAAGGA
	Reverse	ACAGCTTCACAGTCAACTTT
SIRT3	Forward	TCACTACTTTCTCCGGCTG
	Reverse	CAATGTCGGGCTTCACAACG
18S	Forward	TGGTGCATGGCCGTTCT
	Reverse	TAGTTAGCATGCCAGAGTCTCGTT

Figure 21: List of target genes and primer sequences used.

VIII. Western blot analysis

HK-2 cells were seeded in T25 culture dishes (Corning-Costar®, USA) and 24 h later, cell culture media were replaced by fresh K-SFM medium (control cells) or by fresh K-SFM medium containing 0, 0.1, 0.5, 1, 10 or 30 µM of AAI. Cells were then incubated for 24, 48 or 72 h in a humidified atmosphere containing 5 % of CO_2 and at 37 °C. At the end of the incubation period, cells were rinsed with PBS (4 °C). A volume of 200 µL of "DLA" lysis buffer (7 M urea, Merck, Germany; 2 M thiourea, Sigma-Aldrich, USA; 1 % CHAPS, Sigma-Aldrich, USA; 1 % ASB14, Sigma-Aldrich, USA; Tris 30 mM, Invitrogen, USA; pH 8.5; 1 % SDS, Panreac, Spain) containing PIB (phosphatase inhibitor buffer: 120 mM NaF, Merck, Germany; 250 mM β-glycerophosphate, VWR, Belgium; 25 mM Na_3VO_4, Sigma-Aldrich, USA; 250 mM 4-nitrophenylphosphate Sigma-Aldrich, USA) and PIC (protease inhibitor cocktail, [Roche, Switzerland]) was added. Cell lysates were collected with a scraper and

poured in microtubes. Cell lysates were then homogenized during 30 min in a 12 °C-ThermoMixer (under 4 °C, SDS precipitates and behind 25 °C, urea forms cyanates) and centrifuged for 10 min at 14000 g. Finally, supernatants were collected and stored at -80 °C.

a) Protein content determination

The total amount of proteins was determined in each sample by Pierce™ 660 nm reactive (ThermoFisher Scientific, USA), which contains a colorant-ion complex having the property to bind to basic amino acids of proteins. The colorant deprotonation in acidic conditions induces a coloration change from orange to green and a change in the maximal absorption of the colorant. In addition to the Pierce™ 660 nm reactive, the Ionic Detergent Compatibility Reagent (IDCR - ThermoFisher Scientific, USA) was added (1 g/20 mL of Pierce). After 5 min of incubation at room temperature, when the reaction was stabilized, absorbance was read at 660 nm in a spectrophotometer xMark™ Microplate (Biorad, Belgium). A calibration curve was realized with standard samples of known BSA concentration (0, 0.025, 0.125, 0.25, 0.5, 0.75, 1 and 1.5 µg/µL) (ThermoFisher Scientific, USA) which allows the determination of the protein concentration of each sample.

b) Preparation of samples

Based on established protocols (Biorad, Belgium), samples were diluted in distilled water to obtain a total of 12 µg of proteins for SIRT1, 10 to 15 µg of proteins for SIRT3 and 14 µg of proteins for (Ac-)SOD2 and H3(K9) in a volume of 20 µL for the immunodetection analysis. A volume of 5 µL of loading blue (143 mM Tris-HCl; pH 6.8; 20 % SDS; 2 M β-mercaptoethanol; 25 % glycerol and 0.75 mM blue of bromophenol) was added to samples to denature the proteins, burden samples and visualize the migration front. Then, samples were heated for 5 min at 100 °C to denature proteins and then centrifuged 2 min at 13000 g. Finally, 20 µL of each sample were loaded in a homemade polyacrylamide gel (see section VIII.c.). The marker lane was filled with 2.5 µL of ladder (Color Protein Standard, Broad Range (11-245 kDa), Bioké, UK) composed of 20 mM Tris-phosphate; pH 7.5, 2 % SDS, 0.2 mM DTT, 3.6 M urea and 15 % glycerol.

c) Migration

The migration gel is composed of two parts: the stacking gel allowing the concentration of proteins at the entry of the running gel and the running gel allowing the separation/resolution of proteins according to their molecular weight. Gels are composed of 1.5 M Tris-HCl; pH 8.8, Temed (Rooth, France), 30 % acrylamide (BioRad, Belgium), 10 % APS (BioRad, Belgium), 10 % SDS (Sigma-Aldrich, USA) and distilled water. Quantities of these compounds vary according to the gel type and the percentages (12 and 3.75 % in this work). Gels were casted between 2 glass plates (Bio-Rad, USA) and a comb of 0.75 mm was put in the stacking gel to form wells where samples were disposed. Then, gel was disposed in a tank filled with migration buffer (0.25 M Tris Base, Rooth, France; pH 8.5; 1.92 M glycine, Rooth, France; 20 % SDS, Sigma-Aldrich, USA; distilled water). The electrophoretic protein resolution was performed at 150 V for 45 min.

d) Transfer

Proteins were transferred on a polyvinylidene fluoride (PVDF, Bio-Rad, USA) membrane. The membrane was activated for 1 min in methanol and rinsed with transfer buffer (5x Transfer Buffer - composition fixed by the firm BioRad, Belgium -; Ethanol, Univars, Belgium; distilled water). The activated membrane and gel were sandwiched between 2 transfer stacks (Bio-Rad, USA) dipped in transfer buffer and placed at room temperature in the Trans-Blot® Turbo™. A constant amperage current (1.3 A) was applied during 7 min to allow the migration of the proteins from the gel to the PVDF membrane.

e) Immunodetection

The membrane was placed in a solution containing PBS and Odyssey Blocking Buffer PBS, dilution 1:1, (LI-COR, USA) for 1 h in order to allow the saturation of unspecific antigenic sites of the membrane and thus to reduce the background. The membranes were then incubated for 16 h at 4 °C with primary antibody (Figure 22) diluted in Odyssey Blocking Buffer PBS (LI-COR, USA)-0.1 % Tween 20 (BioRad, Belgium). At the end of the incubation, the membrane was rinsed 3 times for 5 min with PBS-0.1 % Tween 20 (BioRad, Belgium) and then incubated for 1 h at room temperature with secondary antibodies coupled with a fluorochrome (Figure 22). Then, membranes were rinsed 3 times during 5 min with 0.1 % PBS-Tween 20 (BioRad, Belgium) and twice with PBS. The membrane was then dried during 30 min in an incubator at 37 °C. Proteins were visualized with Odyssey® imaging system (LI-COR, USA) either at 800 nm or at 700 nm (Figure 22). Finally, fluorescence of each band was quantified with the software Image Studio™ Lite Version 5.2 (LI-COR, USA). For the quantification, the fluorescence of the signals of interest was then normalized for the fluorescence of the α-Tubulin signals:

$$\text{Protein relative abundance} = \frac{fluorescence\ signals\ of\ protein\ of\ interest}{fluorescence\ signals\ of\ \alpha-Tubulin}$$

Primary antibody	**Reference**	**Secondary antibody**	**Molecular weight**
Anti-Sirtuin 3 Rabbit 1:2000 16 h 4 °C (Cell Signaling, USA)	5490S	Goat anti-rabbit 800 nm 1:10000 1 h RT (LI-COR, USA)	28 kDa
Anti-Sirtuin 1 Mouse 1:500 16 h 4 °C (Cell Signaling, USA)	8469S	Goat anti-mouse 700 nm 1:10000 1 h RT (LI-COR, USA)	120 kDa
Anti-SOD2 Rabbit 1:2000 16 h 4 °C (Merck, Germany)	06-984	Goat anti-rabbit 800 nm 1:10000 1 h RT (LI-COR, USA)	24 kDa
Anti-Ac-SOD2 Rabbit 1:2000 16 h 4 °C (Abcam, UK)	ab137037	Goat anti-rabbit 800 nm 1:10000 1 h RT (LI-COR, USA)	24 kDa
Anti-Histone H3 Rabbit 1:2000 16 h 4 °C (Cell Signaling, USA)	4499S	Goat anti-rabbit 800 nm 1:10000 1 h RT (LI-COR, USA)	17 kDa

Anti-Ac-Histone H3 (Lys9) Rabbit 1:1000 16 h 4 °C (Merck, Germany)	06-942	Goat anti-rabbit 800 nm 1:10000 1 h RT (LI-COR, USA)	17 kDa
Anti-α-Tubulin Mouse 1:10000 30 min RT (Sigma-Aldrich, USA)	T5168	Goat anti-mouse 700 nm 1:10000 30 min RT (LI-COR, USA)	50 kDa

Figure 22: List of primary and secondary antibodies *used in this work.*

IX. Statistical analysis

All data are expressed as mean ± SEM (standard error of the mean). For all statistical analyses, analysis of variance I (one-way ANOVA) and a Dunnett test were performed to compare results (GraphPad Prism, version 5.04). Differences between means with a p-value of 0.05 were considered as significantly different.

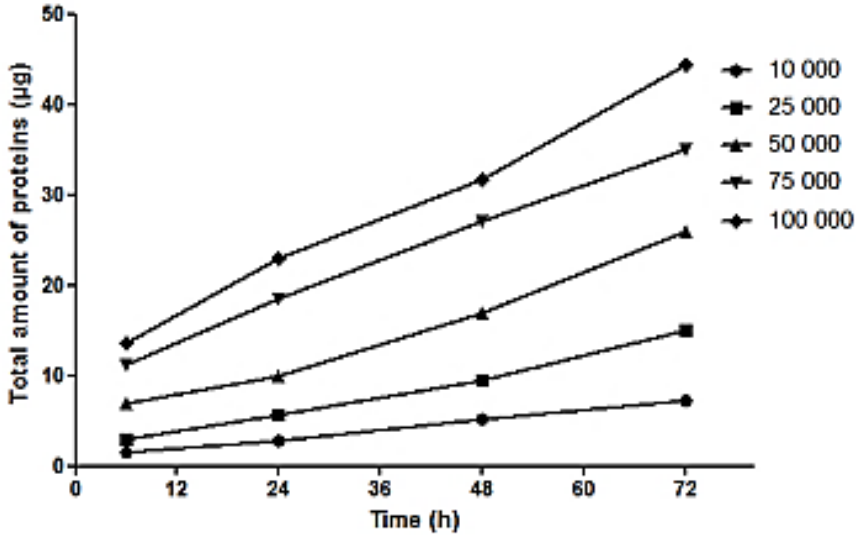

Figure 23: Effects of cell density on HK-2 cell proliferation over time. *Cells were seeded at different densities in 24-well culture dishes and were then incubated for 6, 24, 48 and 72 h. At the end of the incubation periods, protein content associated with cell monolayers was determined by Folin assay. Results are expressed in total amount of proteins as means for 3 technical replicates (n=1, three wells analysed).*

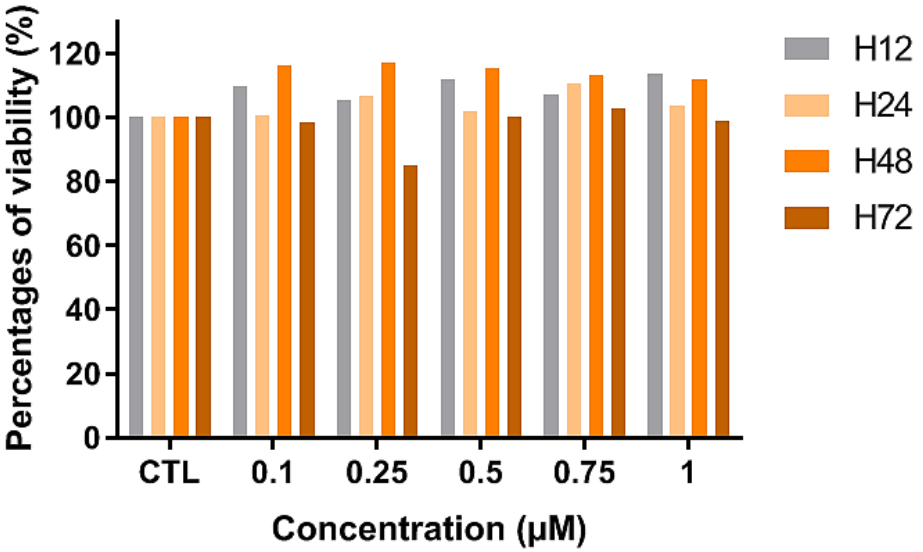

Figure 24: Effects of AAI on HK-2 cell viability assessed by MTT assay. *Cells were seeded at 100000 cells/well in 24-well culture dishes and incubated in the presence of 0, 0.1, 0.25, 0.5, 0.75 or 1 µM of AAI for 12, 24, 48 or 72 h. Results are expressed as means of the percentages of viability compared to control (fixed arbitrarily at 100 % for each control time-point) for three wells (n=1).*

Results

I. Effects of cell density on HK-2 cell proliferation

First, it was necessary to determine the cell density for the seeding of HK-2 cells that is compatible with incubation periods of several days, knowing that the reported doubling time for these cells is about 36 h (Iwata and Zager, 1996). On the one hand, the conduct of the experiment requires getting as much material as possible to allow the different read outs (RNA extraction, western blot analysis …). On the other hand, we did not want that the cells reach "contact inhibition" or start to suffer from a too high cell density leading to cell stress related to culture conditions. Indeed, cell density could be a confounding factor when the toxicity of AAI is analysed. As presented in Figure 23, protein contents are proportional to cell density seeded. Moreover, no slowing or stop of cell proliferation was observed during the first 72 h in culture, no matter what the cell density tested even at the highest cell density (100000 cells/well). Cell micrographs corresponding to this experiment are presented in annexe I (Figure 46).

Based on these results, showing that cell proliferation rate increases with cell density up to 72 h of incubation, a cell density of 100000 cells/well of a 24-plate format was chosen for future experiments, because it allows to get enough of cell material for the analysis without a noticeable alteration of cell proliferation index.

II. Effects of different AAI concentrations on HK-2 cell viability

Our first objective was to determine the optimal conditions to allow the study of SIRT1 and SIRT3 expression/abundance in cells exposed to AAI without important cell death. AAI toxicity on HK-2 cells was first determined by MTT assay. Preliminary data revealed that high concentrations such as 10 and 50 µM were highly toxic for cells (Mosseray, 2018). Cells were then voluntary incubated with low concentrations of AAI (0, 0.1, 0.25, 0.5, 0.75 or 1 µM) for 12, 24, 48 or 72 h. Indeed, the analysis of the expression of a gene of interest in dying cells is always difficult as one can never be sure that the abundance of the gene product analysed revealed the effect of the tested molecule or results from the modifications in gene expression of passenger genes associated with cell death. As observed in Figure 24, AAI does not induce toxicity of HK-2 cells at low concentrations tested. In addition, a representation of the effect of low concentrations of AAI on cell proliferation of HK-2 cells is presented in annexe II (Figure 47).

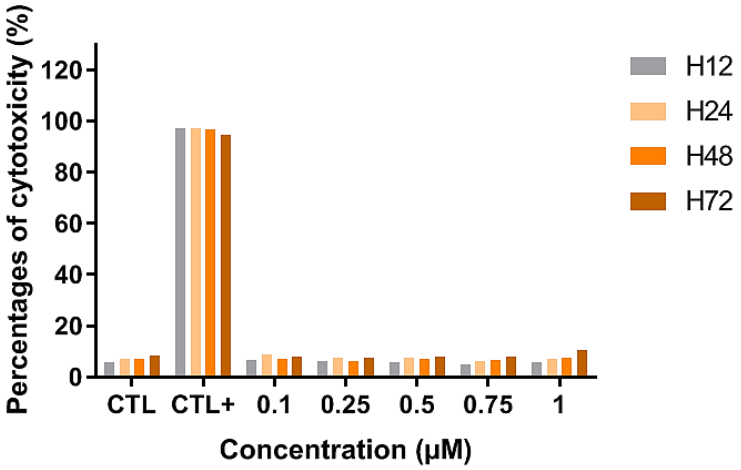

Figure 25: Effects of low AAI concentrations on HK-2 cell cytotoxicity as assessed by LDH assay. *Cells were seeded at 100000 cells/well in 24-well culture dishes and incubated in the presence or in the absence (CTL) of AAI at different concentrations (0.1, 0.25, 0.5, 0.75 or 1 µM) for 12, 24, 48 or 72 h. Results are expressed as means of percentages of cytotoxicity for three wells (n=1).*

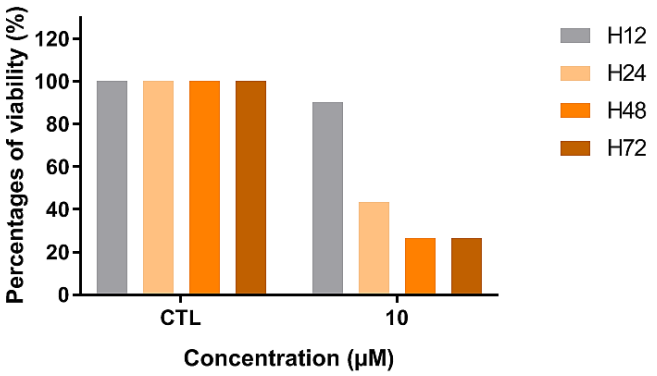

Figure 26: Effects of a higher concentration of AAI on HK-2 cell viability as assessed by MTT assay. *Cells were seeded at 100000 cells/well in 24-well culture dishes and incubated in the presence or in the absence (CTL) of 10 µM of AAI for 12, 24, 48 or 72 h. Results are expressed as means of percentages of viability compared to control (fixed arbitrarily at 100 % for each control time-point) for three wells (n=1).*

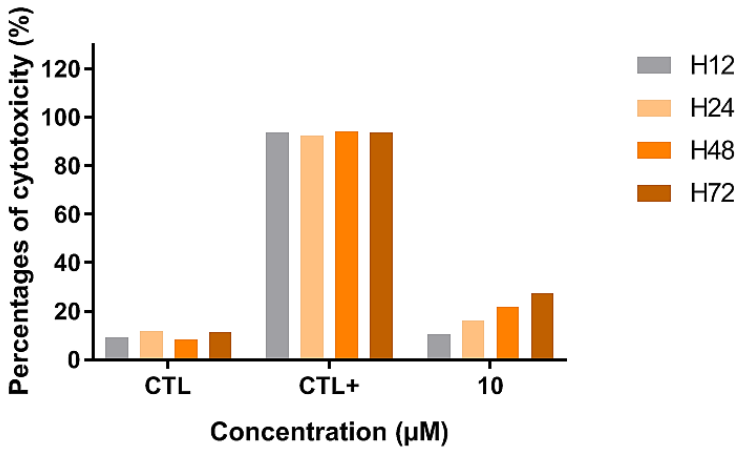

Figure 27: Effects of a higher AAI concentration on HK-2 cell cytotoxicity as assessed by LDH assay. *Cells were seeded at 100000 cells/well in 24-well culture dishes and incubated in the presence of 0 or 10 µM of AAI for 12, 24, 48 or 72 h. Results are expressed as means of percentages of cytotoxicity for three wells (n=1).*

To confirm these results, cell toxicity of AAI was assessed by a LDH assay. HK-2 cells were incubated in the presence or in the absence (CTL) of 0.1, 0.25, 0.5, 0.75 or 1 µM of AAI for 12, 24, 48 or 72 h (Figure 25). There is no difference in cytotoxicity observed, whatever the concentration or incubation time tested. The positive control represents the maximal release of LDH in control cells incubated in the absence of AAI for different periods of time and permeabilized with Triton X-100.

These results on toxicity of low AAI concentrations were next compared to toxicity induced by a higher concentration (10 µM), known to be toxic (Yang et al., 2010). As shown in Figure 26, at the AAI concentration of 10 µM, a time-dependent decrease in cell viability is observed when this parameter is assessed by a MTT assay. An increase in the cytotoxicity, assessed by LDH activity release, was also observed in cells incubated in the presence of 10 µM AAI for 24, 48 or 72 h (Figure 27).

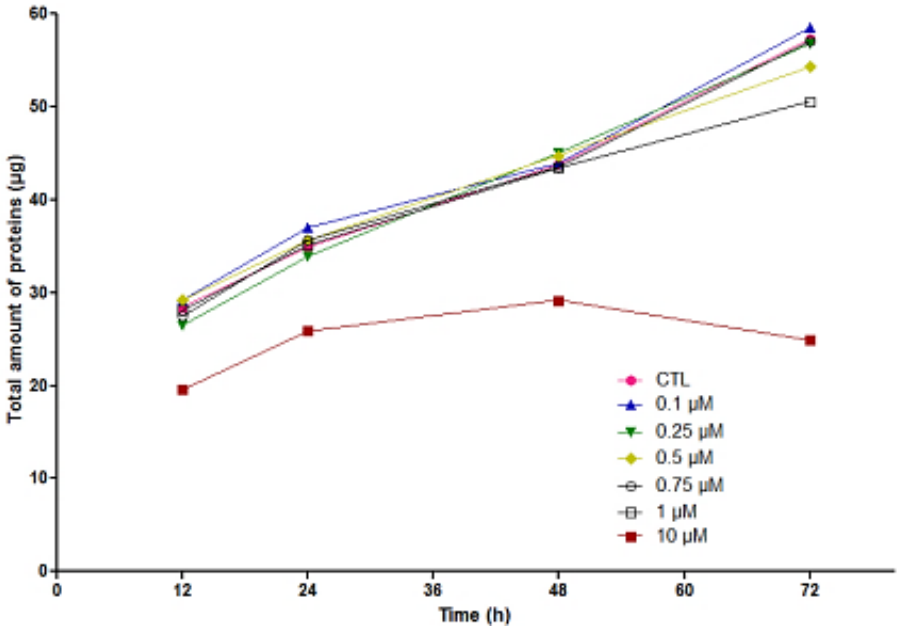

Figure 28: Effects of different AAI concentrations on HK-2 cell proliferation. *Cells were seeded at 100000 cells/well in 24-well culture dishes and incubated in the presence or in the absence (CTL) of different concentrations of AAI (0.1, 0.25, 0.5, 0.75, 1 or 10 µM) for 12, 24, 48 or 72 h. At the end of the different incubation periods, protein content associated with cell monolayers was determined by Folin assay. Results are expressed in total amount of proteins and represent means for three wells (n=1).*

III. Effects of different AAI concentrations on HK-2 cell proliferation

We next addressed the question to know whether low and non-toxic concentrations of AAI are able to affect cell proliferation or not. Cells were incubated with or without different concentrations of AAI during 12, 24, 48 or 72 h before the determination of protein content. As observed in Figure 28, low concentrations of AAI do not strongly affect proliferation of cells even if, at 1 µM, a slight reduction of cell proliferation is observed between 48 and 72 h of incubation. Moreover, a concentration of 10 µM of AAI is toxic (as observed by the reduced amount of proteins obtained after a cell incubation of 12 h) and impairs cell proliferation. For this concentration, toxicity was observed by MTT and LDH assay (Figure 26 and 27, respectively). However, the analysis of cell proliferation by a protein assay cannot discriminate between the alteration of cell cycle/cell proliferation and toxicity.

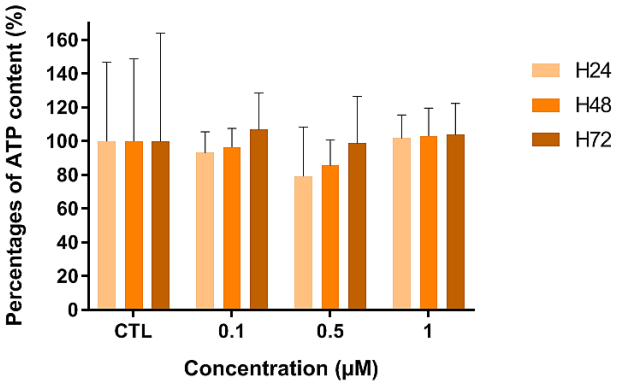

Figure 29: Effects of low AAI concentrations on cellular ATP content. *Cells were seeded at 100000 cells/well in 24-well culture dishes and incubated with or without (CTL) different concentrations of AAI (0.1, 0.5, or 1 µM) for 24, 48 or 72 h. Results are expressed in percentages of ATP content compared to the arbitrarily fixed values of 100 % for control cells at each experimental time-point; ATP content is normalised by protein content of each well. Results are expressed as means ± SEM for n=4. Statistical analysis was performed by one-way ANOVA followed by Dunnett post-test.*

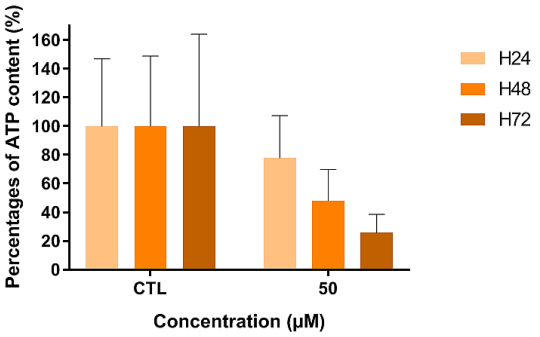

Figure 30: Effects of a high concentration of AAI on cellular ATP content. *Cells were seeded at 100000 cells/well in 24-well culture dishes and incubated with or without 50 µM of AAI for 24, 48 or 72 h. Results are expressed in percentages of ATP content compared to the arbitrarily fixed values of 100 % for control cells at each experimental time-point; ATP content is normalised by protein content of each well. Results are expressed as means ± SEM for n=4. Statistical analysis was performed by one-way ANOVA followed by Dunnett post-test.*

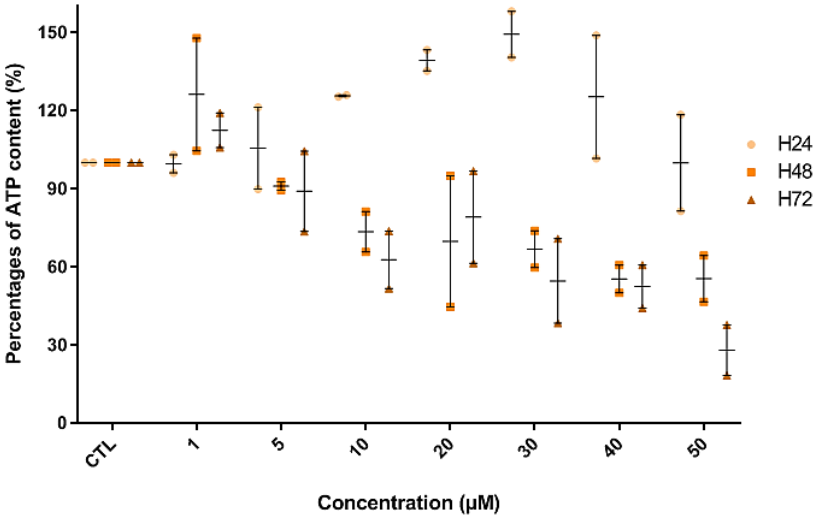

Figure 31: Effects of different AAI concentrations on cellular ATP content. *Cells were seeded at 100000 cells/well in 24-well culture dishes and incubated in the presence or in the absence (CTL) of AAI at different concentrations (1, 5, 10, 20, 30, 40 or 50 µM) for 24, 48 or 72 h. Results are expressed in percentages of ATP content compared to the arbitrarily fixed value of 100 % for control cells at each experimental time-point. Results are expressed as means (bar) for duplicates (n=2).*

IV. Effects of different AAI concentrations on cellular ATP content

Previous work in our laboratory revealed that cells incubated during 24 h in the presence of 50 µM of AAI display a mitochondrial fragmentation (as explained in the introduction, section VI).

As mitochondrial fragmentation observed in cells exposed to a toxic AAI concentration might be accompanied by ATP production alterations, in this work, an ATP assay was used to assess ATP contents in cells exposed to AAI (Figures 29 and 30). While there is no major change in ATP contents for cells incubated with concentrations up to 1 µM (Figure 29), a time-dependent decrease in ATP contents is observed in cells exposed to 50 µM of AAI during 24, 48 or 72 h (Figure 30). This decrease is thus correlated to mitochondrial fragmentation observed in cells incubated with 50 µM during 24 h, suggesting that changes in mitochondria dynamics and fragmentation are associated with alterations of mitochondrial ATP production.

To cover the range between the highest concentration used in this work (1 µM) and the concentration used by P. Mosseray (50 µM), an ATP assay was performed on cells incubated in the presence of 0, 1, 5, 10, 20, 30, 40 or 50 µM of AAI for 24, 48 or 72 h. A time- and concentration-dependent decrease in ATP contents is observed for cells incubated with 10 µM and higher concentrations for 48 and 72 h (Figure 31).

Additionally, the concentration range between 1 and 10 µM in AAI and shorter incubation times have been tested in order to assess the cytotoxicity of the molecule. However, no alteration of ATP contents was observed in cells incubated for 3, 6, 12, 24 or 48 h in the presence of 0, 1, 2.5, 5, 7.5, 10 or 50 µM of AAI, when compared to the ATP contents in control cells, except at 50 µm for 48 h (data not shown).

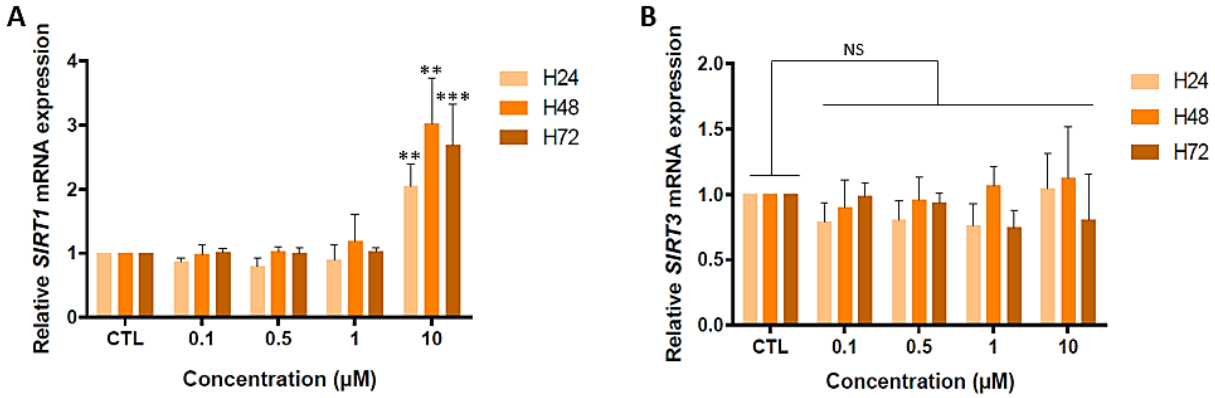

Figure 32: Effects of AAI on the relative mRNA abundance of SIRT1 (A) or SIRT3 (B). *Cells were seeded at 1.25x10^6 cells/T25 culture dishes and incubated in the presence or in the absence (CTL) of different AAI concentrations (0.1, 0.5, 1 or 10 µM) for 24, 48 or 72 h (n=4 for CTL, 0.1, 0.5 and 1 µM conditions, 2 wells per condition; n=3 for 10 µM condition, 2 wells per condition). Results are expressed as relative mRNA abundance for SIRT1 (A) or SIRT3 (B) and represent as means ± SEM. Statistical analysis was performed by one-way ANOVA followed by Dunnett post-test. AA vs CTL conditions: **: p< 0.01; ***: p< 0.001; NS, Non-Significantly different when compared to CTL.*

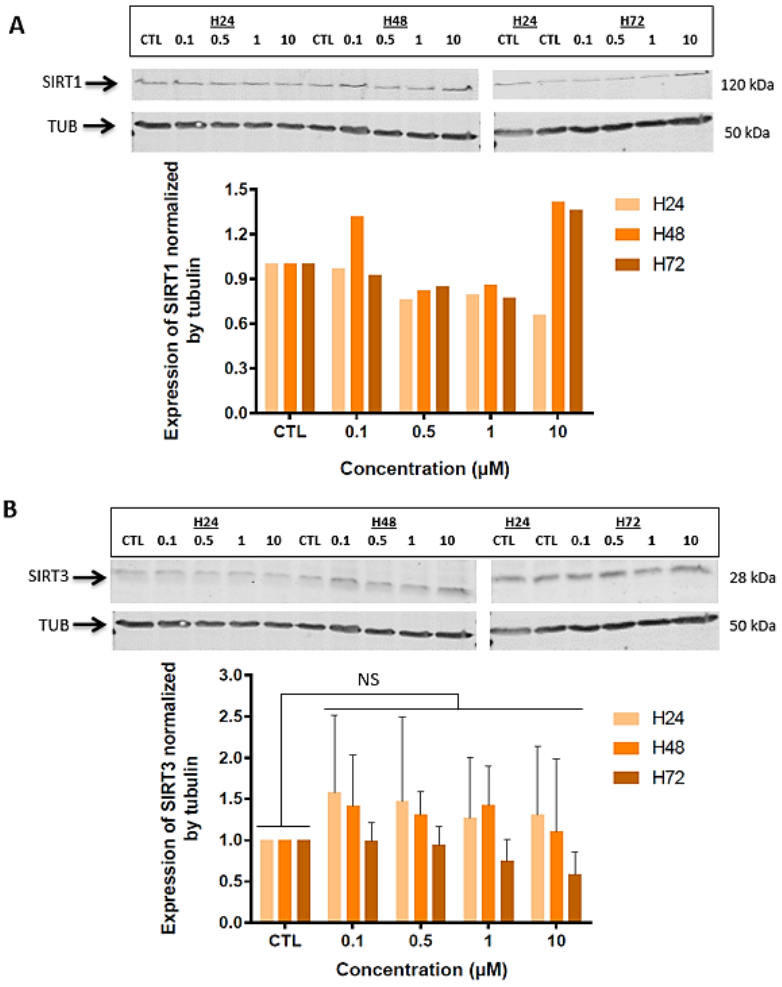

Figure 33: Effects of AAI on the relative abundance of SIRT1 (A) and SIRT3 (B) enzymes. *Cells were seeded at 1.25x10^6 cells/T25 culture dishes and incubated in the presence or in the absence (CTL) of AAI at different concentrations (0.1, 0.5, 1 or 10 µM) for 24, 48 or 72 h (n=1 for SIRT1; n=3 for SIRT3). For western blot analysis of SIRT1, 12 µg of proteins were loaded (A). For SIRT3 western blot, 12 µg of proteins were loaded (B). Results are expressed as protein relative abundance and normalised by a-tubulin used as a loading control. Statistical analysis was performed by one-way ANOVA, followed by Dunnett post-test. AAI-treated cells vs control cells: NS, Non-Significant.*

V. Effects of AAI on sirtuins 1 and 3 abundance

Previous work in our laboratory reported that the relative mRNA abundance of *SIRT1* is significantly increased in cells exposed to 50 µM during 12 or 24 h and that the relative protein abundance of SIRT1 is significantly increased at 24 h (data not shown (Mosseray, 2018)). Moreover, it is also known that the relative mRNA abundance of *SIRT3* is significantly decreased in cells incubated in the presence of AAI at 50 µM during 6 h, but significantly increased at 24 h. Strikingly, no significant difference was found for the protein abundance of SIRT3 in cells exposed to 50 µM of AAI, no matter what the time of incubation considered (data not shown (Mosseray, 2018)).

To evaluate the putative effects of low concentrations of AAI on the abundance of SIRT1 and SIRT3, the relative expression of these sirtuins was evaluated at both mRNA (Figure 32) and protein (Figure 33) levels. As shown in Figure 32 A, the relative mRNA abundance of *SIRT1* remains stable for subtoxic concentrations, but is increased in cells exposed to AAI at 10 µM for 24, 48 or 72 h. For *SIRT3*, AAI does not have any effect on the mRNA abundance in cells incubated either in the presence of low AAI concentrations or in the presence of the toxic 10 µM concentration (Figure 32 B).

As shown in Figure 33, few changes in the abundance of SIRT1 at the protein level are observed in cells exposed to 0, 0.1, 0.5 or 1 µM AAI for 24, 48 or 72 h, and a slight increase in the 10 µM condition, for 48 or 72 h, is also observed. For SIRT3, a non-significant decrease of its abundance is observed in cells incubated for 72 h with 10 µM of AAI.

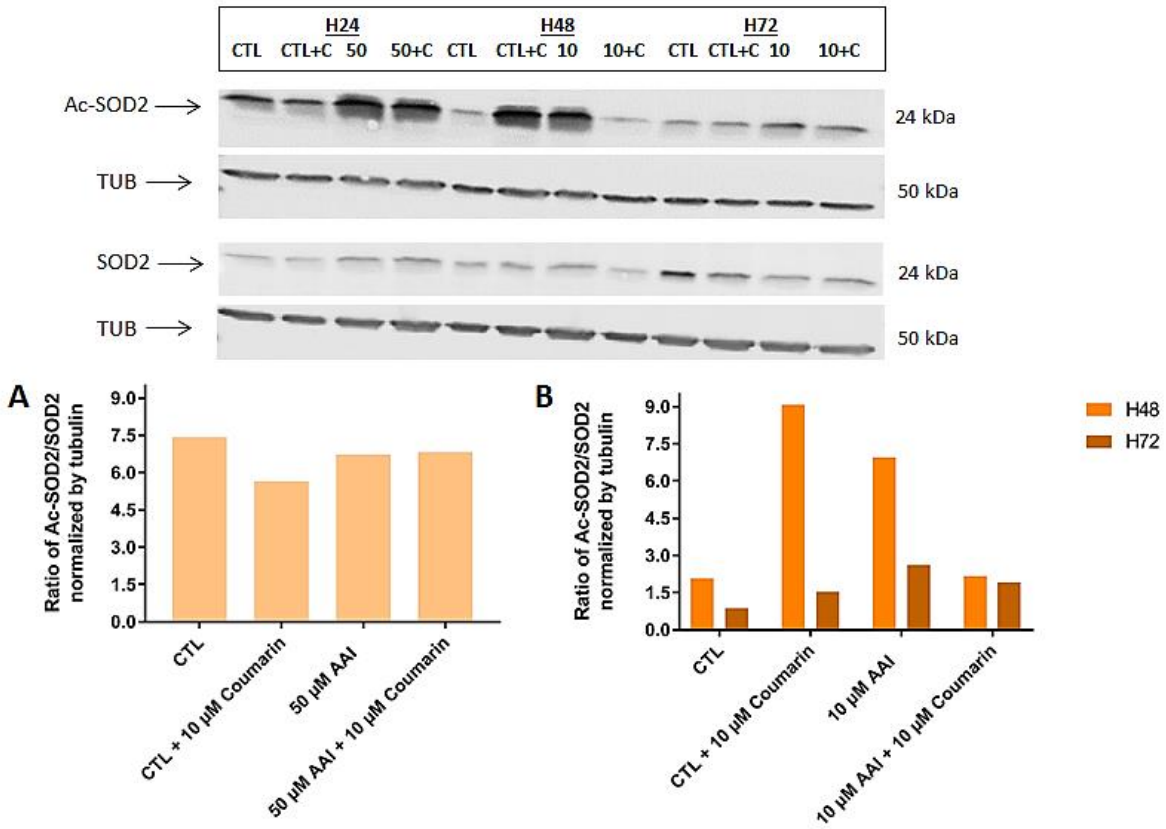

Figure 34: Effects of Coumarin on the abundance of Ac-SOD2 (A for 24 h and B for 48 and 72 h). *Cells were seeded at 1.25x10^6 cells/T25 dishes and incubated in the presence (CTL + Coumarin) or in the absence (CTL) of Coumarin and in the presence of 50 µM of AAI (50 µM) with (50 µM + Coumarin) or without (50 µM) additional 10 µM of Coumarin for 24 h (A). For 48 or 72 h (B), cells were incubated in the presence (CTL + Coumarin) or in the absence (CTL) of Coumarin and in the presence of 10 µM of AAI (10 µM) with (10 µM + Coumarin) or without (10 µM) additional 10 µM of Coumarin (n=1). For this western blot analysis, 14 µg of proteins were loaded in the gel. Results are expressed as protein relative abundance and normalised by a-tubulin used as a loading control.*

VI. Effects of sirtuins 1 and 3 activators or inhibitors on acetylated targets of both enzymes, cytotoxicity and cell proliferation

As mentioned, four molecules (Coumarin, 3-TYP, SRT2104 and EX527) were tested, in order to evaluate a putative sensitisation of sirtuins inhibitors (3-TYP and EX527) or a potential protection of sirtuins activators (Coumarin and SRT2104) against the AAI-induced toxicity for HK-2 cells, respectively with a concentration of 1 or 10 and 50 µM. They are the topics of the following developments.

For the experiments evaluating the putative protection, two concentrations of AAI have been used: 10 and 50 µM. The concentration of 10 µM was used for long time period and the concentration of 50 µM was used for short time period. Indeed, 50 µM is too toxic to keep enough material until 72 h-incubation.

The first tested molecule was the Coumarin, an activator of SIRT3 activity.

a) Effects of Coumarin on the acetylation status of SOD2, a sirtuin 3 target

As observed in Figure 34 A, there is a slight decrease in the SOD2 acetylation in cells incubated for 24 h with 10 µM of Coumarin, when compared to control cells. At 24 h, we do not see any modification of SOD2 acetylation in cells exposed to 50 µM of AAI and the presence of Coumarin does not affect the acetylation level of the antioxidant enzyme (Figure 34 A).

However, surprisingly, for 48 h of incubation, we observed an increase in the acetylation status of SOD2 (Figure 34 B). In addition, in cells incubated with 10 µM of AAI alone, the acetylation of the antioxidant enzyme is also increased and this acetylation is prevented in cells incubated for 48 h with 10 µM of AAI and 10 µM of Coumarin (Figure 34 B).

For 72 h-incubation, we still observed an increase in SOD2 acetylation in cells incubated with 10 µM of AAI, but the presence of Coumarin does not change the acetylation level of the enzyme (Figure 34 B).

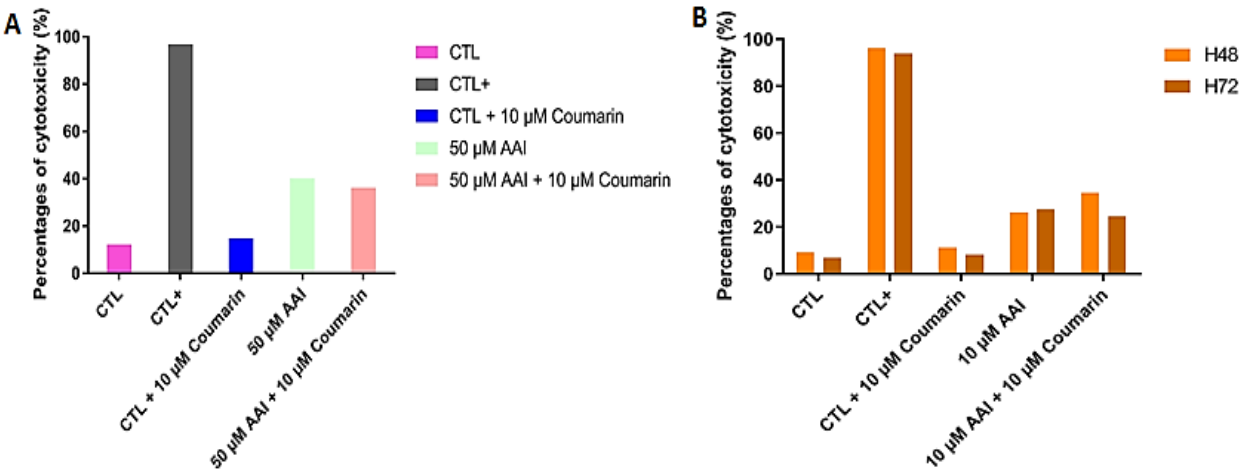

Figure 35: Effect of Coumarin on HK-2 cytotoxicity in the presence or in the absence of high concentration of AAI as assessed by LDH (A for 24 h; B for 48 or 72 h) assay. *Cells were seeded at 100000 cells/well in 24-well culture dishes and incubated in the presence or in the absence (CTL) of 50 µM of AAI for 24 h (A) or in the presence or in the absence (CTL) of 10 µM of AAI for 48 or 72 h (B). As indicated, in some conditions, 10 µM of Coumarin were added to cells for the same period of time. Results are expressed as means of percentages of cytotoxicity for three wells (n=1).*

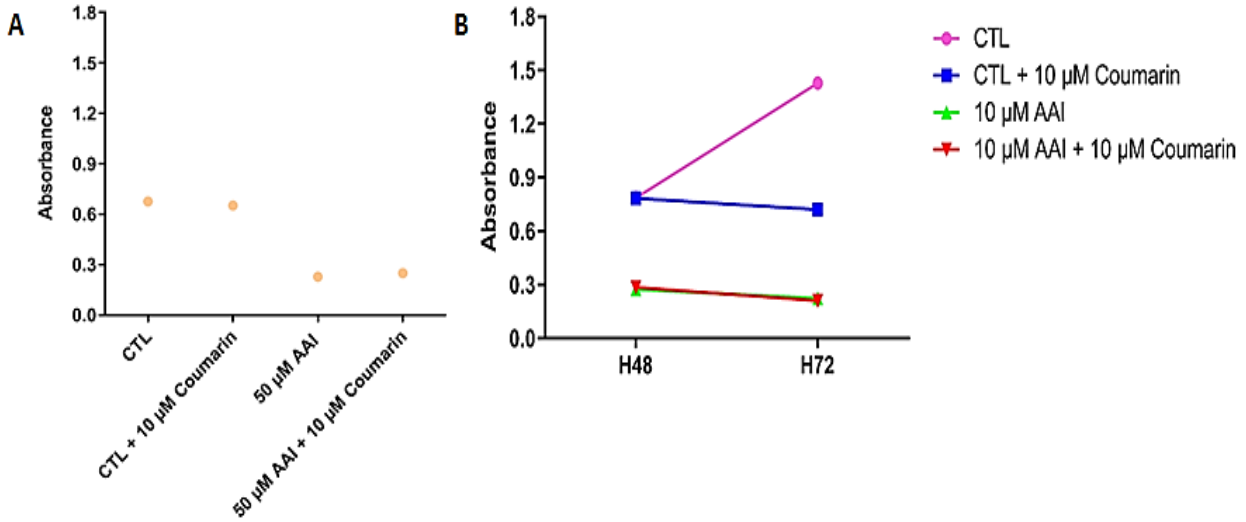

Figure 36: Effect of Coumarin on HK-2 cell proliferation in the presence or in the absence of high concentration of AAI as assessed by MTT (A for 24 h; B for 48 or 72 h) assay. *Cells were seeded at 100000 cells/well in 24-well culture dishes and incubated in the presence or in the absence (CTL) of 50 µM of AAI for 24 h (A) or in the presence or in the absence (CTL) of 10 µM of AAI for 48 or 72 h (B). As indicated, in some conditions, 10 µM of Coumarin were added to cells for the same period of time. Results are expressed as absorbance unit and represent means of absorbance for three wells (n=1).*

b) Effects of Coumarin, an activator of SIRT3, on cell toxicity and proliferation

Regarding the cytotoxicity, Coumarin does not reduce the toxicity of AAI for HK-2 cells (Figure 35 A and 35 B), when compared to the toxicity induced by 10 or 50 µM of AAI. In addition, there is no toxicity of Coumarin alone on HK-2 cells for 24, 48 or 72 h.

As shown in Figure 36, the proliferation of cells incubated in the presence of 10 µM of Coumarin does not seem to be affected during the first 24 h (Figure 36 A) and is inhibited during 48 and 72 h (Figure 36 B) in comparison with the proliferation determined for control cells. However, while AAI inhibits the proliferation of cells, the presence of Coumarin does not have any effect on the proliferation of cells incubated with either 10 or 50 µM of AAI (Figure 36 A and 36 B).

These results suggest that, in the experimental conditions, Coumarin does not induce a protection against toxicity of AAI for HK-2 cells.

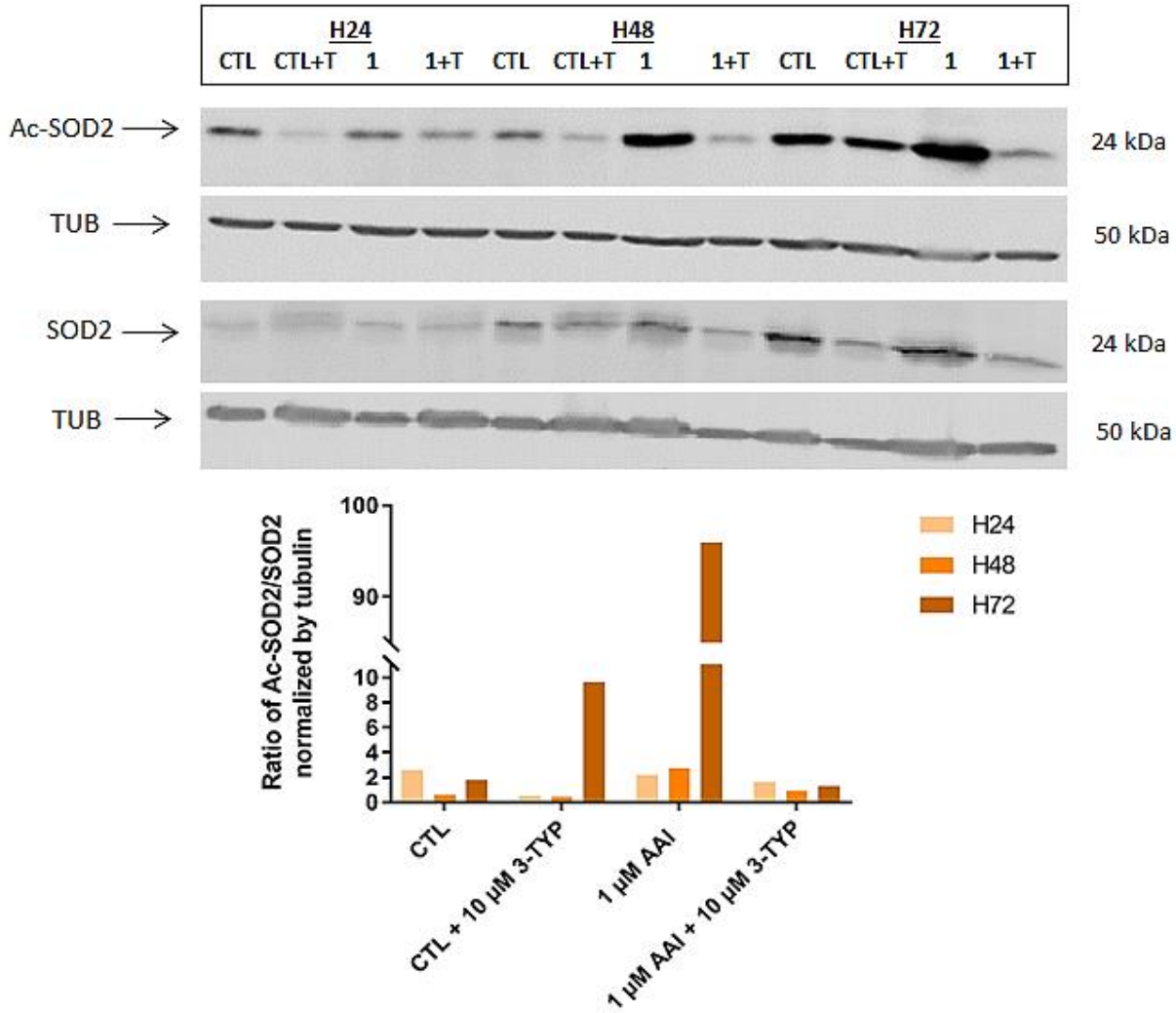

Figure 37: Effects of 3-TYP on the abundance of Ac-SOD2. *Cells were seeded at 1.25x10^6 cells/T25 dishes and incubated in the presence (CTL + 3-TYP) or in the absence (CTL) of 3-TYP and in the presence of 1 µM of AAI (1 µM) with (1 µM + 3-TYP) or without (1 µM) additional 10 µM of 3-TYP for 24, 48 or 72 h (n=1). For this western blot analysis, 14 µg of proteins were loaded in the gel. Results are expressed as protein relative abundance and normalised by a-tubulin used as a loading control.*

The second molecule tested on HK-2 cells was the 3-TYP, an inhibitor of SIRT3 activity.

c) Effects of 3-TYP on the acetylation status of SOD2, a sirtuin 3 target

For western blot analysis, the loading control is not conclusive for Ac-SOD2 and leads to a difficult interpretation for 72 h (Figure 37).

For 24 and 48 h, a slight decrease of the SOD2 acetylation was observed, when comparing control cells and control cells with 10 µM of 3-TYP or cells incubated with AAI and cells in the presence of AAI and 3-TYP. At 48 h, when comparing control cells and cells incubated in the presence of AAI, an increase of the SOD2 acetylation was also observed in the presence of AAI alone (Figure 37).

However, surprisingly, it appears clear that the inhibition of SIRT3 using 10 µM of 3-TYP does not increase the acetylation of SOD2 (Figure 37).

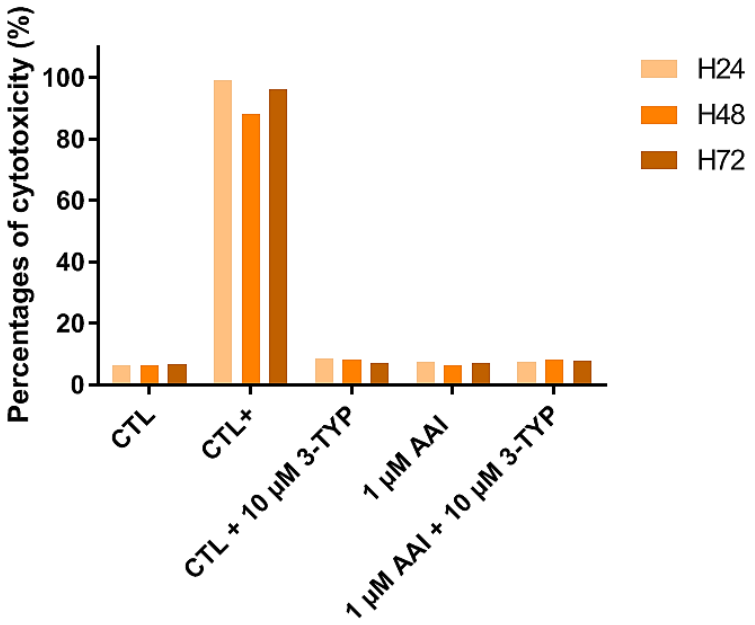

Figure 38: Effect of 3-TYP on HK-2 cytotoxicity in the presence or in the absence of low concentration of AAI as assessed by LDH assay. *Cells were seeded at 100000 cells/well in 24-well culture dishes and incubated in the presence or in the absence (CTL) of 1 µM of AAI for 24, 48 or 72 h. As indicated, in some conditions, 10 µM of 3-TYP were added to cells for the same period of time. Results are expressed as means of percentages of cytotoxicity for three wells (n=1).*

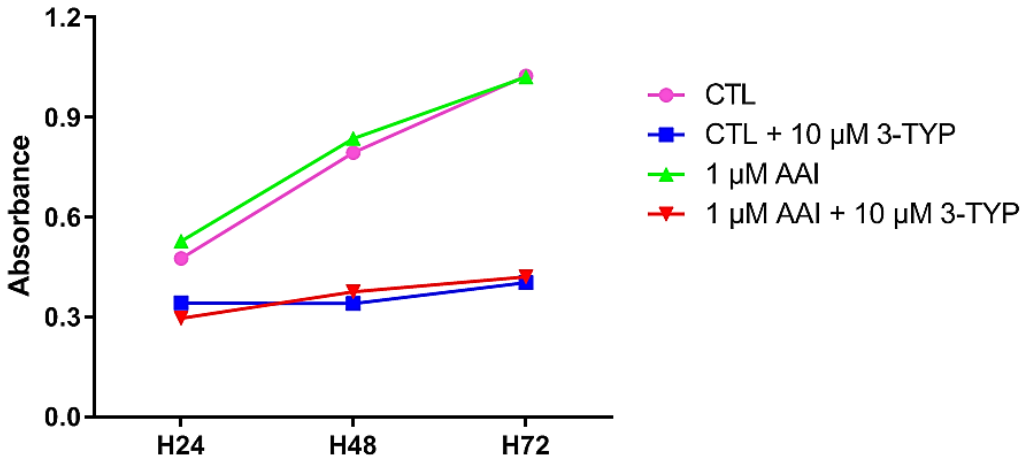

Figure 39: Effect of 3-TYP on HK-2 cell proliferation in the presence or in the absence of low concentration of AAI as assessed by MTT assay. *Cells were seeded at 100000 cells/well in 24-well culture dishes and incubated in the presence or in the absence (CTL) of 1 µM of AAI for 24, 48 or 72 h. As indicated, in some conditions, 10 µM of 3-TYP were added to cells for the same period of time. Results are expressed as absorbance unit and represent means of absorbance for three wells (n=1).*

d) Effects of 3-TYP, an inhibitor of SIRT3, on cell toxicity and proliferation

We wanted to test the putative effect of a SIRT3 inhibition on the sensitisation of HK-2 cells to AAI. There is no cytotoxicity observed for cells incubated in the presence of 3-TYP alone or with 3-TYP in the presence of AAI (Figure 38).

However, as shown in Figure 39, the proliferation of HK-2 cells incubated with or without AAI was inhibited by the presence of this inhibitor for the different timings. The impact was the same for control cells incubated in the presence of 10 µM of 3-TYP than for AAI-treated cells (1 µM) incubated in the presence of 3-TYP (Figure 39).

These results suggest that 3-TYP does not induce sensitisation of HK-2 cells to AAI, but 3-TYP slows down the cell proliferation.

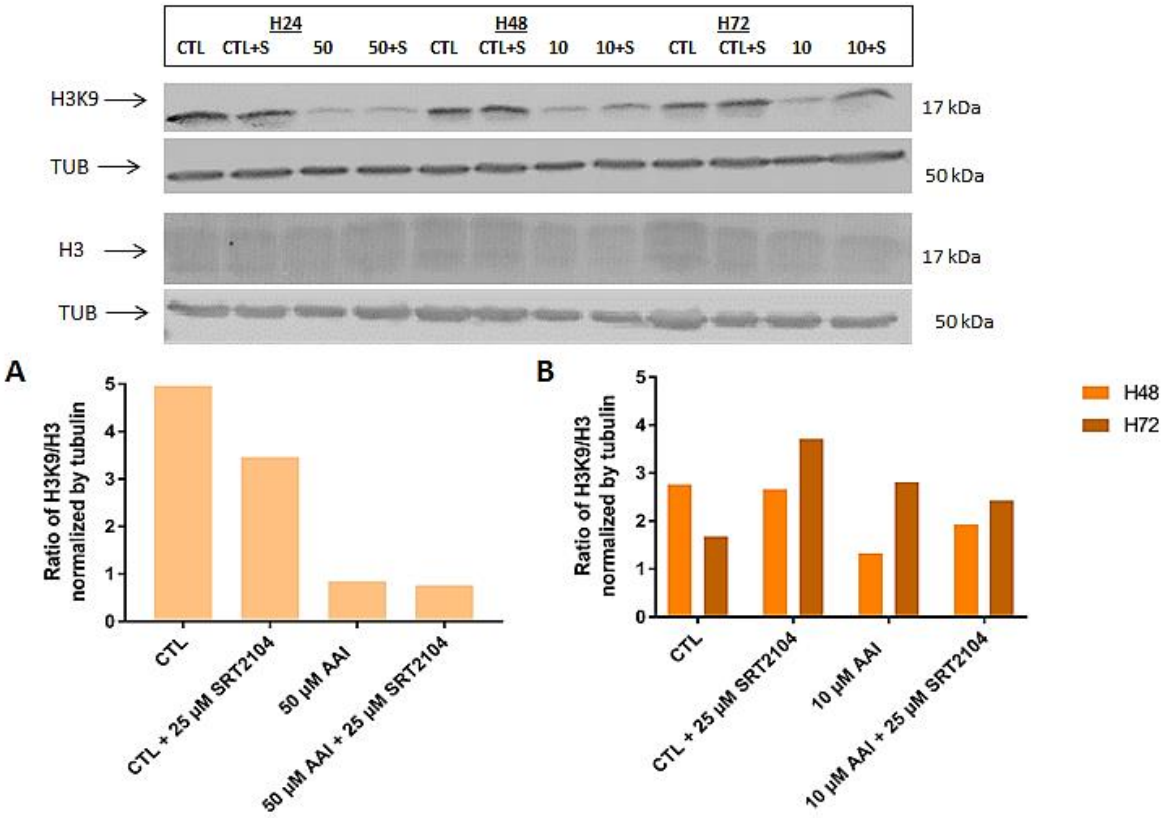

Figure 40: Effects of SRT2104 on the abundance of H3K9 (A for 24 h and B for 48 and 72 h). *Cells were seeded at 1.25x10^6 cells/T25 dishes and incubated in the presence (CTL + SRT2104) or in the absence (CTL) of SRT2104 and in the presence of 50 µM of AAI (50 µM) with (50 µM + SRT2104) or without (50 µM) additional 25 µM of SRT2104 for 24 h (A). For 48 or 72 h (B), cells were incubated in the presence (CTL + SRT2104) or in the absence (CTL) of SRT2104 and in the presence of 10 µM of AAI (10 µM) with (10 µM + SRT2104) or without (10 µM) additional 25 µM of SRT2104 (n=1). For this western blot analysis, 14 µg of proteins were loaded in the gel. Results are expressed as protein relative abundance and normalised by a-tubulin used as a loading control.*

The third experienced molecule is the SRT2104, an activator of SIRT1 activity.

e) Effects of SRT2104 on the acetylation status of H3, a sirtuin 1 target

As observed in Figure 40 A, SRT2104 induces a decrease in the H3 acetylation at the 24 h time-point, when comparing control cells and control cells with 25 µM of SRT2104. However, no modifications are observed, when comparing 50 µM of AAI and 50 µM of AAI with 25 µM of SRT2104 (Figure 40 A).

For 48 and 72 h, the expression is slightly modified by the use of SRT2104, when comparing 10 µM of AAI and 10 µM of AAI with 25 µM of SRT2104 (Figure 40 B).

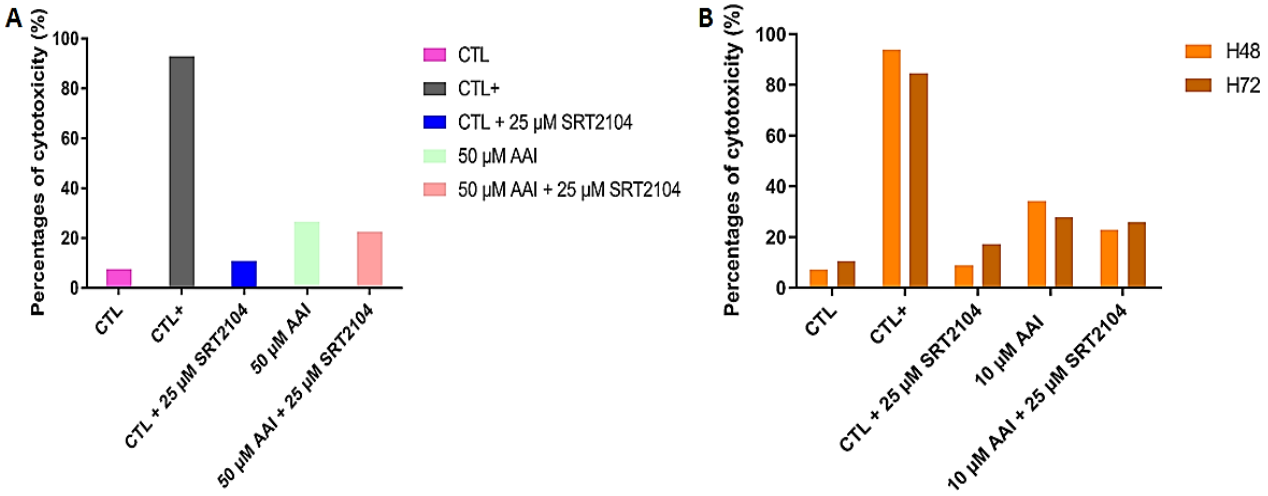

Figure 41: Effect of SRT2104 on HK-2 cytotoxicity in the presence or in the absence of high concentration of AAI as assessed by LDH (A for 24 h; B for 48 or 72 h) assay. *Cells were seeded at 100000 cells/well in 24-well culture dishes and incubated in the presence or in the absence (CTL) of 50 µM of AAI for 24 h (A) or in the presence or in the absence (CTL) of 10 µM of AAI for 48 or 72 h (B). As indicated, in some conditions, 25 µM of SRT2104 were added to cells for the same period of time. Results are expressed as means of percentages of cytotoxicity for three wells (n=1).*

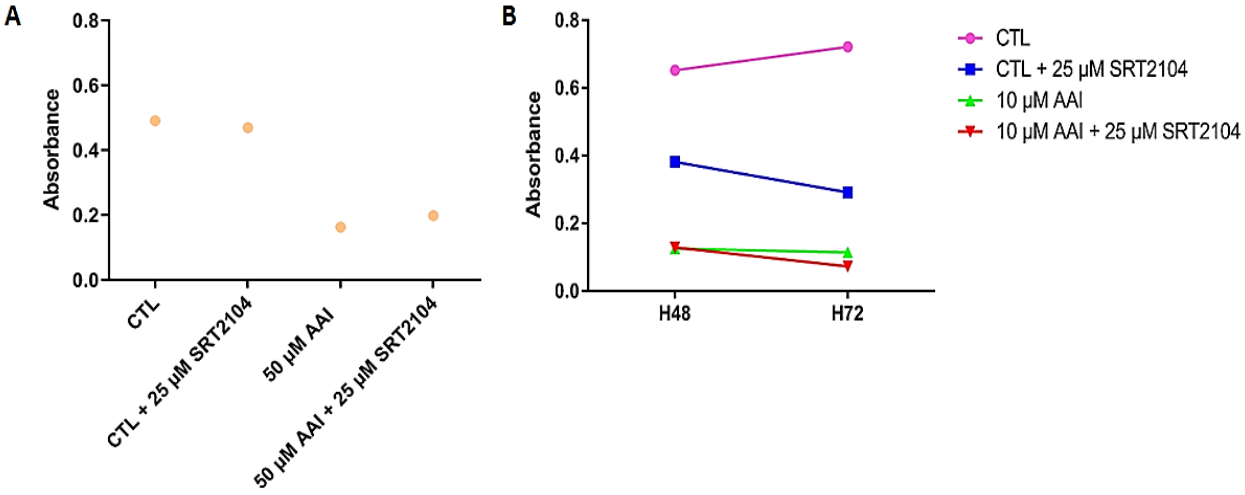

Figure 42: Effect of SRT2104 on HK-2 cell proliferation in the presence or in the absence of high concentration of AAI as assessed by MTT (A for 24 h; B for 48 or 72 h) assay. *Cells were seeded at 100000 cells/well in 24-well culture dishes and incubated in the presence or in the absence (CTL) of 50 µM of AAI for 24 h (A) or in the presence or in the absence (CTL) of 10 µM of AAI for 48 or 72 h (B). As indicated, in some conditions, 25 µM of SRT2104 were added to cells for the same period of time. Results are expressed as absorbance unit and represent means of absorbance for three wells (n=1).*

f) Effects of SRT2104, an activator of SIRT1, on cell toxicity and proliferation

Regarding the cytotoxicity, the molecule SRT2104 does not seem to be toxic at the tested concentration (25 µM) and does not change the increase in LDH released by cells incubated for 24 h with 50 µM of AAI (Figure 41 A). However, there is a slight increase (from 10 to 17 %) in the toxicity observed in cells incubated in the presence of 25 µM of SRT2104 for 72 h (Figure 41 B). A slight decrease (from 34 to 23 %) in the toxicity is only observed for 48 h, when comparing the release by cells incubated with 10 µM of AAI and cells incubated with 10 µM of AAI in the presence of 25 µM of SRT2104 (Figure 41 B).

As shown in Figure 42 A, the proliferation of HK-2 cells was not affected by the presence of this activator at a concentration of 25 µM during 24 h, but there is a decrease in cell proliferation at 48 and 72 h of incubation (Figure 42 B). In addition, the presence of SRT2104 in the culture media does not change the inhibitory effect of AAI on the proliferation of HK-2 cells incubated with 50 µM of AAI (for 24 h) or 10 µM of AAI (48 or 72 h) (Figure 42 A and 42 B, respectively).

As an effect has only been only seen for a 48 h-incubation time, it is very difficult and even impossible to draw a conclusion on the putative effect of the SIRT1 activator on the toxicity for HK-2 cells.

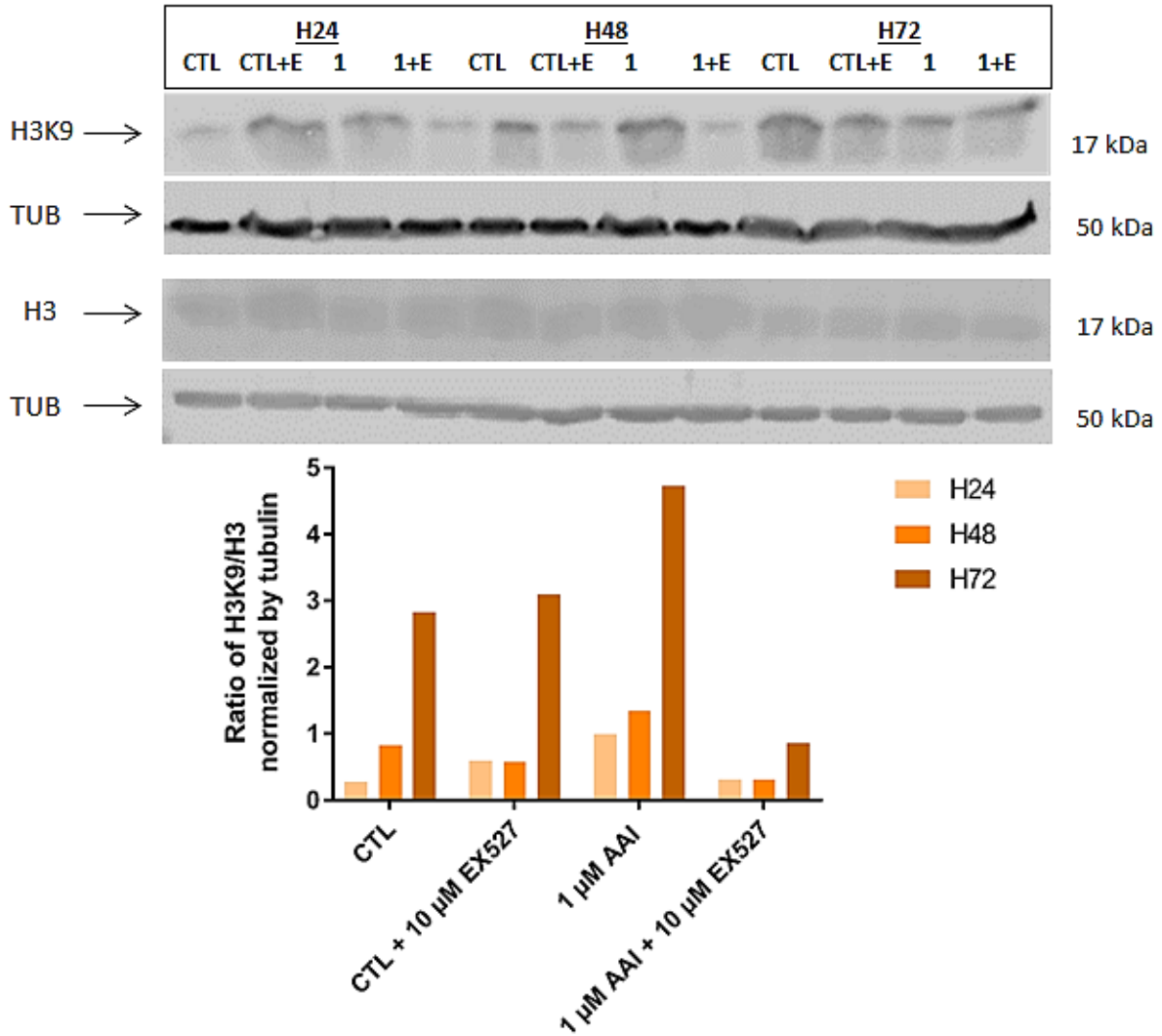

Figure 43: Effects of EX527 on the abundance of H3K9. *Cells were seeded at 1.25x10^6 cells/T25 dishes and incubated in the presence (CTL + EX527) or in the absence (CTL) of EX527 and in the presence of 1 µM of AAI (1 µM) with (1 µM + EX527) or without (1 µM) additional 10 µM of EX527 for 24, 48 or 72 h (n=1). For this western blot analysis, 14 µg of proteins were loaded in the gel. Results are expressed as protein relative abundance and normalised by a-tubulin used as a loading control.*

The fourth and last tested molecule is the EX527, an inhibitor of SIRT1 catalytic activity.

g) Effects of EX527 on the acetylation status of H3, a sirtuin 1 target

Despite the quality of the western blot, one can observe that the presence of 10 µM of EX527 does not change the acetylation level of the histone protein when compared to the abundance of the acetylated form of the H3 in control cells for 24, 48 or 72 h. In addition, a slight increase in the H3 acetylation is found in cells incubated with 1 µM of AAI for 24, 48 or 72 h (Figure 43). Surprisingly, the acetylation seems to be reduced in cells incubated with 1 µM of AAI in the presence of the SIRT1 inhibitor for each time tested in this work.

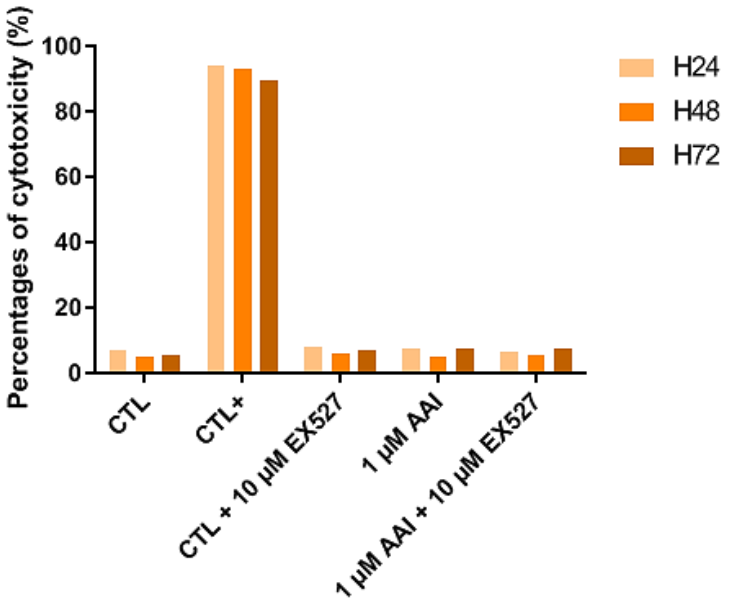

Figure 44: Effect of EX527 on HK-2 cytotoxicity in the presence or in the absence of low concentration of AAI as assessed by LDH assay. *Cells were seeded at 100000 cells/well in 24-well culture dishes and incubated in the presence or in the absence (CTL) of 1 µM of AAI for 24, 48 or 72 h. As indicated, in some conditions, 10 µM of EX527 were added to cells for the same period of time. Results are expressed as means of percentages of cytotoxicity for three wells (n=1).*

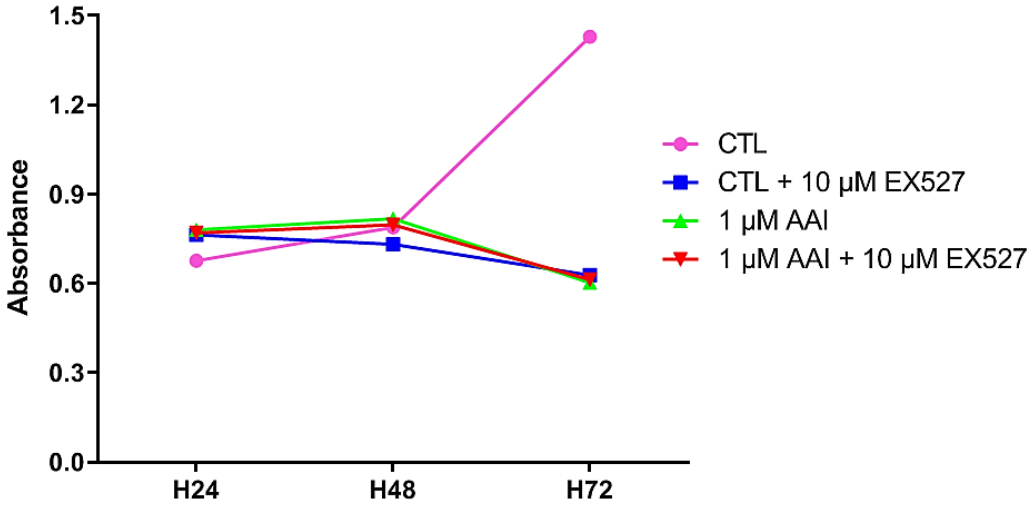

Figure 45: Effect of EX527 on HK-2 cell proliferation in the presence or in the absence of low concentration of AAI as assessed by MTT assay. *Cells were seeded at 100000 cells/well in 24-well culture dishes and incubated in the presence or in the absence (CTL) of 1 µM of AAI for 24, 48 or 72 h. As indicated, in some conditions, 10 µM of EX527 were added to cells for the same period of time. Results are expressed as absorbance unit and represent means of absorbance for three wells (n=1).*

h) Effects of EX527, an inhibitor of SIRT1, on cell toxicity and proliferation

The molecule used at 10 µM does not induce any toxicity of the cells and the presence of EX527 at the concentration used for this experiment does not affect the LDH release measured for cells incubated with 1 µM of AAI for 24, 48 or 72 h (Figure 44).

As shown in Figure 45, the proliferation of HK-2 cells is inhibited in the presence of either 1 µM of AAI or the inhibitor of SIRT1 at 10 µM, but the effect is mainly visible between 48 and 72 h. In addition, the presence of EX527 does not have any effect on the proliferation of cells incubated with 1 µM AAI (Figure 45).

These results suggest that EX527 does not induce a sensitisation of HK-2 cells to AAI toxicity.

Discussion

Aristolochic acid nephropathy (AAN) is a worldwide problem, which was initially reported as a consequence of the ingestion of slimming pills containing aristolochic acids (AA), genotoxic, cytotoxic and carcinogenic compounds (Romanov et al., 2015; Shibutani et al., 2007). This nephropathy leads to an extensive and progressive interstitial fibrosis, mainly located in the cortex and characterized by a tubular atrophy of proximal tubules and by inflammatory cells infiltration in the interstitial tissue (Debelle et al., 2008; Jadot et al., 2017b; Vanherweghem et al., 1993). Tubular atrophy is the consequence of the loss of integrity of the proximal tubular epithelial cells (PTEC). Indeed, it was described that PTEC constitute the preferential cell target of AA (Debelle et al., 2008; Depierreux et al., 1994; Nortier et al., 2015).

Therefore, for the experiments described in this work, we used human kidney-2 (HK-2) cells, which are PTEC from normal adult human kidney, immortalized by human papillomavirus-16 (HPV-16). Indeed, it is an immortalized human cell line realized from PTEC, which are the main target of AA. Moreover, HK-2 possess many characteristics which are found into physiological PTEC (Ryan et al., 1994).

Sirtuins (SIRT) 1 and 3 are NAD^+-dependent enzymes catalysing the deacetylation of many different substrates, which were already investigated in other kidney diseases models such as cisplatin- (Morigi et al., 2015), ischemia-reperfusion (I/R)- (Hasegawa et al., 2010) or sepsis-induced acute kidney injury (AKI) models (Zhao et al., 2016). In these models, SIRT1 was reported as protective against oxidative stress triggered by I/R in C57Bl/6 mice (Hasegawa et al., 2010). SIRT3 was also reported as protective against renal mitochondrial damages in cisplatin- and sepsis-induced AKI models (Morigi et al., 2015; Zhao et al., 2016).

As regards *in vitro* studies, focus of the present work, it was reported that overexpression of SIRT3 in normal rat kidney tubular epithelial (NRK52E) cells allows the suppression of angiotensin II (Ang II)-induced decrease in mitochondrial membrane potential. Ang II plays an important role in the progression of renal injury and most particularly in progressive renal fibrosis. He and his colleagues (2018) have also demonstrated that SIRT3 overexpression reversed the superoxide dismutase 2 (SOD2) accumulation induced by Ang II. This study suggests that SIRT3 might ameliorate mitochondrial dysfunction (He et al., 2018).

I/R can cause AKI and is characterized by, among others, increased production of ROS and mitochondrial damages. I/R injury (IRI), causing hypoxia/reoxygenation, increases cell death, reduces mitochondrial membrane potential and reduces SIRT3 expression in HK-2 cells. The expression of SIRT3 can be preserved and the mitochondrial alterations can be attenuated by the use of the dexmedetomidine molecule, an α2-adrenoreceptors agonist. This molecule inhibits mitochondrial disruption, likely by preventing mitochondrial membrane potential impairment and cytochrome c release. Therefore, *in vitro,* dexmedetomidine possesses protective effects and up-regulates SIRT3. In turn, SIRT3 contributes to dexmedetomidine effects by preserving mitochondrial structure and function (Si et al., 2018).

The first part of the present study was to determine the optimal concentration and incubation time in the presence of AAI that are minimizing the toxicity without cell death in order to study AAI effects on the expression of SIRT1 and SIRT3. It was observed that concentrations used in this work are not toxic, as compared to 10 µM which was used as a positive control because known as cytotoxic (Yang et al., 2010). Indeed, these authors showed that HK-2 cells incubated with a concentration of 14 µM of AAI arrest cell cycle at G2/M checkpoint after 48 h of incubation. In addition, Romanov and his colleagues have shown that

a concentration of AAI as low as 4 µM already induces activation of DNA damage signalling pathway and cell cycle arrest in G2/M phase (Romanov et al., 2015).

The significant decrease in the viability observed for 0.25 µM at 72 h time-point is difficult to interpret as the toxicity is not observed for higher concentrations and is most likely due to an experimental problem. In addition, at 10 µM, a decrease in cell proliferation was observed, when compared to control cells, as revealed by both MTT and LDH assays. The second tests confirm the first ones. In addition, it was demonstrated that only the toxic concentration of 10 µM does affect the proliferation of HK-2 cells for a 72 h-incubation.

In the second part of this work, ATP contents were determined in HK-2 cells exposed to AAI. Indeed, it was demonstrated that, in Sprague-Dawley rats intoxicated during 7 days with 5, 20 or 80 mg/kg/day, ATP contents decrease in a concentration-dependent manner (Jiang et al., 2013). A decrease in ATP contents was only observed for an AA concentration of 50 µM. Thus, subtoxic concentrations should not affect the morphology of the mitochondrial population in HK-2 cells. Therefore, the morphology of the mitochondrial population in HK-2 cells exposed to low concentrations of AAI should be analysed to confirm previous results and to establish a correlation between mitochondrial fragmentation and decrease in ATP contents. In the thesis of P. Mosseray, the mitochondrial network has been assessed after HK-2 incubation in the presence of 5 µM of AAI during 24, 48 or 72 h. The morphology of the mitochondrial population was not affected in these conditions (data not shown – unpublished data, P. Mosseray, ongoing PhD thesis).

As described in the introduction, AAI can possibly be secreted outside PTEC by multidrug resistance-associated proteins (MRP) 2 and 4 transporters and these transporters need ATP to carry organic anions (Hagos and Wolff, 2010). However, it appears that AAI decreases cellular ATP contents. This impairment could potentially induce a reduction of AAI transport in PTEC, leading to an accumulation of AAI and, finally, result in an increase in the toxicity induced by AA exposure (Hagos and Wolff, 2010).

A transient increase in ATP contents in cells, incubated in the presence of AAI in a range between 1 and 50 µM, was only observed for a 24 h-incubation. It might be supported by several explanations: 1) a potential activation of glycolysis to compensate a mitochondrial injury, 2) a reduction of ATP-consuming biological processes or an increase of the ATP production, in order to spare and preserve ATP contents, and 3) an attempt to adjust and compensate in response to stress. For example, related to the second point, on the one hand, it could be a reduction of ATP-consuming processes such as protein synthesis, RNA/DNA synthesis, Na^+ cycling, Ca^{2+} cycling and proton leak (Wieser and Krumschnabel, 2001). On the other hand, it could be a stimulation of the ATP production induced by the activation of Ca^{2+}-signalling cascade to compensate the energy loss induced by calcium signals. These hypotheses could be tested by the use of thapsigargin or ionomycin, two molecules able to increase the calcium concentration, in order to assess the effects of an increase of calcium-concentration on ATP contents (Voronina et al., 2010). Nevertheless, these preliminary results need to be confirmed.

Another perspective will be to assess the dynamin-related protein 1 (Drp1) phosphorylation level in HK-2 cells incubated in the presence of AAI (from 10 µM up to 50 µM). Indeed, it was demonstrated that, in cultured tubular cells, ATP depletion caused Drp1 translocation to mitochondria and mitochondrial fragmentation, leading to cytochrome c release and apoptosis (Tabara et al., 2014). In fact, during ATP depletion, Drp1 dephosphorylation at Ser637 was observed and contributes to mitochondrial fragmentation (Zhan et al., 2013).

Zheng and colleagues also reported defects in mitochondrial structure and a decrease in ATP levels in a model of iron overload in mesenchymal stromal cells (Zheng et al., 2018). It is also known that high concentrations of AAI (20 or 100 μM) induce an increase of ROS concentrations in NRK-52E (Wu et al., 2015). In fact, in a context of oxidative stress, mitochondrial fragmentation is correlated to reduced ATP levels in a model of iron overload (Zheng et al., 2018). Indeed, high ROS levels can lead to defects in mitochondrial structure by damaging the mitochondrial respiration chain and inhibiting the synthesis of DNA and proteins. In addition, mitochondrial dynamics by fusion and fission process are closely linked to cellular energy metabolism and the mitochondrial morphology can also be regulated by ATP concentration (Zheng et al., 2018). The results of the present study developed and based on another model will not confirm or invalidate the results developed by Zheng and his team. Therefore, the morphology of the mitochondrial population in HK-2 cells exposed to AAI should be analysed in a context of oxidative stress.

Several perspectives for future studies about mitochondria exist. For example, it is possible to measure mitochondrial respiration levels, which are a useful indicator of mitochondrial biogenesis. It could be performed by the assessment of the carbonyl cyanide-4 (tri-fluoromethoxy) phenylhydrazone (FCCP)-uncoupled respiration, a marker of maximal mitochondrial ETC activity of renal proximal tubular cells. It was reported that this respiration increased when the mitochondrial biogenesis increases (Whitaker et al., 2016). A second option would be the evaluation of the glutathione/oxidized glutathione (GSH/GSSG) ratio, as the oxidative stress and the mitochondrial damages seem be linked (Zheng et al., 2018) and as AAI-intoxication induces GSH depletion in rats (Yu et al., 2011). If this ratio increases, the oxidative stress decreases (Ouyang et al., 2019). We could determine this by a colorimetric assay based on the reaction between 5', 5'-dithiobis-2-nitrobenzoic acid (DTNB) and GSH to form 2-nitro-5-thiobenzoic acid (TNB), which exhibits maximum absorbance at 412 nm. The intensity of the absorbance is proportional to the GSH level in the sample (ScienceCell^{TM}, Research Laboratories). In addition, after I/R in HK-2 cells, it was observed a decrease of the expression levels of three mitochondrial respiratory chain genes: 1) adenosine triphosphate synthase subunit β (ATPS-β), 2) nicotinamide adenine dinucleotide: ubiquinone oxidoreductase subunit B8 (NDUFB8) and 3) cytochrome c oxidase subunit 1 (COX1). As these proteins are associated with mitochondrial damages, another possibility of additional study could be to assess protein levels of ATPS-β, NDUFB8 and/or COX1 by western blot analysis (Huang et al., 2018).

In the third part of the study, we aimed to investigate the expression levels of SIRT1 and SIRT3 in HK-2 cells exposed to subtoxic concentrations of AAI, at both protein and mRNA levels. No changes were observed in cells exposed to subtoxic concentrations, mainly for SIRT1. The expression of SIRT3 was more variable at protein level. The mechanisms responsible for a lower abundance of the enzymes with these different concentrations should be analysed in a future development.

It was reported that SIRT1 expression increases with the cellular accumulation of ROS (Hasegawa et al., 2008). In the current work, SIRT1 levels are unchanged; it is probable that the subtoxic concentrations induce no or minor oxidative stress. As regards SIRT3, this protein was studied in a model of cisplatin-induced AKI in C57BL/6J mice and is known to have antioxidant properties. This nephropathy model is characterized by tubular cells impairment and one of the major tubular cell injuries in this model is the mitochondrial dysfunction, which is manifested by oxidative stress, inflammation and cell damages. A decrease of SIRT3 expression was reported as exacerbating cisplatin-nephrotoxicity by an impairment of the mitochondrial morphology (Huang et al., 2019). The SIRT3 expression has no significant modification in the present study, but it would be interesting in the future to

evaluate oxidative stress level, by the assessment of SOD2 acetylation level for example, to know whether SIRT3 protects against this stress. Indeed, it was demonstrated that ROS levels are tightly linked with SIRT3 activity (Huang et al., 2019). The hypothesis, to confirm during upcoming studies, would be that the tested subtoxic concentrations should not trigger oxidative stress, inflammation or mitochondrial damages.

The last part of this work covered an assessment of the effect on the one hand on the acetylation of specific targets and on the other hand on the cytotoxicity and the cell proliferation, either by activation of SIRT1 and SIRT3 or by inhibition of these proteins, respectively by two molecules for inhibition and two molecules for activation.

First, we will discuss about the effects of an activator (Coumarin) and an inhibitor (3-TYP) of SIRT3 activity.

The selected activator of SIRT3 activity was the Coumarin. It is extended into the NAD^+ binding pocket of SIRT3 and it has been shown that Coumarin treatment in primary cultured cortical astrocytes isolated from rats induces several effects. This treatment, increasing SIRT3 activity, activates SOD2 and, by the way, reduces the mitochondrial superoxide level and the Lys68 acetylation of SOD2 (Lu et al., 2017). In this work, a slight decrease of the SOD2 acetylation was observed at 24 h, only in control cells incubated with 10 µM of Coumarin. An increase in the SOD2 acetylation was observed for 48 or 72 h in cells incubated in the presence of AAI alone, but this acetylation is decreased in cells exposed to 10 µM of AAI and 10 µM of Coumarin for 48 h-incubation. We can postulate that AAI would inactivate SOD2 and we can hypothesize an activation of SIRT3 by Coumarin, which can be confirmed by the measure of SIRT3 protein or mRNA expression and the SIRT3 activity level. Nevertheless, the activation of SIRT3 seems not sufficient to induce a protection against an exposure of 10 or 50 µM of AAI. Indeed, in this study, we observed a similar cytotoxicity in cells incubated with AAI alone compared to cells with AAI and Coumarin. For future experiments, the concentration of Coumarin could be increased in order to obtain a stronger effect of the activation of SIRT3.

The second molecule, 3-TYP, can inhibit SIRT3 activity to a similar extent compared to nicotinamide. It was reported that, after an exposure of HeLa cells during 1-6 h in the presence of 1 mM of this compound, the acetylation of mitochondrial proteins increases (Galli et al., 2012). After, it was shown in a model of cadmium-induced hepatotoxicity in human hepatocellular carcinoma cell line (HepG2) that an overexpression of *SIRT3* mRNA allows: 1) a reduction of the acetylated-SOD2, 2) an increase of SOD2 activity and, finally, 3) a decrease in mitochondrial ROS production. The activity of SOD2 is inversely proportional to its acetylation. In this study, the use of 50 µM of 3-TYP attenuated these modifications (Pi et al., 2015). In fact, SOD2 activity is mediated by SIRT3. SIRT3 reduces cellular levels of ROS according to the levels of SOD2, by the deacetylation of two critical lysine residues on SOD2, promoting then its antioxidative activity. More importantly, the ability of SOD2 to reduce cellular levels of ROS and to promote resistance to oxidative stress is enhanced considerably by SIRT3. Moreover, 3-TYP inhibits only the activity and not the expression of SIRT3 (Zeng et al., 2016). However, in this work, only a slight decrease of the SOD2 acetylation was observed for 24 or 48 h, in cells exposed to 10 µM of 3-TYP. Moreover, an increase of acetylated-SOD2 was observed in the presence of AAI alone for 48 h. Nevertheless and surprisingly, the inhibition of SIRT3 with this concentration of inhibitor does not increase the acetylation of SOD2. To know whether the concentration of 3-TYP used in this work is able to induce a modification of SIRT3, we could evaluate the enzymatic SIRT3 activity by a fluorimetric assay. And as regards the cell proliferation and the cytotoxicity, it appears that 10 µM of 3-TYP is not toxic for HK-2 cells for 24, 48 or 72 h-incubation periods, but that affects only the proliferation. No sensitisation was observed in this work.

Secondly, we will discuss about the effects of an activator (SRT2104) and an inhibitor (EX527) of SIRT1 activity.

The selected activator of SIRT1 activity was the SRT2104, our third molecule. Previously, it was reported that transgenic mice overexpression SIRT1 shows neuroprotection during Huntington disease (HD), whereas a deficiency of SIRT1 exacerbates the HD phenotype. Jiang and his team have used SRT2104 in N171-82Q HD mice in order to activate SIRT1 activity. They have provided the evidence that this compound ameliorates motor deficits, rescues brain atrophy, and extends survival in HD mouse model (Jiang et al., 2014). In addition, the use of 100 mg/kg of SRT2104 in C57BL/6 mice allows an overall downregulation of inflammatory pathways in muscles. Moreover, the exposure of 3 µM of SRT2104 on C2C12 myofibroblasts induces a lower acetylation of the p65 subunit of nuclear factor-kappa B (NF-κB), which suggests that SRT2104 suppresses NF-κB activity. And as regards oxidative stress, it is reported in the study of Mercken (2014) that, in an experimental model of atrophy using mice, short-term SRT2104 treatment preserves bone and muscle mass and that levels of SOD2 were increased only in muscles and not in liver (Mercken et al., 2014). It was also established that 100 mg/kg of SRT2104 reduces the expression of oxidative stress and inflammation markers in the aortic endothelium of C57BL/6 mice, in addition to the increase of SIRT1 protein expression (Wu et al., 2018). In this work, the histone H3 acetylation decreases at the 24 h for cells incubated in the presence of 25 µM of SRT2104. And at 48 or 72 h, the expression is slightly modified for cells exposed to both 10 µM of AAI and 25 µM of SRT2104. At 72 h-incubation, the acetylation of cells incubated with both AAI and SRT2104 increases irrationally. It might be due to the instability of the molecule and we have to keep in mind that these results come from only one experiment. In addition, the use of 25 µM of SRT2104 induces a decrease of the HK-2 cells proliferation between 48 and 72 h, accompanied by an increase of the cytotoxicity. But a slight protection, marked by a decrease of the toxicity, is observed at 48 h time-point, when comparing cells exposed to both 10 µM of AAI and 25 µM of SRT2104 and cells exclusively exposed to 10 µM of AAI. From these results, it is very difficult to draw a conclusion on the putative effect of SRT2104 on the cytotoxicity for HK-2 cells. In this case, the concentration of the activator could be increased in order to obtain a stronger effect or the stability of SRT2104 could be studied.

The last molecule, EX527, is a selective inhibitor of SIRT1's catalytic site (Solomon et al., 2006). It seems that, after formation of a complex SIRT1 - substrate, EX527 binds to this complex and blocks the product release (Blum et al., 2011). In a model of I/R injury in C57BL/6J mice evaluating the protective effect of melatonin treatment and its potential effects on the cerebral mitochondrial redox state and function, it was demonstrated that EX527 reversed the beneficial effects of melatonin by SIRT1 activity decrease (Yang et al., 2015). In addition, in the study of Solomon (2006), it was reported that the use of 1 µM of EX527 does not influence the cell proliferation (Solomon et al., 2006). In the present study, EX527 does not affect the acetylation of histone H3 for 24, 48 or 72 h-incubation periods, but the use of 1 µM of AAI increases the acetylation level. Surprisingly, in the presence of both AAI and EX527, a decrease of the H3 acetylation is observed. It might be due to an interaction between both molecules, which would inhibit the effect of EX527 alone. In addition, a decrease of the cell proliferation of control cells incubated in the presence of 10 µM of EX527 was only observed after 72 h, with or without 1 µM of AAI. That might suggest that cell proliferation is affected by the inhibition of the catalytic activity of SIRT1 and that 10 µM of EX527 does not induce a sensitisation of HK-2 cells to AAI cytotoxicity. In perspectives to this study, we might evaluate the SIRT1 expression to know whether the concentration of EX527 used is sufficient to modify the expression of the enzyme.

Moreover, additional *in vitro* experiments could be conducted by using other models, either microfluidic organs-on-chips (Chang et al., 2017) or integrated discrete multiple organ co-culture (IdMOC) (Gayathri et al., 2015). These co-culture methods allow to identify the toxicological mechanisms of hepatic and renal enzymes in the activation or detoxification of AAI in humans and the organ-organ interactions (Chang et al., 2017).

Both models have several advantages. The first is to get complete information about the induction or inhibition of hepatic Phase I and Phase II enzymes. As a result, the cellular changes that happened to the target organ - the kidney in this case - can be obtained simultaneously. Another is that the major pathway involved in the drug metabolism can be identified by the use of selective inhibitors or inducers of the selected specific pathway. A third is the identification of the drug-drug interaction, in which a drug can affect the metabolic stability of the other drug (Gayathri et al., 2015). In addition, these models also allow to mimic *in vivo* situation under *in vitro* condition (Gayathri et al., 2015).

The first approach, microfluidic organs-on-chips, is also called micro-physiological systems (MPS) and allows to link a human kidney MPS to a human liver MPS via polyethylene tubing. The kidney MPS recapitulates the renal proximal tubule by the use of primary PTEC (Chang et al., 2017). Primary human PTEC were seeded inside the MPS filled with type I collagen, allowing to adhere for 24 hours, and perfusion of media was initiated inside the lumen. Cells inside the lumen exhibited characteristic features of mature PTEC (Bajaj et al., 2018; Chang et al., 2017). This MPS 1) exhibits long-term viability (up to four weeks), 2) preserves polarized expression and function of proteins crucial for absorptive and secretory transport, 3) reacts to physiological stimuli and 4) performs biochemical synthetic activities (Weber et al., 2016). The second MPS is composed of human hepatic parenchymal cells (Chang et al., 2017). These cells possess high viabilities and are operational for long-term culture (Chang et al., 2017). In addition, they are the closest model for the liver *in vivo* (Gayathri et al., 2015) and have human hepatic metabolism capacity (Li, 2007b). Indeed, they maintained various intact cell properties such as the intact cell membrane with active transporter functions, complete and uninterrupted metabolic pathways, and metabolic enzymes and cofactors at physiologically relevant concentrations (Li, 2015).

The second device allows the use of primary cells or organ slices, multiple organ interaction and analysis of metabolic cytotoxicity. The concept is the following: a culture plate possesses chambers containing wells, which have six small inner wells. This provide a culture with six different cell types, three cell types in duplicate or two cell types in triplicate. The diverse cell types, after culturing in their own media, are interconnected by filling the chamber with a universal medium (Gayathri et al., 2015), which is akin to the blood circulation connecting organs in the human body (Li, 2007a). In this case, cell types could be the same that for the MPS: primary PTEC and hepatocytes.

By the use of several cell types simultaneously, IdMOC and MPS are less time-consuming methods (Gayathri et al., 2015). Moreover, these approaches have the ability to evaluate each cell type separately for cytotoxicity after co-culturing and under near-identical experimental conditions (Li, 2007b; Li, 2015) and well-to-well or plate-to-plate differences are eliminated for the IdMOC (Li, 2009).

After the establishment of one of these models of co-culture, it might be possible to investigate the effects induced by AAI on liver and renal cells with regard to inflammation, oxidative stress or mitochondrial damages in order to mimic most the complete metabolization of AAI.

Finally, additional *in vivo* experiments could be performed. The AAN mice model, previously developed in our laboratory (Jadot et al., 2017a), should be tested in *SIRT3*$^{-/-}$ mice or in transgenic mice overexpressing *SIRT3*.

References

Abe, K., and N. Matsuki. 2000. Measurement of cellular 3-(4,5-dimethylthiazol-2-yl)-2,5-diphenyltetrazolium bromide (MTT) reduction activity and lactate dehydrogenase release using MTT. *Neurosci Res*. 38:325-329.

Allen, M., P. Millett, E. Dawes, and N. Rushton. 1994. Lactate dehydrogenase activity as a rapid and sensitive test for the quantification of cell numbers in vitro. *Clin Mater*. 16:189-194.

Austin, S., and J. St-Pierre. 2012. PGC1alpha and mitochondrial metabolism--emerging concepts and relevance in ageing and neurodegenerative disorders. *J Cell Sci*. 125:4963-4971.

Babu, E., M. Takeda, R. Nishida, R. Noshiro-Kofuji, M. Yoshida, S. Ueda, T. Fukutomi, N. Anzai, and H. Endou. 2010. Interactions of human organic anion transporters with aristolochic acids. *Journal of pharmacological sciences*. 113:192-196.

Bajaj, P., S.K. Chowdhury, R. Yucha, E.J. Kelly, and G. Xiao. 2018. Emerging Kidney Models to Investigate Metabolism, Transport and Toxicity of Drugs and Xenobiotics. *Drug Metab Dispos*.

Bakhiya, N., V.M. Arlt, A. Bahn, G. Burckhardt, D.H. Phillips, and H. Glatt. 2009. Molecular evidence for an involvement of organic anion transporters (OATs) in aristolochic acid nephropathy. *Toxicology*. 264:74-79.

Baudoux, T.E., A.A. Pozdzik, V.M. Arlt, E.G. De Prez, M.H. Antoine, N. Quellard, J.M. Goujon, and J.L. Nortier. 2012. Probenecid prevents acute tubular necrosis in a mouse model of aristolochic acid nephropathy. *Kidney Int*. 82:1105-1113.

Benigni, A., L. Perico, and D. Macconi. 2016. Mitochondrial Dynamics Is Linked to Longevity and Protects from End-Organ Injury: The Emerging Role of Sirtuin 3. *Antioxid Redox Signal*. 25:185-199.

Bethea, M., and D.T. Forman. 1990. Beta 2-microglobulin: its significance and clinical usefulness. *Annals of clinical and laboratory science*. 20:163-168.

Biomnis. 2012. Retinol-binding protein.

Blum, C.A., J.L. Ellis, C. Loh, P.Y. Ng, R.B. Perni, and R.L. Stein. 2011. SIRT1 modulation as a novel approach to the treatment of diseases of aging. *Journal of medicinal chemistry*. 54:417-432.

Bustin, S.A., V. Benes, J.A. Garson, J. Hellemans, J. Huggett, M. Kubista, R. Mueller, T. Nolan, M.W. Pfaffl, G.L. Shipley, J. Vandesompele, and C.T. Wittwer. 2009. The MIQE guidelines: minimum information for publication of quantitative real-time PCR experiments. *Clinical chemistry*. 55:611-622.

Callard, P. 2016. Eléments d'histologie rénale. *In* Physiologie et physiopathologies rénales. CUEN.

Carafa, V., A. Nebbioso, and L. Altucci. 2012. Sirtuins and disease: the road ahead. *Front Pharmacol*. 3:4.

Chang, S.Y., E.J. Weber, V.S. Sidorenko, A. Chapron, C.K. Yeung, C. Gao, Q. Mao, D. Shen, J. Wang, T.A. Rosenquist, K.G. Dickman, T. Neumann, A.P. Grollman, E.J. Kelly, J. Himmelfarb, and D.L. Eaton. 2017. Human liver-kidney model elucidates the mechanisms of aristolochic acid nephrotoxicity. *JCI Insight*. 2.

Chen, Y.Y., S.Y. Chiang, H.C. Wu, S.T. Kao, C.Y. Hsiang, T.Y. Ho, and J.G. Lin. 2010. Microarray analysis reveals the inhibition of nuclear factor-kappa B signaling by aristolochic acid in normal human kidney (HK-2) cells. *Acta Pharmacol Sin*. 31:227-236.

Coll, E., A. Botey, L. Alvarez, E. Poch, L. Quinto, A. Saurina, M. Vera, C. Piera, and A. Darnell. 2000. Serum cystatin C as a new marker for noninvasive estimation of glomerular filtration rate and as a marker for early renal impairment. *Am J Kidney Dis*. 36:29-34.

Cooper, G. 2000. The cell: a molecular approach.

Cooper, H.M., J.Y. Huang, E. Verdin, and J.N. Spelbrink. 2009. A new splice variant of the mouse SIRT3 gene encodes the mitochondrial precursor protein. *PLoS One*. 4:e4986.

Debelle, F.D., J.L. Vanherweghem, and J.L. Nortier. 2008. Aristolochic acid nephropathy: a worldwide problem. *Kidney Int*. 74:158-169.

Depierreux, M., B. Van Damme, K. Vanden Houte, and J.L. Vanherweghem. 1994. Pathologic aspects of a newly described nephropathy related to the prolonged use of Chinese herbs. *Am J Kidney Dis*. 24:172-180.

Finkel, T., C.X. Deng, and R. Mostoslavsky. 2009. Recent progress in the biology and physiology of sirtuins. *Nature*. 460:587-591.

Flick, F., and B. Luscher. 2012. Regulation of sirtuin function by posttranslational modifications. *Front Pharmacol*. 3:29.

Galli, U., O. Mesenzani, C. Coppo, G. Sorba, P.L. Canonico, G.C. Tron, and A.A. Genazzani. 2012. Identification of a sirtuin 3 inhibitor that displays selectivity over sirtuin 1 and 2. *European journal of medicinal chemistry*. 55:58-66.

Galvan, D.L., N.H. Green, and F.R. Danesh. 2017. The hallmarks of mitochondrial dysfunction in chronic kidney disease. *Kidney Int*. 92:1051-1057.

Gayathri, L., D. Dhanasekaran, and M.A. Akbarsha. 2015. Scientific concepts and applications of integrated discrete multiple organ co-culture technology. *Journal of pharmacology & pharmacotherapeutics*. 6:63-70.

Gueutin, V., G. Deray, and C. Isnard-Bagnis. 2012. [Renal physiology]. *Bull Cancer*. 99:237-249.

Hagos, Y., and N.A. Wolff. 2010. Assessment of the role of renal organic anion transporters in drug-induced nephrotoxicity. *Toxins (Basel)*. 2:2055-2082.

Hasegawa, K., S. Wakino, K. Yoshioka, S. Tatematsu, Y. Hara, H. Minakuchi, K. Sueyasu, N. Washida, H. Tokuyama, M. Tzukerman, K. Skorecki, K. Hayashi, and H. Itoh. 2010. Kidney-specific overexpression of Sirt1 protects against acute kidney injury by retaining peroxisome function. *J Biol Chem*. 285:13045-13056.

Hasegawa, K., S. Wakino, K. Yoshioka, S. Tatematsu, Y. Hara, H. Minakuchi, N. Washida, H. Tokuyama, K. Hayashi, and H. Itoh. 2008. Sirt1 protects against oxidative stress-induced renal tubular cell apoptosis by the bidirectional regulation of catalase expression. *Biochem Biophys Res Commun*. 372:51-56.

He, P., Z. Li, Z. Yue, H. Gao, G. Feng, P. Wang, Y. Huang, W. Luo, H. Hong, L. Liang, S. Chen, and P. Liu. 2018. SIRT3 prevents angiotensin II-induced renal tubular epithelial-mesenchymal transition by ameliorating oxidative stress and mitochondrial dysfunction. *Molecular and cellular endocrinology*. 460:1-13.

Houtkooper, R.H., E. Pirinen, and J. Auwerx. 2012. Sirtuins as regulators of metabolism and healthspan. *Nat Rev Mol Cell Biol*. 13:225-238.

Huang, L.L., R.T. Long, G.P. Jiang, X. Jiang, H. Sun, H. Guo, and X.H. Liao. 2018. Augmenter of liver regeneration promotes mitochondrial biogenesis in renal ischemia-reperfusion injury. *Apoptosis : an international journal on programmed cell death*. 23:695-706.

Huang, S., and A.H. Millar. 2013. Succinate dehydrogenase: the complex roles of a simple enzyme. *Current opinion in plant biology*. 16:344-349.

Huang, Z., Q. Li, Y. Yuan, C. Zhang, L. Wu, X. Liu, W. Cao, H. Guo, S. Duan, X. Xu, B. Zhang, and C. Xing. 2019. Renalase attenuates mitochondrial fission in cisplatin-induced acute kidney injury via modulating sirtuin-3. *Life sciences*. 222:78-87.

Iwata, M., and R.A. Zager. 1996. Myoglobin inhibits proliferation of cultured human proximal tubular (HK-2) cells. *Kidney Int*. 50:796-804.

Jadot, I., V. Colombaro, B. Martin, I. Habsch, O. Botton, J. Nortier, A.E. Decleves, and N. Caron. 2017a. Restored nitric oxide bioavailability reduces the severity of acute-to-chronic transition in a mouse model of aristolochic acid nephropathy. *PLoS One*. 12:e0183604.

Jadot, I., A.E. Decleves, J. Nortier, and N. Caron. 2017b. An Integrated View of Aristolochic Acid Nephropathy: Update of the Literature. *Int J Mol Sci*. 18.

Jiang, M., J. Zheng, Q. Peng, Z. Hou, J. Zhang, S. Mori, J.L. Ellis, G.P. Vlasuk, H. Fries, V. Suri, and W. Duan. 2014. Sirtuin 1 activator SRT2104 protects Huntington's disease mice. *Annals of clinical and translational neurology*. 1:1047-1052.

Jiang, Z., Q. Bao, L. Sun, X. Huang, T. Wang, S. Zhang, H. Li, and L. Zhang. 2013. Possible role of mtDNA depletion and respiratory chain defects in aristolochic acid I-induced acute nephrotoxicity. *Toxicol Appl Pharmacol*. 266:198-203.

Jorens, P.G., Y. Sibille, N.J. Goulding, F.J. van Overveld, A.G. Herman, L. Bossaert, W.A. De Backer, R. Lauwerys, R.J. Flower, and A. Bernard. 1995. Potential role of Clara cell protein, an endogenous phospholipase A2 inhibitor, in acute lung injury. *Eur Respir J*. 8:1647-1653.

Kabanda, A., M. Jadoul, R. Lauwerys, A. Bernard, and C. van Ypersele de Strihou. 1995. Low molecular weight proteinuria in Chinese herbs nephropathy. *Kidney Int*. 48:1571-1576.

Kincaid, B., and E. Bossy-Wetzel. 2013. Forever young: SIRT3 a shield against mitochondrial meltdown, aging, and neurodegeneration. *Frontiers in aging neuroscience*. 5:48.

Kitada, M., S. Kume, A. Takeda-Watanabe, K. Kanasaki, and D. Koya. 2013. Sirtuins and renal diseases: relationship with aging and diabetic nephropathy. *Clin Sci (Lond)*. 124:153-164.

Kupis, W., J. Palyga, E. Tomal, and E. Niewiadomska. 2016. The role of sirtuins in cellular homeostasis. *J Physiol Biochem*. 72:371-380.

Lacour, B. 2013. Physiologie du rein et bases physiopathologiques des maladies rénales. *In* Revue francophone des laboratoires. 25-37.

Lebeau, C., V.M. Arlt, H.H. Schmeiser, A. Boom, P.J. Verroust, O. Devuyst, and R. Beauwens. 2001. Aristolochic acid impedes endocytosis and induces DNA adducts in proximal tubule cells. *Kidney Int*. 60:1332-1342.

Lebeau, C., F.D. Debelle, V.M. Arlt, A. Pozdzik, E.G. De Prez, D.H. Phillips, M.M. Deschodt-Lanckman, J.L. Vanherweghem, and J.L. Nortier. 2005. Early proximal tubule injury in experimental aristolochic acid nephropathy: functional and histological studies. *Nephrol Dial Transplant*. 20:2321-2332.

Li, A.P. 2007a. Human hepatocytes: isolation, cryopreservation and applications in drug development. *Chemico-biological interactions*. 168:16-29.

Li, A.P. 2007b. In Vitro Evaluation of Human Xenobiotic Toxicity: Scientific Concepts and the Novel Integrated Discrete Multiple Cell CoCulture (IdMOC) Technology. *ALTEX*.

Li, A.P. 2009. The use of the Integrated Discrete Multiple Organ Co-culture (IdMOC) system for the evaluation of multiple organ toxicity. *Alternatives to laboratory animals : ATLA*. 37:377-385.

Li, A.P. 2015. Evaluation of Adverse Drug Properties with Cryopreserved Human Hepatocytes and the Integrated Discrete Multiple Organ Co-culture (IdMOC(TM)) System. *Toxicological research*. 31:137-149.

Li, L., M. Dong, and X.G. Wang. 2016. The Implication and Significance of Beta 2 Microglobulin: A Conservative Multifunctional Regulator. *Chinese medical journal*. 129:448-455.

Li, Q., F. Lei, Y. Tang, J.S. Pan, Q. Tong, Y. Sun, and D. Sheikh-Hamad. 2018. Megalin mediates plasma membrane to mitochondria cross-talk and regulates mitochondrial metabolism. *Cellular and molecular life sciences : CMLS*. 75:4021-4040.

Li, Y., Z. Liu, X. Guo, J. Shu, Z. Chen, and L. Li. 2006. Aristolochic acid I-induced DNA damage and cell cycle arrest in renal tubular epithelial cells in vitro. *Arch Toxicol*. 80:524-532.

Lin, X., X. Duan, Y.Y. Liang, Y. Su, K.H. Wrighton, J. Long, M. Hu, C.M. Davis, J. Wang, F.C. Brunicardi, Y. Shi, Y.G. Chen, A. Meng, and X.H. Feng. 2006. PPM1A functions as a Smad phosphatase to terminate TGFbeta signaling. *Cell*. 125:915-928.

Liu, M.C., T.H. Lin, T.S. Wu, F.Y. Yu, C.C. Lu, and B.H. Liu. 2011. Aristolochic acid I suppressed iNOS gene expression and NF-kappaB activation in stimulated macrophage cells. *Toxicol Lett*. 202:93-99.

Lowry, O.H., N.J. Rosebrough, A.L. Farr, and R.J. Randall. 1951. Protein measurement with the Folin phenol reagent. *J Biol Chem*. 193:265-275.

Lu, J., H. Zhang, X. Chen, Y. Zou, J. Li, L. Wang, M. Wu, J. Zang, Y. Yu, W. Zhuang, Q. Xia, and J. Wang. 2017. A small molecule activator of SIRT3 promotes deacetylation and activation of manganese superoxide dismutase. *Free Radic Biol Med*. 112:287-297.

Mercken, E.M., S.J. Mitchell, A. Martin-Montalvo, R.K. Minor, M. Almeida, A.P. Gomes, M. Scheibye-Knudsen, H.H. Palacios, J.J. Licata, Y. Zhang, K.G. Becker, H. Khraiwesh, J.A. Gonzalez-Reyes, J.M. Villalba, J.A. Baur, P. Elliott, C. Westphal, G.P. Vlasuk, J.L. Ellis, D.A. Sinclair, M. Bernier, and R. de Cabo. 2014. SRT2104 extends survival of male mice on a standard diet and preserves bone and muscle mass. *Aging cell*. 13:787-796.

Morigi, M., L. Perico, C. Rota, L. Longaretti, S. Conti, D. Rottoli, R. Novelli, G. Remuzzi, and A. Benigni. 2015. Sirtuin 3-dependent mitochondrial dynamic improvements protect against acute kidney injury. *J Clin Invest*. 125:715-726.

Mosseray, P. 2018. ETUDE DES SIRTUINES 1 ET 3 DANS DES MODELES IN VIVO ET IN VITRO DE NEPHROTOXICITE AUX ACIDES ARISTOLOCHIQUES. UNamur, editor.

Mount, D.B. 2014. Thick ascending limb of the loop of Henle. *Clinical journal of the American Society of Nephrology : CJASN*. 9:1974-1986.

Murty, M.S., U.K. Sharma, V.B. Pandey, and S.B. Kankare. 2013. Serum cystatin C as a marker of renal function in detection of early acute kidney injury. *Indian J Nephrol*. 23:180-183.

Mussap, M., and M. Plebani. 2004. Biochemistry and clinical role of human cystatin C. *Crit Rev Clin Lab Sci*. 41:467-550.

Nogueiras, R., K.M. Habegger, N. Chaudhary, B. Finan, A.S. Banks, M.O. Dietrich, T.L. Horvath, D.A. Sinclair, P.T. Pfluger, and M.H. Tschop. 2012. Sirtuin 1 and sirtuin 3: physiological modulators of metabolism. *Physiol Rev*. 92:1479-1514.

Nortier, J., A. Pozdzik, T. Roumeguere, and J.L. Vanherweghem. 2015. [Aristolochic acid nephropathy ("Chinese herb nephropathy")]. *Nephrol Ther*. 11:574-588.

Ouyang, J., Z. Zeng, H. Fang, F. Li, X. Zhang, and W. Tan. 2019. SIRT3 Inactivation Promotes Acute Kidney Injury Through Elevated Acetylation of SOD2 and p53. *The Journal of surgical research*. 233:221-230.

Penders, J., and J.R. Delanghe. 2004. Alpha 1-microglobulin: clinical laboratory aspects and applications. *Clin Chim Acta*. 346:107-118.

Perico, L., M. Morigi, and A. Benigni. 2016. Mitochondrial Sirtuin 3 and Renal Diseases. *Nephron*. 134:14-19.

Pi, H., S. Xu, R.J. Reiter, P. Guo, L. Zhang, Y. Li, M. Li, Z. Cao, L. Tian, J. Xie, R. Zhang, M. He, Y. Lu, C. Liu, W. Duan, Z. Yu, and Z. Zhou. 2015. SIRT3-SOD2-mROS-dependent autophagy in cadmium-induced hepatotoxicity and salvage by melatonin. *Autophagy*. 11:1037-1051.

Polak-Jonkisz, D., K. Laszki-Szczachor, L. Rehan, W. Pilecki, H. Filipowski, and M. Sobieszczanska. 2013. Nephroprotective action of sirtuin 1 (SIRT1). *J Physiol Biochem*. 69:957-961.

Prakash, S., et al. 2011. Biological cytotoxicity evaluation of spiro[azetidine-2, 3'-indole]-2', 4(1'H)-dione derivatives for anti-lung and anti-breast cancer activity *Der Pharmacia Lettre*. 3:236-243.

Qi, X., Y. Cai, L. Gong, L. Liu, F. Chen, Y. Xiao, X. Wu, Y. Li, X. Xue, and J. Ren. 2007. Role of mitochondrial permeability transition in human renal tubular epithelial cell death induced by aristolochic acid. *Toxicol Appl Pharmacol*. 222:105-110.

Romanov, V., T.C. Whyard, W.C. Waltzer, A.P. Grollman, and T. Rosenquist. 2015. Aristolochic acid-induced apoptosis and G2 cell cycle arrest depends on ROS generation and MAP kinases activation. *Arch Toxicol*. 89:47-56.

Ryan, M.J., G. Johnson, J. Kirk, S.M. Fuerstenberg, R.A. Zager, and B. Torok-Storb. 1994. HK-2: an immortalized proximal tubule epithelial cell line from normal adult human kidney. *Kidney Int*. 45:48-57.

Samarakoon, R., A. Rehfuss, N.S. Khakoo, L.L. Falke, A.D. Dobberfuhl, S. Helo, J.M. Overstreet, R. Goldschmeding, and P.J. Higgins. 2016. Loss of expression of protein phosphatase magnesium-dependent 1A during kidney injury promotes fibrotic maladaptive repair. *FASEB journal : official publication of the Federation of American Societies for Experimental Biology*. 30:3308-3320.

Sansoe, G., M. Aragno, R. Mastrocola, J.C. Cutrin, S. Silvano, G. Mengozzi, A. Smedile, F. Rosina, O. Danni, and M. Rizzetto. 2006. Overexpression of kidney neutral endopeptidase (EC 3.4.24.11) and renal function in experimental cirrhosis. *Am J Physiol Renal Physiol*. 290:F1337-1343.

Schmeiser, H.H., C.A. Bieler, M. Wiessler, C. van Ypersele de Strihou, and J.P. Cosyns. 1996. Detection of DNA adducts formed by aristolochic acid in renal tissue from patients with Chinese herbs nephropathy. *Cancer Res*. 56:2025-2028.

Shibutani, S., H. Dong, N. Suzuki, S. Ueda, F. Miller, and A.P. Grollman. 2007. Selective toxicity of aristolochic acids I and II. *Drug Metab Dispos*. 35:1217-1222.

Shui, G.X., D. Sang, X. Yin, Y. Cai, and W. Sun. 2017. Dahuang Fuzi Decoction Attenuates Renal Fibrosis and Ameliorates Mitochondrial Dysfunction in Chronic Aristolochic Acid Nephropathy. *Evidence-based complementary and alternative medicine : eCAM*. 2017:9536458.

Si, Y., H. Bao, L. Han, L. Chen, L. Zeng, L. Jing, Y. Xing, and Y. Geng. 2018. Dexmedetomidine attenuation of renal ischaemia-reperfusion injury requires sirtuin 3 activation. *British journal of anaesthesia*. 121:1260-1271.

Solomon, J.M., R. Pasupuleti, L. Xu, T. McDonagh, R. Curtis, P.S. DiStefano, and L.J. Huber. 2006. Inhibition of SIRT1 catalytic activity increases p53 acetylation but does not alter cell survival following DNA damage. *Mol Cell Biol*. 26:28-38.

Stiborova, M., V.M. Arlt, and H.H. Schmeiser. 2017. DNA Adducts Formed by Aristolochic Acid Are Unique Biomarkers of Exposure and Explain the Initiation Phase of Upper Urothelial Cancer. *Int J Mol Sci*. 18.

Sun, W., Y. Yu, G. Dotti, T. Shen, X. Tan, B. Savoldo, A.K. Pass, M. Chu, D. Zhang, X. Lu, S. Fu, X. Lin, and J. Yang. 2009. PPM1A and PPM1B act as IKKbeta phosphatases to terminate TNFalpha-induced IKKbeta-NF-kappaB activation. *Cell Signal*. 21:95-102.

Tabara, L.C., J. Poveda, C. Martin-Cleary, R. Selgas, A. Ortiz, and M.D. Sanchez-Nino. 2014. Mitochondria-targeted therapies for acute kidney injury. *Expert reviews in molecular medicine*. 16:e13.

van Meerloo, J., G.J. Kaspers, and J. Cloos. 2011. Cell sensitivity assays: the MTT assay. *Methods Mol Biol*. 731:237-245.

Vanherweghem, J.L., and E. al. 2003. Aristolochic acid nephropathy after Chinese herbal remedies. *In* Clinical nephrotoxins. Renal injury from drugs and chemicals. G.A.P. M.E. De Broe, W.M. Bennett, G.A. Verpooten, editor. 579-589.

Vanherweghem, J.L., M. Depierreux, C. Tielemans, D. Abramowicz, M. Dratwa, M. Jadoul, C. Richard, D. Vandervelde, D. Verbeelen, R. Vanhaelen-Fastre, and et al. 1993. Rapidly progressive interstitial renal fibrosis in young women: association with slimming regimen including Chinese herbs. *Lancet*. 341:387-391.

Verroust, P.J., R. Kozyraki, T.G. Hammond, S.K. Moestrup, and E.I. Christensen. 2000. Physiopathologic role of cubilin and megalin. *Advances in nephrology from the Necker Hospital*. 30:127-145.

Voronina, S.G., S.L. Barrow, A.W. Simpson, O.V. Gerasimenko, G. da Silva Xavier, G.A. Rutter, O.H. Petersen, and A.V. Tepikin. 2010. Dynamic changes in cytosolic and mitochondrial ATP levels in pancreatic acinar cells. *Gastroenterology*. 138:1976-1987.

Weber, E.J., A. Chapron, B.D. Chapron, J.L. Voellinger, K.A. Lidberg, C.K. Yeung, Z. Wang, Y. Yamaura, D.W. Hailey, T. Neumann, D.D. Shen, K.E. Thummel, K.A. Muczynski, J. Himmelfarb, and E.J. Kelly. 2016. Development of a microphysiological model of human kidney proximal tubule function. *Kidney Int*. 90:627-637.

Whitaker, R.M., D. Corum, C.C. Beeson, and R.G. Schnellmann. 2016. Mitochondrial Biogenesis as a Pharmacological Target: A New Approach to Acute and Chronic Diseases. *Annual review of pharmacology and toxicology*. 56:229-249.

Wieser, W., and G. Krumschnabel. 2001. Hierarchies of ATP-consuming processes: direct compared with indirect measurements, and comparative aspects. *Biochem J*. 355:389-395.

Wu, H., J. Wu, S. Zhou, W. Huang, Y. Li, H. Zhang, J. Wang, and Y. Jia. 2018. SRT2104 attenuates diabetes-induced aortic endothelial dysfunction via inhibition of P53. *The Journal of endocrinology*. 237:1-14.

Wu, T.K., C.W. Wei, Y.R. Pan, S.H. Cherng, W.J. Chang, H.F. Wang, and Y.L. Yu. 2015. Vitamin C attenuates the toxic effect of aristolochic acid on renal tubular cells via decreasing oxidative stressmediated cell death pathways. *Mol Med Rep*. 12:6086-6092.

Xue, X., L.K. Gong, K. Maeda, Y. Luan, X.M. Qi, Y. Sugiyama, and J. Ren. 2011. Critical role of organic anion transporters 1 and 3 in kidney accumulation and toxicity of aristolochic acid I. *Molecular pharmaceutics*. 8:2183-2192.

Yamamoto, H., K. Schoonjans, and J. Auwerx. 2007. Sirtuin functions in health and disease. *Mol Endocrinol*. 21:1745-1755.

Yang, L., T.Y. Besschetnova, C.R. Brooks, J.V. Shah, and J.V. Bonventre. 2010. Epithelial cell cycle arrest in G2/M mediates kidney fibrosis after injury. *Nat Med*. 16:535-543, 531p following 143.

Yang, Y., S. Jiang, Y. Dong, C. Fan, L. Zhao, X. Yang, J. Li, S. Di, L. Yue, G. Liang, R.J. Reiter, and Y. Qu. 2015. Melatonin prevents cell death and mitochondrial dysfunction via a SIRT1-dependent mechanism during ischemic-stroke in mice. *Journal of pineal research*. 58:61-70.

Yu, F.Y., T.S. Wu, T.W. Chen, and B.H. Liu. 2011. Aristolochic acid I induced oxidative DNA damage associated with glutathione depletion and ERK1/2 activation in human cells. *Toxicol In Vitro*. 25:810-816.

Yu, H., Y. Yanagisawa, M.A. Forbes, E.H. Cooper, R.A. Crockson, and I.C. MacLennan. 1983. Alpha-1-microglobulin: an indicator protein for renal tubular function. *J Clin Pathol*. 36:253-259.

Yu, J., and J. Auwerx. 2009. The role of sirtuins in the control of metabolic homeostasis. *Ann N Y Acad Sci*. 1173 Suppl 1:E10-19.

Yuan, J., X. Luo, M. Guo, J. Wu, W. Yang, R. Yu, and S. Yao. 2009. Determination of aristolochic acid I and its metabolites in cell culture with a hyphenated high-performance liquid chromatographic technique for cell toxicology. *Talanta*. 78:1141-1147.

Zeng, Z., Y. Yang, X. Dai, S. Xu, T. Li, Q. Zhang, K.S. Zhao, and Z. Chen. 2016. Polydatin ameliorates injury to the small intestine induced by hemorrhagic shock via SIRT3 activation-mediated mitochondrial protection. *Expert opinion on therapeutic targets*. 20:645-652.

Zhan, M., C. Brooks, F. Liu, L. Sun, and Z. Dong. 2013. Mitochondrial dynamics: regulatory mechanisms and emerging role in renal pathophysiology. *Kidney Int*. 83:568-581.

Zhao, W.Y., L. Zhang, M.X. Sui, Y.H. Zhu, and L. Zeng. 2016. Protective effects of sirtuin 3 in a murine model of sepsis-induced acute kidney injury. *Sci Rep*. 6:33201.

Zheng, Q., Y. Zhao, J. Guo, S. Zhao, C. Fei, C. Xiao, D. Wu, L. Wu, X. Li, and C. Chang. 2018. Iron overload promotes mitochondrial fragmentation in mesenchymal stromal cells from myelodysplastic syndrome patients through activation of the AMPK/MFF/Drp1 pathway. *Cell death & disease*. 9:515.

Zhuo, J.L., and X.C. Li. 2013. Proximal nephron. *Comprehensive Physiology*. 3:1079-1123.

Zschoernig, B., and U. Mahlknecht. 2008. SIRTUIN 1: regulating the regulator. *Biochem Biophys Res Commun*. 376:251-255.

Table of annexes

Annex I - Micrographs of cell proliferation of HK-2 cells overtime

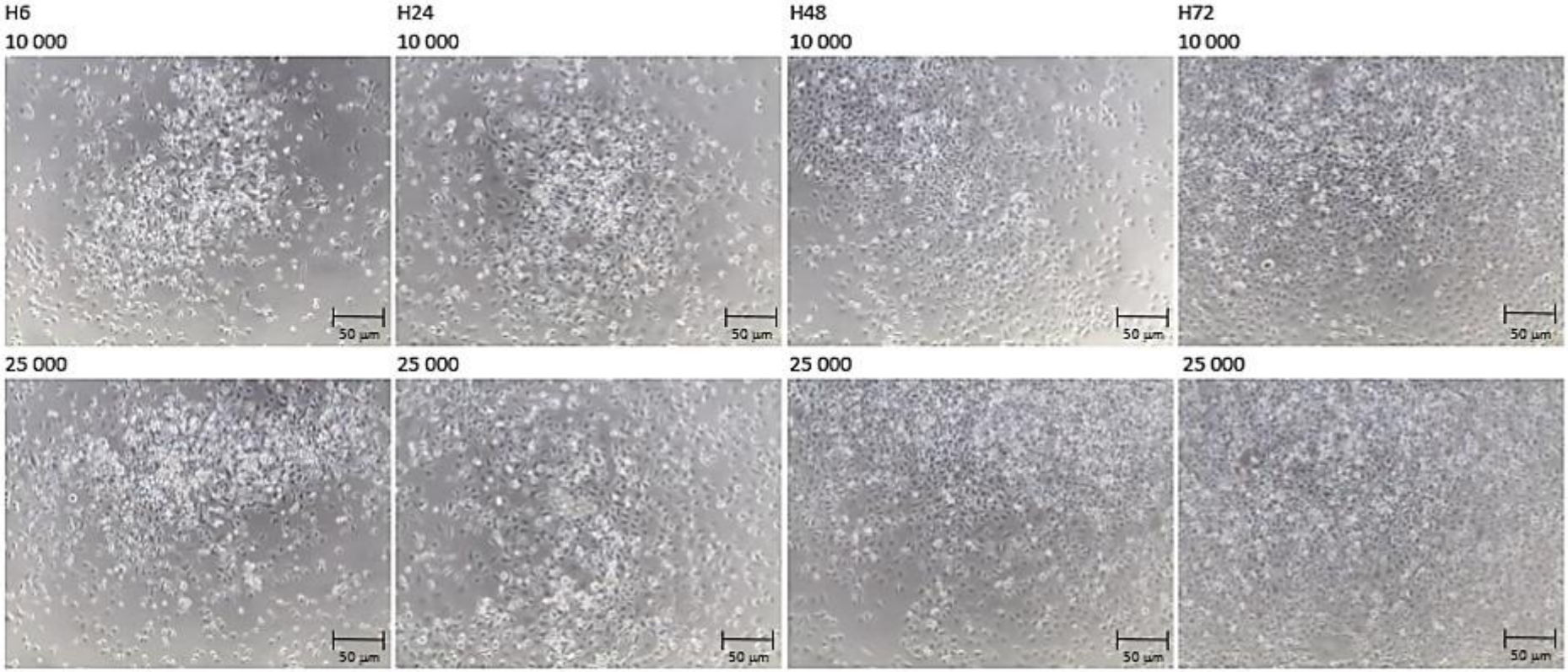

Figure 46: Micrographs of cell proliferation of HK-2 cells overtime. *Cells were seeded at different densities in 24-well culture plate during 6, 24, 48 or 72 h. Magnification 60x.*

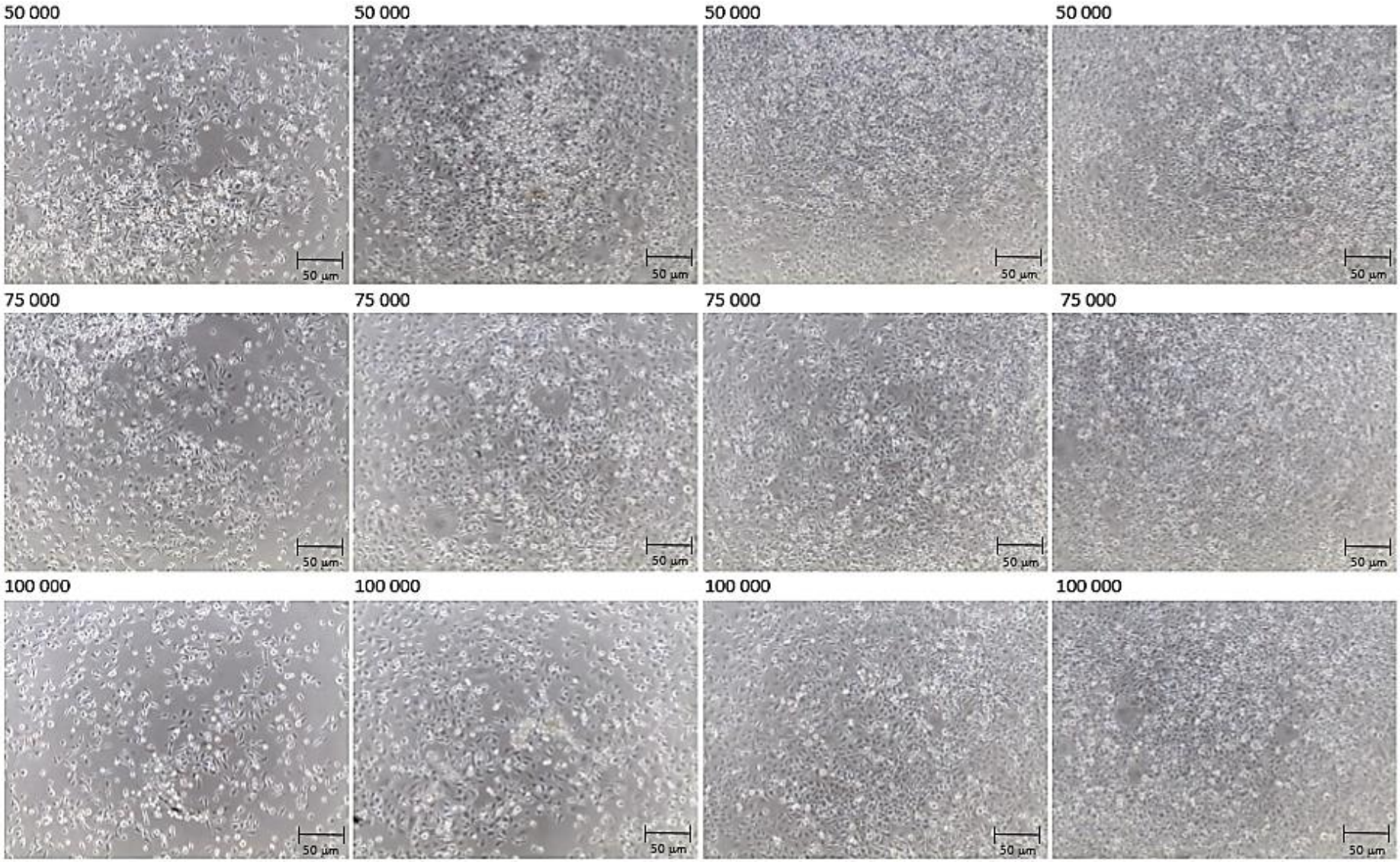

Figure 46: Micrographs of cell proliferation of HK-2 cells overtime. *Cells were seeded at different densities in 24-well culture plate during 6, 24, 48 or 72 h. Magnification 60x.*

Annex II - Effects of low concentrations of AAI on cell proliferation

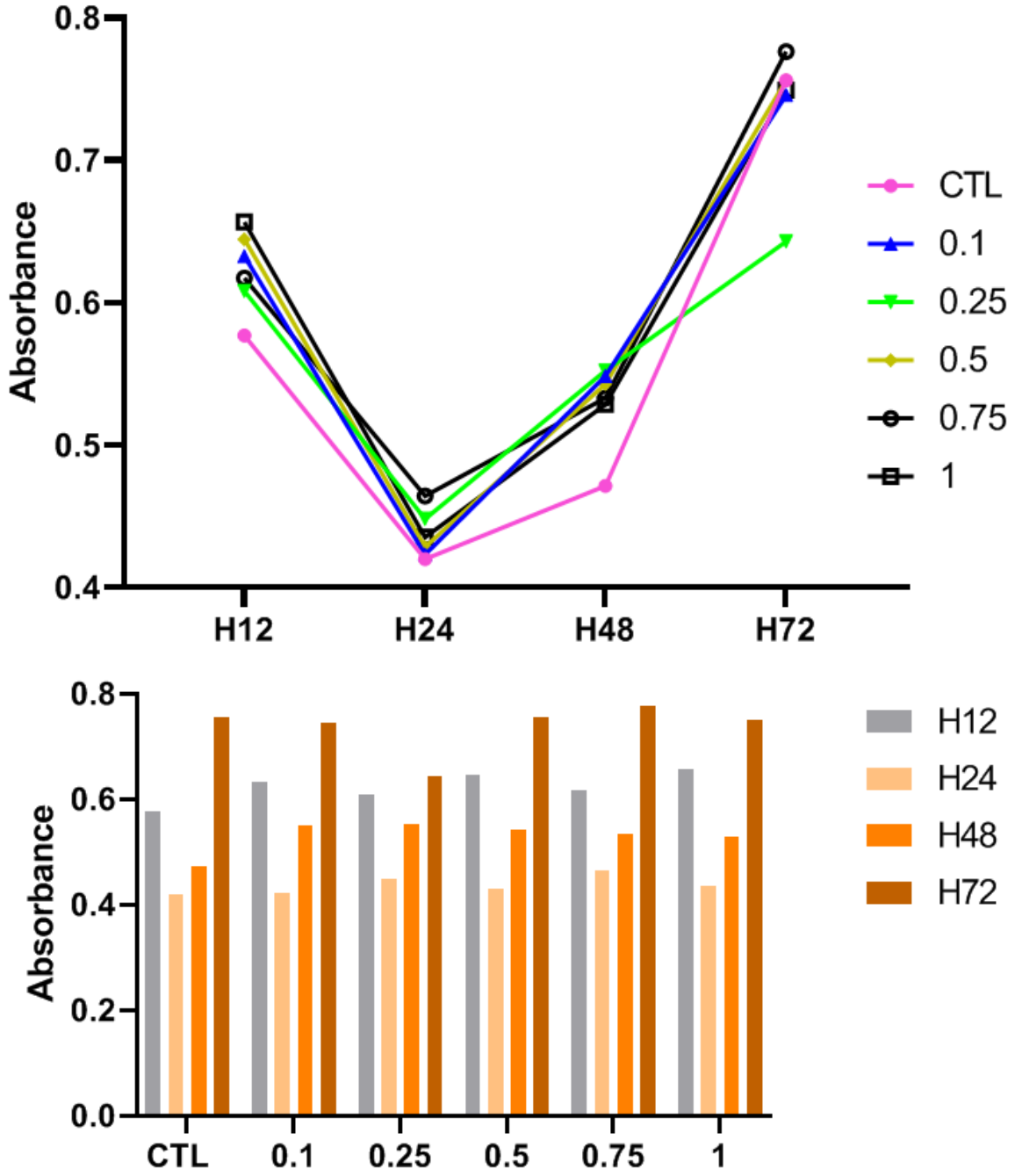

Figure 47: Effect of low concentrations of AAI on HK-2 cell assessed by MTT assay. *Cells were seeded at 100000 cells/well in 24-well culture dishes and incubated in the presence of 0, 0.1, 0.25, 0.5, 0.75 or 1 µM of AAI for 12, 24, 48 or 72 h. Results are expressed as absorbance unit and represent means of absorbance for three wells (n=1).*

Annex III - Micrographs of cell proliferation of HK-2 cells

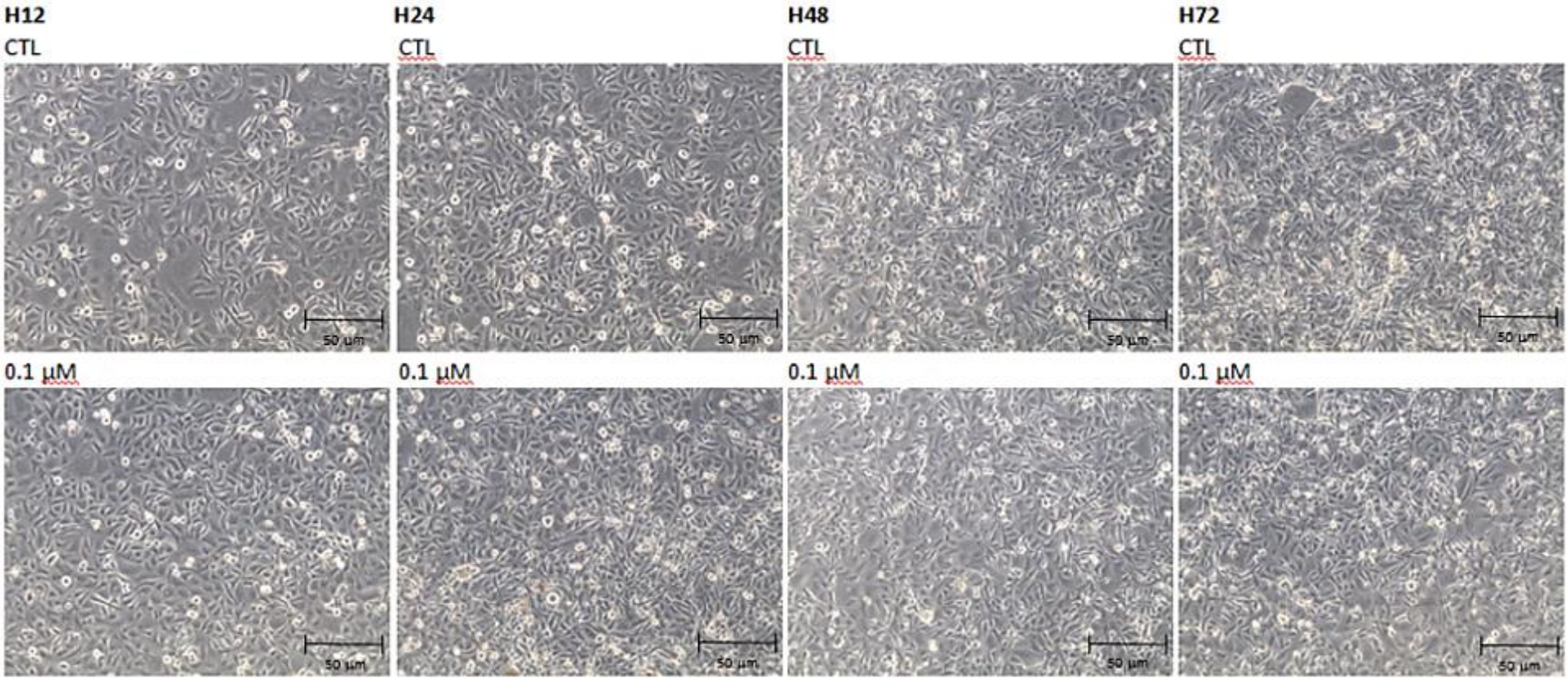

Figure 48: Micrographs of cell proliferation of HK-2 cells *seeded at 100 000 cells/well in 24-well culture plate or 1.25x10^{6} cells/T25 culture flask and incubated with 0.1, 0.25, 0.5, 0.75, 1, 10 or 50 µM of AAI during 12, 24, 48 or 72 h with AAI. Magnification 100x.*

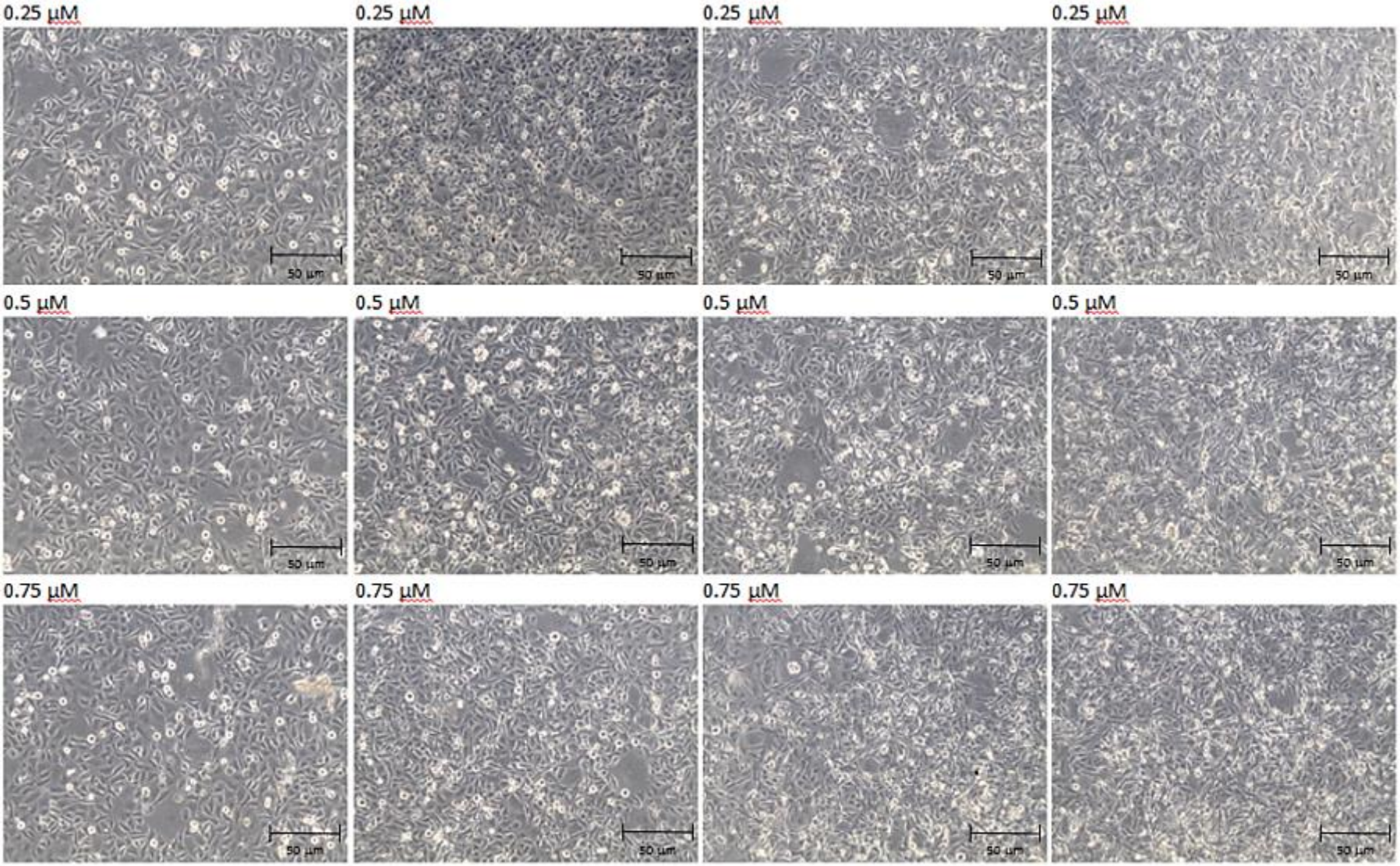

Figure 48: Micrographs of cell proliferation of HK-2 cells *seeded at 100 000 cells/well in 24-well culture plate or 1.25x10^6 cells/T25 culture flask and incubated with 0.1, 0.25, 0.5, 0.75, 1, 10 or 50 µM of AAI during 12, 24, 48 or 72 h with AAI. Magnification 100x.*

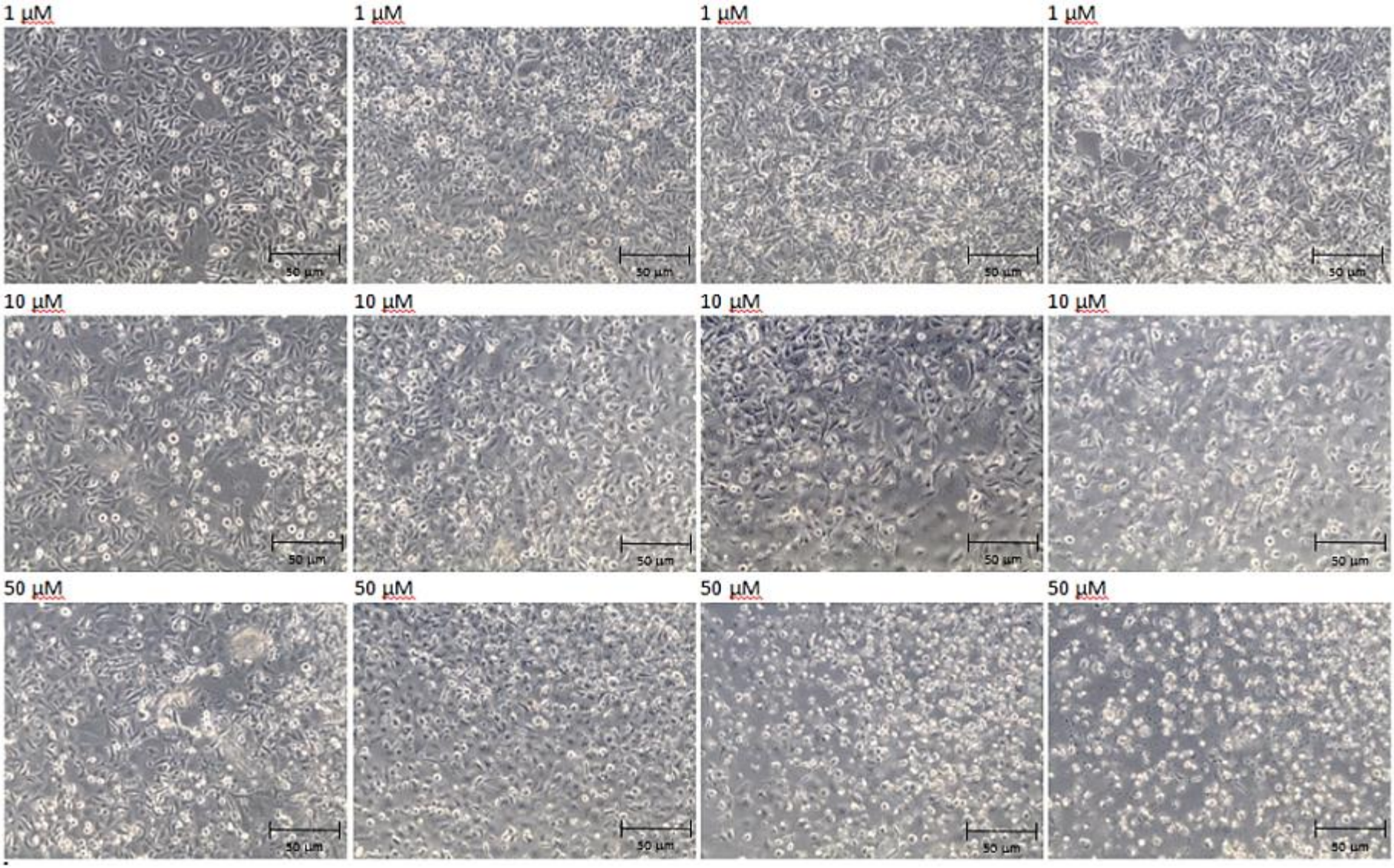

Figure 48: Micrographs of cell proliferation of HK-2 cells *seeded at 100 000 cells/well in 24-well culture plate or 1.25x10^{6} cells/T25 culture flask and incubated with 0.1, 0.25, 0.5, 0.75, 1, 10 or 50 µM of AAI during 12, 24, 48 or 72 h with AAI. Magnification 100x.*